Washington University in St. Louis
Washington University Open Scholarship

Engineering and Applied Science Theses & Dissertations | McKelvey School of Engineering

Winter 1-15-2021

Neural Dynamics, Adaptive Computations, and Sensory Invariance in an Olfactory System

Srinath Nizampatnam
Washington University in St. Louis

Follow this and additional works at: https://openscholarship.wustl.edu/eng_etds

 Part of the Electrical and Electronics Commons, and the Neuroscience and Neurobiology Commons

Recommended Citation

Nizampatnam, Srinath, "Neural Dynamics, Adaptive Computations, and Sensory Invariance in an Olfactory System" (2021). *Engineering and Applied Science Theses & Dissertations*. 612.
https://openscholarship.wustl.edu/eng_etds/612

This Dissertation is brought to you for free and open access by the McKelvey School of Engineering at Washington University Open Scholarship. It has been accepted for inclusion in Engineering and Applied Science Theses & Dissertations by an authorized administrator of Washington University Open Scholarship. For more information, please contact digital@wumail.wustl.edu.

WASHINGTON UNIVERSITY IN ST. LOUIS

School of Engineering and Applied Science

Department of Electrical & Systems Engineering

Dissertation Examination Committee:
Baranidharan Raman, Chair
Dennis Barbour
Shatanu Chakrabartty
Shinung Ching
Daniel Moran

Neural Dynamics, Adaptive Computations, and Sensory Invariance in an Olfactory System

by

Srinath Nizampatnam

A dissertation presented to
The Graduate School
of Washington University in
partial fulfillment of the
requirements for the degree
of Doctor of Philosophy

January 2021
St. Louis, Missouri

© 2021, Srinath Nizampatnam

Table of Contents

List of Figures

Acknowledgments

I am deeply thankful for the exceptional research opportunities that my advisor, Dr. Barani Raman, has presented to me during my time at Washington University. While I spent my initial days in his lab on purely quantitative aspects of systems neuroscience, I slowly transitioned to performing electrophysiology experiments – an amazing experience that makes this field so exciting! I am very thankful to Barani for encouraging me to pursue this path where I could work on analytical methods while staying excited through experiments. Beyond giving me this opportunity, his unwavering patience and understanding have contributed immensely to my growth in my early scientific years. I have also learned a great deal about presenting and writing from his well-timed advice. I am truly blessed to have had the opportunity to work with and learn from him.

I sincerely thank the rest of my dissertation committee members: Dr. Dennis Barbour, Dr. Shantanu Chakrabartty, Dr. Shinung Ching, and Dr. Daniel Moran for their interest in this research, and for the feedback I received.

It has been a great experience working with an amazing group of people in Raman lab. I sincerely thank all the members of the lab for all the feedback and discussions I have had with them. I am thankful to have worked with Dr. Debajit Saha, who was a postdoctoral researcher in the lab. His amazing guidance in performing electrophysiology experiments has helped me to get off to a good start, and his advice on planning projects and prioritizing key questions has been invaluable. I like to thank Lijun Zhang for always being a great team member and for assisting me with issues related to quantitative analysis. I would also like to thank all my friends in St. Louis for making this journey a truly memorable and amazing one.

I express my sincere gratitude to Dr. V. U. Reddy for his guidance during my undergraduate studies and for inspiring me to pursue a Ph.D. His immense knowledge and passion for the field of signal processing, and his patience while solving problems served me as a great inspiration. I like to thank Dr. Arye Nehorai for all his support during my initial years at Washington University. I also like to thank Dr. Mark Anastasio and Dr. Xuan Zhang for the research experience that I gained working with them.

I will be forever grateful to my parents and my sister, whose love and support have always encouraged me to go a step further. Being away from them has been the hardest, but this has been a journey worth chasing.

Srinath Nizampatnam

Washington University in St. Louis

January 2021

Dedicated to my parents.

ABSTRACT OF THE DISSERTATION

Neural dynamics, adaptive computations, and sensory invariance in an olfactory system

by

Srinath Nizampatnam

Doctor of Philosophy in Electrical Engineering

Washington University in St. Louis, 2020

Professor Baranidharan Raman, Chair

Sensory stimuli evoke spiking activities that are patterned across neurons and time in the early processing stages of olfactory systems. What features of these spatiotemporal neural response patterns encode stimulus-specific information (i.e. 'neural code'), and how they are translated to generate behavioral output are fundamental questions in systems neuroscience. The objective of this dissertation is to examine this issue in the locust olfactory system.

In the locust antennal lobe (analogous to the vertebrate olfactory bulb), a neural circuit directly downstream to the olfactory sensory neurons, even simple stimuli evoke neural responses that are complex and dynamic. We found each odorant activated a distinct neural ensemble during stimulus presentation (ON response) and following its termination (OFF response). Our results indicate that the ON and OFF ensemble neural activities differed in their ability to recruit recurrent inhibition, entrain field-potential oscillations, and more importantly in their relevance to behavior (initiate versus reset conditioned responses).

Furthermore, when the same stimulus was encountered in a multitude of ways, we found that the neural response patterns in individual neurons varied unpredictably. Intriguingly, a simple, linear logical classifier (OR-of-ANDs) that can decode information distributed in flexible

subsets of ON neurons was sufficient to achieve robust recognition. We found that the incorporation of OFF neurons could enhance pattern discriminability and reduce false positives thereby further improving performance. These results indicate that a trade-off between stability and flexibility in sensory coding can be achieved using a simple computational logic.

Lastly, we examined how the ON and OFF neural ensembles varied with stimulus intensity. We found that neurons that were ON responsive at low intensity switched and became OFF responsive at higher intensities. Similarly, OFF responsive neurons at low intensity were recruited and responded during odor stimulation at higher intensities. We found a competitive network involving two sub-categories of GABAergic local neurons can mediate this switch between ON and OFF responsive ensembles and how they vary as a function of stimulus intensity.

In sum, our results provide a comprehensive understanding of how a relatively simple invertebrate olfactory system could perform complex adaptive computations with very simple individual components.

Chapter 1: Introduction

Olfactory systems have evolved over millions of years to recognize complex multi-molecular mixtures. While the dimensionality of the chemical space is immense, the olfactory system has found solutions to efficiently and robustly represent sensory stimuli. In addition to their high dimensionality, sensory stimuli encountered in the natural environment are often dynamic in nature with several factors influencing robust recognition such as competing stimuli, or distracting stimuli, or intensity variations. Here we sought to understand how odorants can be detected and recognized in an invariant fashion. Furthermore, we investigated whether a single computational framework can provide robust recognition under all these perturbations.

While there are many external interferences, which are irrelevant, impacting how the odorants are received, are there meaningful changes in how a stimulus gets processed that might also impact its recognition? Adaptation is a widespread property of sensory systems, occurring at many stages of processing[1] and across time scales spanning from hundreds of milliseconds to tens of seconds[2]. In most sensory systems, an important objective of this adaptation process is to suppress redundant information in order to attend to salient features in the stimuli [3, 4]. While this computational task can be achieved relatively easily in sensory systems with labeled-line coding schemes, it becomes particularly challenging in modalities where a majority of stimuli are encoded in a combinatorial fashion and with considerable neural overlap [5-9]. Whether neural circuits adapt to one stimulus without varying the encoding of other stimuli, or whether they achieve a balance between variability and robustness in other ways is not understood.

In this work, we investigated how the neural responses adapt under complex stimulus encounters and an invariant stimulus recognition can be achieved using the locust (*Schistocerca americana*) olfactory system. This model is advantageous as not only many of its neuronal populations are accessible for recording [10], but also can be studied to understand how neural dynamics translate to behavior [11-14].

1.1 Insect Olfactory Anatomy

In the insect olfactory system, odorants are sensed by olfactory receptor neurons (ORNs), which are located in the antennae within hair-like structures called sensilla [15]. ORNs transduce the chemical stimuli into trains of action potentials that are relayed to downstream centers. A given receptor generally responds to a range of odorants, and the number of ORNs activated increase with intensity [16-18]. The current dogma is that each odorant activates a unique combination of ORNs—suggesting a combinatorial representation of odorants intensity [17, 19].

Excitatory ORN signals are relayed downstream to the ipsilateral antennal lobe, where the axons of multiple ORNs converge onto spherical structures known as glomeruli[20] (**Fig. 1.1**). This combination of outputs from multiple, spatially distributed ORNs that express the same olfactory receptor protein (the transducing element) increases signal strength, and minimizes noise due to fluctuations in intensities[21]. At these centers, ORNs synapse directly to two different cell types: cholinergic projection neurons (PNs – excitatory) and GABAergic local neurons (LNs – inhibitory) [22, 23]. Anatomical studies have shown that there are approximately 830 PNs and 300 LNs in the locust antennal lobe[22]. PNs extend their dendrites to multiple glomeruli, which makes this model system relatively unique. Axon-less LNs project broadly within the antennal lobe and form inhibitory synapses with a large number of PNs[20]. LNs

display different spontaneous activity and different response patterns to odors in different insect species. However, in locusts, only non-spiking LNs are described so far [20].

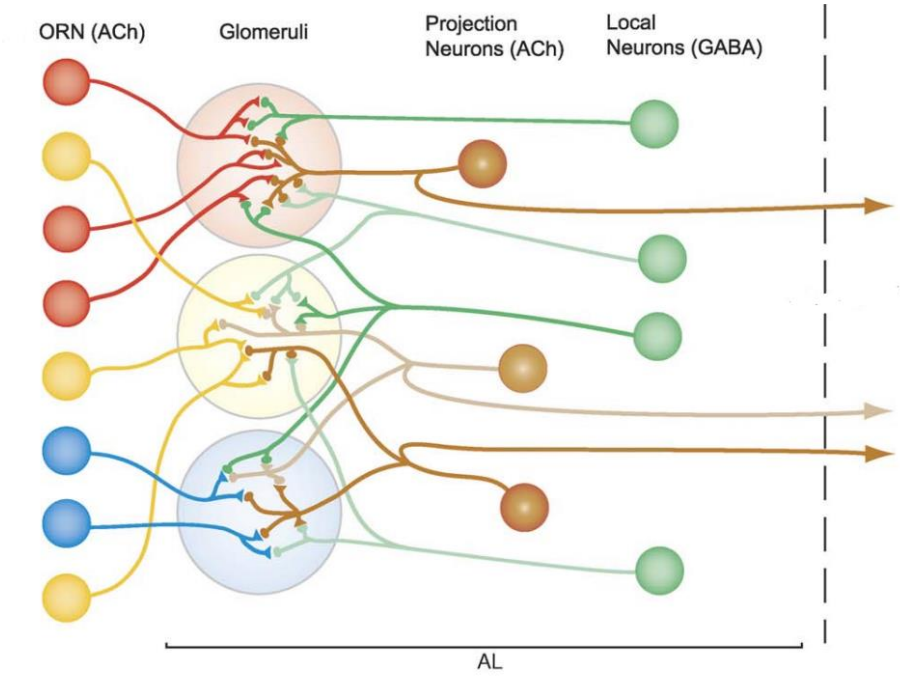

Figure 1.1: The anatomy of insect antennal lobe. A schematic of the anatomy of insect olfactory system is shown (reproduced as is from [24]). ORNs send excitatory outputs to both PNs and LNs. PNs and LNs have recurrent connections within the antennal lobe, PNs send their outputs to the higher brain centers.

The PN outputs project onto downstream circuits in the mushroom body and lateral horns, the higher order circuits that are thought to underlie associative learning[25, 26] and innate behaviors[27], respectively. There are approximately 50,000 neurons called Kenyon cells (KCs) in the locust mushroom body[28]. Each KC receives input from approximately half of the PN population through weak synapses [29].

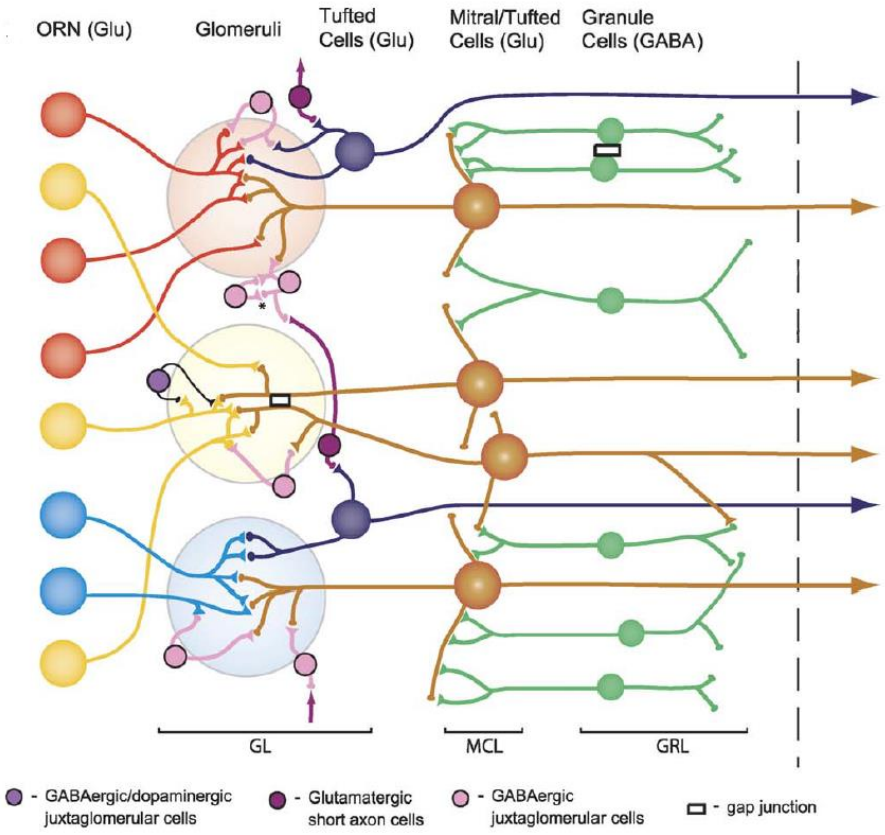

Figure 1.2: The anatomy of vertebrate olfactory bulb. Glutamatergic ORNs expressing the same receptors send their excitatory signals to the olfactory bulb (OB). Within the OB, glutamatergic mitral and tufted (M/T) cells, GABAergic short axon cells, periglomerular cells, and granule cells, form synaptic interactions. M/T cells provide the output of the OB to higher olfactory center. GL: glomerular layer. MCL: mitral cell layer. GRL: granule cell layer (reproduced as is from [24])

The vertebrate olfactory system (**Fig. 1.2**) shares circuit motifs similar to the insect olfactory system, even though they evolved independently [24, 30]. In mammals, the receptor neurons are located in the olfactory epithelium within the nasal cavity. Excitatory signals from the receptor units project their signals onto glomeruli in the olfactory bulb, analogous to the antennal lobe in the insect olfactory system. Within glomeruli, glutamatergic mitral and tufted (M/T) cells (analogous to PNs) and GABAergic periglomerular cells form synaptic connections. Additionally, GABAergic juxtaglomerular interneurons, which are axon-less, form inter-

glomerular connections with M/T cells [31]. Next, M/T cells send their signals to the piriform cortex and other cortical targets in the brain.

1.2 Sensory coding and neural dynamics in the locust antennal lobe

1.2.1 Olfactory Coding

The topic of how the sensory stimuli are represented in brain and how those representations transform to robust behaviors has been a subject of great debate [32-37]. Broadly, there are two hypotheses: 'spatial code' and 'temporal code'. The key understanding behind spatial coding is that the stimulus-specific information gets encoded by a unique combination of spatially adjacent neurons [38-40]. In flies, attractive odors were found to activate the medial regions of the antennal lobe, while repulsive odors activated the lateral regions [39, 40]. Temporal coding suggests that the useful stimulus-specific information can be found along the temporal dimension of neural responses, since odor-evoked neural responses are also temporally patterned. The temporal response features such as response latency and response patterns [11, 12, 35, 41-44] of spiking activities have been shown to be important for sensory coding.

To understand how the coding principles in the early processing stages of olfactory processing, neural responses have been well characterized by many physiological studies [8, 11, 45-48]. At the level of first-order olfactory receptor neurons, both firing rates and firing patterns of the odor-evoked responses were shown to be odor-specific and temporally heterogeneous [8]. This temporally structured input from ORNs drives more elaborate spatiotemporal activity patterns [49-52] at the level of second-order projection neurons in the antennal lobe. The highly

convergent nature of ORNs (~100,000) to PNs (~830) connection often results in activation – either excitation or inhibition – of a high percentage of PNs in the presence of odors [53].

The responses evoked by the projection neurons vary with the odor stimulus presented, and at the ensemble level, these responses are shown to encode both stimulus identity and intensity [35, 45-48, 51, 54]. The representations of these ensemble neural responses were found to be organized into odor-specific manifolds, and with the intensity-specific trajectories lying within the odor-specific manifold (**Fig. 1.3**) [48]. In other words, the variability with respect to intensity changes of a stimulus was found to be less when compared to the variability with respect to the identity of stimulus.

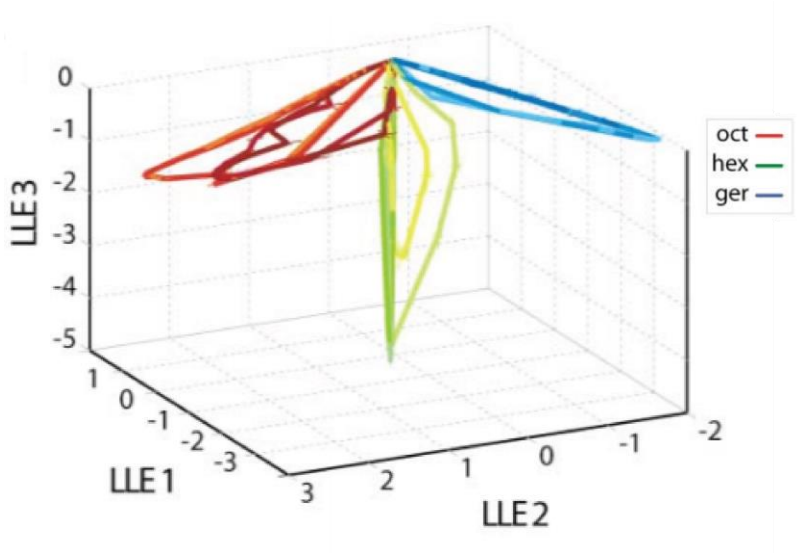

Figure 1.3: Visualization of population projection neuron responses as trajectories. Spatiotemporal neural responses (110 PNs) are plotted as trajectories for four concentrations of three odors (octanol – red, hex – green, geraniol – blue). Note that the changes due to intensities are much less when compared to changes due to identity (reproduced as is from [48]).

The spatiotemporal projection neuron response patterns for a given stimulus, however, have been shown to be variable when encountered in complex environments [45, 54, 55]. Previous studies have shown that the response patterns can vary depending on the stimulus

dynamics, examples of which include a stimulus encountered in a temporally overlapping fashion with other stimuli [45, 55], and when a stimulus is encountered in a pulsatile fashion [12, 54]. While the activity of individual projection neurons varied, the activity patterns based on the ensemble of neurons were found to be odor-specific and reliable. Any overlap in these spatiotemporal activity patterns across environments was found to be sufficient to decode an odor in a background-independent manner [45]. Overall, ensemble-based stimulus decoding methods have been shown to be reliable and can disambiguate complex stimulus encounters [54].

1.2.2 Role of inhibition from local neurons

In additions to variations due to the stimulus dynamics, the temporal patterns of stimulus-evoked activity can also vary due to changes in interactions between individual neurons (and therefore, in a way that is 'intrinsic' to the neural network). This is evident in the neural response variations observed over repeated presentations of the same stimulus [47]. In the antennal lobe, local neurons provide both presynaptic inhibition [56] onto ORN axons and post-synaptic inhibition [57] onto projection neurons dendrites. Furthermore, inhibition onto PNs can come in both feedback and feedforward configurations [22, 57, 58]. While the recurrent inhibition corresponds to the feedback provided by LNs in response to the excitatory input from PNs, the feedforward inhibition corresponds to the inhibition provided by LNs in response to the ORN input (**Fig. 1.4**).

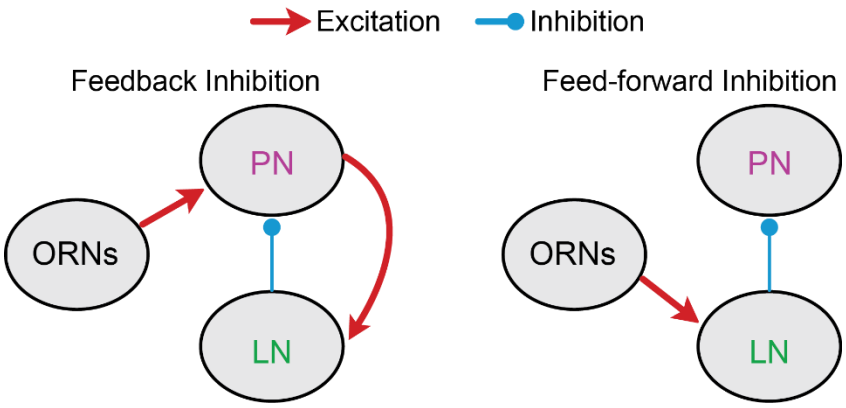

Figure 1.4: A schematic showing feedback and feed-forward inhibition in the antennal lobe. Left, ORNs send their excitatory input to a PN, which excites a LN that provides inhibitory feedback to the same PN. Right, ORNs send their excitatory input to a LN, which provides inhibition to a PN.

The feedback inhibition provided by LNs is non-static and has been hypothesized to undergo changes with repeated exposures of the same stimulus [47, 59]. Upon repeated stimulus presentations, the integrated power of local field potential (averaged antennal lobe response) oscillations of later trials of exposure was found to be significantly higher when compared to the first few trials of exposure (**Fig. 1.5**). Besides the increasing oscillatory power with the repeated exposures of a stimulus, both the LN activity and PN spike time were found to be in increased coherence with the local field potential waveform. The number of PN spikes evoked by the stimulus also decreased as the stimulus became more familiar. This change was found to be stimulus-specific and intrinsic to the antennal lobe circuit as a form of short-term memory [47].

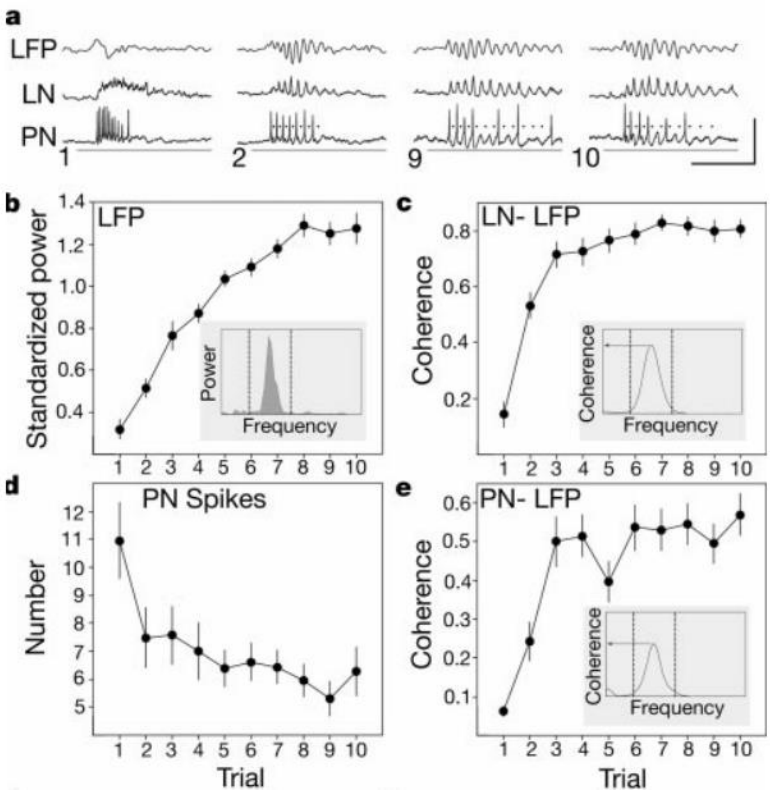

Figure 1.5: Coherence and spike time precision increase over repeated stimulus presentations. (a) Comparison between the initial (trials 1–2) and later trials (trials 9–10) of the same stimulation is shown for local field potential (LFP), local neuron (LN), and projection neuron (PN). **(b)** LFP power spectrum increased during the first 7 or 8 trials before reaching asymptote. **(c)** Coherence between LN and LFP increased rapidly in the first two trials. **(d)** Number of odor-elicited PN spikes is plotted with the trial. **(e)** Coherence between PN spike time and LFP increased over trials (reproduced as is from [47]).

Furthermore, the reduced PN activity to repeated stimulus encounters has been hypothesized to cause the olfactory habituation [60-62]. While examining the role of feedback inhibition from local neurons in behavioral habituation, prior studies found strengthening of inhibitory synapses from LNs to a subset of PNs [60]. This synapse-specific enhancement of recurrent inhibition was hypothesized to cause odorant-selective response adaptation in the PNs [58, 61].

While feedback inhibition is implicated with oscillatory synchronization of the PN activity and habituation, the feedforward inhibition has been hypothesized to support gain

control function [56, 63] in the antennal lobe (i.e. prevent the responses of PNs from saturating). Notably, when the concentration of an odorant increased, the lateral inhibitory input (from LNs) was shown to scale linearly with the total ORN activity in fruit fly [63]. Such scaling of inhibitory strength with the input was shown to prevent a stimulus from saturating the dynamic range of PNs. Whether the local neurons in the locust antennal lobe play a similar role is not understood. While it is known that LNs reshape PN activity and that there is a diverse set of local neurons [20], how this diversity within local neurons reshape PN activity to encode odorants is not understood.

1.3 Odor Coding in Mushroom Body

In addition to examining the neural response patterns in the antennal lobe, several studies have also examined the neural responses evoked by Kenyon cells (KCs) lobe [45, 48] in the mushroom body, a site that has been associated with learning and memory [64-67]. Anatomical studies showed that each Kenyon cell receives input from multiple projection neurons (roughly half) [29, 68].

While the projection neurons are spontaneously active and respond to odors in a temporally elaborate manner, KCs are nearly silent during spontaneous periods and respond to odors with very few spikes [45, 48, 53, 69-72] (i.e. temporally sparse; **Fig. 1.6**). Recurrent connections between KCs and a giant GABAergic neuron[73] (GGN – inhibitory), and integration of inputs in cyclic windows[53, 74] are the reasons hypothesized for the sparse encoding by KCs. Interestingly, unlike the PNs, these sparsened KC responses were found to be widely separated for similar stimuli [71] (i.e. de-correlated neural representation).

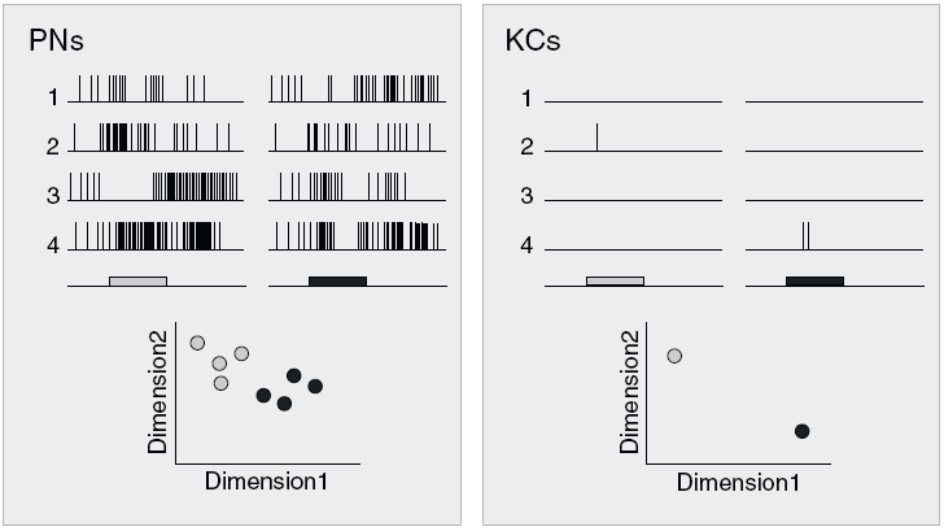

Figure 1.6: Kenyon cells respond sparsely and selectively. Comparison of odor-evoked responses of projection neurons and Kenyon cells is shown (reproduced as is from [72]). Left, raster plots of 4 projection neurons and their representation in 2-dimensions is shown. Right, raster plots of 4 Kenyon cells and their representation in 2-dimensions is shown.

1.4 Behavioral Relevance

Several behavioral assays have been developed to study olfactory insect behavior[75-77] and understand their neural basis[41, 78, 79]. These assays had been developed to investigate relation between physiological responses and a particular behavior, such as studying innate behavior[41] or odor valence[40]. Pavlovian conditioning paradigm has also been adapted to study olfactory learning[80, 81]. In locusts, behavioral studies have been recently developed to study associative learning [46, 76]. Locusts can be trained using an appetitive-conditioning paradigm, in which they are presented with a conditioned stimulus followed by a food reward (wheat grass) with significant stimulus-reward overlap. When trained locusts are presented with the conditioned stimulus, the locusts open their maxillary palps in anticipation of the food reward (**Fig. 1.7**).

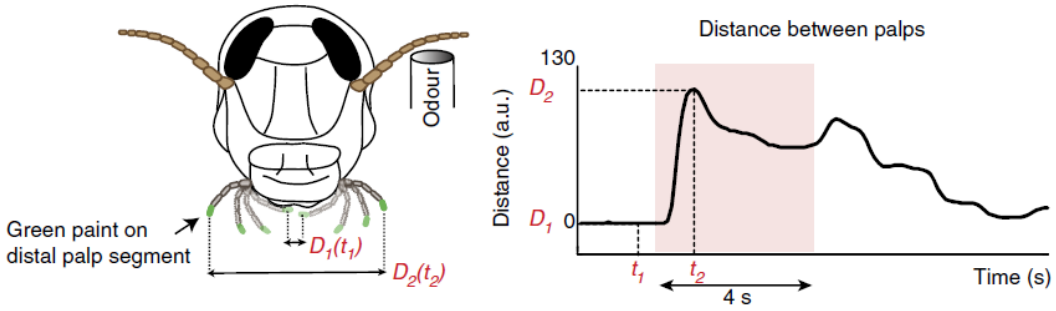

Figure 1.7: Behavioral response to the conditioned stimulus. A schematic of the locust palp-opening response (POR) behavioral assay is shown. Maxillary palps were painted with a non-odorous green paint to facilitate tracking. Opening of the palps can be tracked as a distance that can be used an indicator for acquired memory (reproduced as is from [46]).

While investigating how competing cues impact olfactory learning, researchers have found that locusts can recognize the conditioned stimulus in a background invariant manner [45]. This indicates that locusts can not only discriminate between different stimuli, but neural responses have been translated to a robust behavior even in complex stimulus encounters. A prior study has also noted that the combinatorial PN ensembles encode stimulus identity, whereas temporal structure of ensemble PN response emphasize novel stimuli [46].

The translation from neural responses at early processing stages to the final behavior in locusts remains unknown. Noting that finding an accurate mapping can be a complex mapping, can we find what features of neural responses are most important?

1.5 Thesis Outline

The overall organization of this thesis is as follows: All experimental and analytical methods used in this dissertation are discussed in Chapter 2. Computational models that were developed to model neural dynamics observed in locust antennal lobe are also shown here. In Chapter 3, I investigate the role of recurrent inhibition in activating two distinct neural ensembles in the

antennal lobe—primarily occurring at the onset and offset of a stimulus. More importantly, the behavioral relevance of these distinct neural ensembles is also discussed here. This work has been published in Nature Communications (2017). In Chapter 4, I examine the robustness of the neural code using a sequential stimulation protocol and propose a flexible coding approach that presents a novel way of robustly encoding stimulus-specific information. This helps us understand how a sensory system can maintain robustness while allowing the circuit to adapt. This work has been published in Nature Communications (2018). In Chapter 5, I examine how projection neuron responses are perturbed when the stimulus encounters are more complex. Reliability of the flexible coding approach is also investigated using this data. In Chapter 6, I investigate the role of feedforward inhibition from local neurons in reshaping the activity of projection neurons. Subpopulations within local neurons are identified and their role in intensity coding is hypothesized. A possible network mechanism is also explained using a computational model. In Chapter 6, the overall focus and results of this study are shown along with some results that require further work to arrive at conclusions.

Chapter 2: Methods

This chapter contains methods, both experimental and analytical, which were designed to examine adaptive computations in locust olfactory neural circuit. Experiments include extracellular (multi-unit) and whole-cell (single-unit) *in vivo* neural recordings and behavioral experiments. While extracellular experiments were designed to study network-level (population) computations, intracellular experiments were aimed at examining cell-intrinsic mechanisms. Behavioral experiments were designed to understand how different adaptive computations in the brain translate to final behavior. Moreover, statistical and machine learning methods that were used to analyze neural and behavioral data are also shown. This chapter is organized as follows: electrophysiology, behavior, analyses and computational modeling.

2.1 Electrophysiology

2.1.1 Extracellular studies

Odor stimulation: Odor stimuli were delivered using a standard procedure [45, 46, 54, 82]. The following odor panel was used: hexanol, geraniol, 2-octanol, isoamyl acetate, benzaldehyde, citral, apple, and cyclohexanone. All odorants were diluted to their 1% concentration by volume (v/v) in mineral oil. A carrier stream of desiccated and filtered air stream (0.75 L min^{-1}) was directed at the antenna to provide a constant flux. A constant volume (0.1 L min^{-1}) from the odor bottle headspace (60 ml sealed bottles contained 20 ml diluted odor solutions) was injected into the carrier stream using a pneumatic pico-pump (WPI Inc., PV-820) during stimulus presentations. A vacuum funnel placed right behind the locust antenna ensured removal of odor

vapors. Each solitary or sequential presentation of an odorant was delivered in a pseudorandomized manner (blocks of 10 trials) with 60 s inter-trial intervals.

Olfactory electrophysiology: Young locusts (*Schistocerca americana*) of either sex with fully developed wings (post fifth instar) were selected from a crowded colony. After immobilizing locusts, the brain was exposed, desheathed, and continually perfused with locust saline as reported previously [54, 83]. Extracellular recordings from the antennal lobe were made using a 16-channel, 4×4 silicon probes (NeuroNexus). Each electrode contact pad was gold plated such that its impedance was in the 200 – 300 kΩ range. Raw extracellular signals were filtered between 0.3 to 6 kHz and amplified at 10 k gain using a custom-made 16-channel amplifier (Biology Electronics Shop; Caltech, Pasadena, CA). Raw data were acquired at 15 kHz sampling rate using a custom LabView data acquisition program.

PN spike sorting: For spike sorting, we used a conservative approach that was described in earlier works[84]. We used the following criteria for the single-unit identification: cluster separation > 5 noise s.d., the number of spikes within 20 ms < 6.5%, and spike waveform variance < 6.5 noise s.d. Using this approach, a total of 85 PNs were identified from 9 locusts (11 antennal lobes).

PID experiment: We used a fast photo-ionization detector (miniPID, Aurora Scientific) to characterize the dynamics of stimulus delivered. Raw data were amplified (gain = 5) and acquired at 15 kHz sampling rate using a custom LabView data acquisition program.

2.1.2 Intracellular studies

Surgery process and olfactory stimulation is same as what we described in extracellular studies. Intracellular studies were done using patch-clamp technique (whole cell recordings) by holding the current at a specific level i.e. current clamp. Patch-electrodes were prepared by pulling glass pipettes (BF 120-69-10) using a micropipette puller (Sutter instrument – model P1000). Pipettes were filled with locust intracellular solution[85]: 155mM K aspartate, 1.5mM MgCl2, 1mM CaCl2, 10mMHEPES, 10mM EGTA, 2mM ATP disodium salt, 3mM D-Glucose, 0.1mM cAMP. All these chemicals were purchased from Sigma-Aldrich. The pH of the patch solution was adjusted to7.0 using 1M NaOH and the osmolarity was adjusted to 320-325mM range using sucrose.

Steps followed for current clamp experiment:

- Pull the micro pipettes with a microforge using a custom-made program to achieve impedances within the range of 5–15MΩ.
- Fill the electrodes with intracellular solution before connecting to a head stage of amplifier (Axoclamp 700b, Molecular Devices). Maintain a constant air pressure at the tip of the patch electrode.
- Navigate the electrode towards the cell bodies as shown in **Fig. 2.1** and by holding a current pulse (-1nA at 2Hz).
- Once a cell was targeted, release the pressure and apply brief suctions until there is a significant voltage drop (confirm a Giga-ohm seal). Change the holding current to zero, and apply bigger suctions until we confirm that the cell-wall is broken (i.e. low impedance).

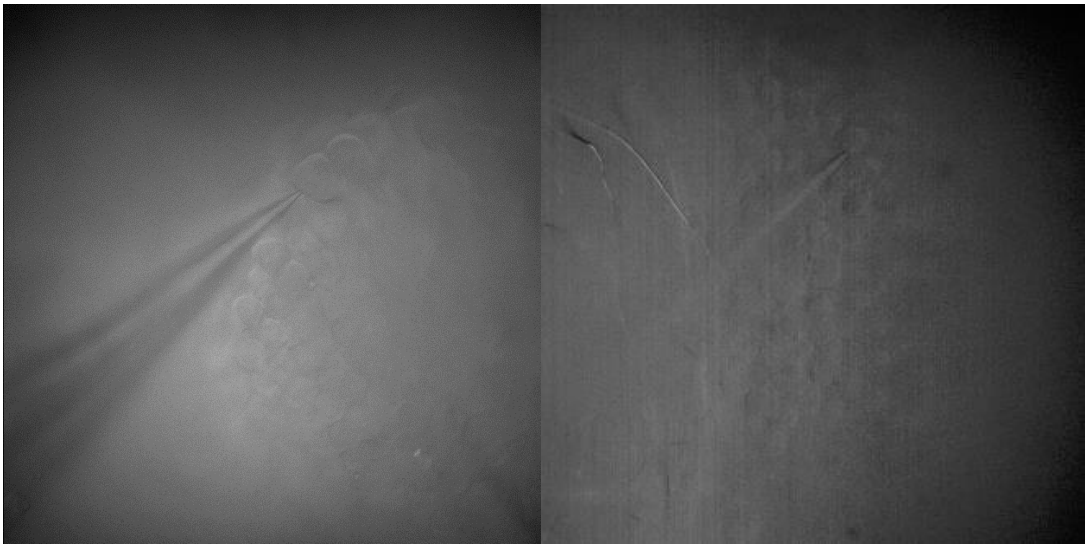

Figure 2.1: Whole-cell intracellular experiment. Images of the locust brain are shown while doing a patch-clamp experiment (viewed with 40x lens). Left panel shows an electrode targeting a neuron in the antennal lobe, and the right panel shows an electrode targeting a Kenyon cell in the mushroom body. Notice that Kenyon cells are small and densely packed compared to antennal lobe neurons.

Electrical stimulations: We used electrical stimulations to study some of the cell-intrinsic mechanisms that cause stimulus response adaptation. Current pulses with magnitudes of 100-200 pA (+ve or -ve) were used to stimulate the neurons. Voltage responses were recorded while electrical pulses were delivered (blocks of 5 trials) with 60 s inter-trial intervals.

2.2 Behavioral experiments

Behavioral experiments were performed using locusts of either sex. All locusts used were from a crowded colony that was kept on a 12 h day – 12 h night cycle (7 am – 7 pm day). All behavioral experiments were performed between 10 am – 3:30 pm.

Locusts were starved for 24 hours prior to their use in the appetitive-conditioning assay. The protocols that we used in this study for training locusts and tracking their palp-movements were identical to an earlier study[46]. The odor delivery setup and the stimulus sequences used

were identical to that described for the electrophysiology experiments.

Hexanol diluted in mineral oil (hex 1%) was used as the conditioned stimulus for all behavioral experiments in this study. Wheat grass was used as the unconditioned stimulus. During each training trial, the conditioned stimulus was presented for 6 s. Food reward was given 3 s after the onset of the conditioned stimulus. Food was given manually for the duration of approximately 10 seconds. The training phase included a total of six training trials with a ten-minute interval between successive trials. Only locusts that accepted food reward in at least four out of the six training trials and had a palp-opening response (POR) in at least three training trials were regarded as 'trained locusts' and retained for the testing phase (75% of the locusts (30/40) fell into this category). The imaging software was not able to robustly track the palp movements of three of the trained locusts (3/30) and, therefore, these locusts were excluded from all analyses.

In the unrewarded testing phase, locust PORs were evaluated using six test trials. The first trial in all tests was the solitary presentation of 4 s of hexanol. This was done to ensure that trained locusts were able to recognize the solitary presentations of the trained stimulus (26/27 locusts had a strong POR to solitary hexanol). In the subsequent five trials, the conditioned stimulus was presented in non-overlapping two odor sequences used in electrophysiology experiments. The two odor stimulus sequences were presented in a pseudo-randomized manner. The inter-trial delay between test phase trials was set to at least 20 minutes.

Locust response categorization: We classified a locust to be 'responsive' when the POR to an odor presentation was 6.5 s.d. above pre-stimulus baseline response. Further, the POR during

odor presentation had to remain greater than 20% of its peak value for at least 1 s. All the other cases were marked as ‘non-responsive’.

2.3 Neural data analysis

Dimensionality reduction analyses for PN responses:

We used two dimensionality reduction techniques for visualizing ensemble PN responses: principal component analysis (PCA) and linear discriminant analysis (LDA). For both analyses, spiking activity of each PN was binned in 50 ms non-overlapping time bins and averaged across trials. Spike counts of all recorded PNs were aligned with respect to the stimulus onset and concatenated to form an N-dimensional PN response vector per 50 ms time window. Therefore, for each odorant, we obtained a response matrix of the following dimensions: N neurons (rows) x 80-time bins (columns; 4s of activity).

To perform the PCA analysis, we first concatenated the responses of the N PNs to all the odorants (N PNs x k x 80 time bins [k odors x 80 time bins]). Response covariance matrices (N x N) were computed for these concatenated data matrices. Each N-dimensional PN response vector was then projected onto the three principal eigenvectors (for visualization).

For generating figures, PN responses after PCA dimensionality reduction were linked in the temporal order of occurrence to create odor trajectories. The pre-stimulus baseline activity in the first time bin was subtracted before plotting each response trajectory. The odor trajectories shown were also smoothed using a three-point moving-average, low-pass filter.

LDA dimensionality reduction[86] analysis was also performed by first concatenating all high-dimensional PN response vectors that needed to be visualized. The projection vectors were

determined such that they maximized separation between responses of different stimuli while at the same time also reducing variance within responses generated by a single stimulus.

Sorting of PN response: PN responses were sorted in **Fig. 3.1b–e** based on the following metric:

$$Response\ Difference\ = \frac{\text{norm Peak ON} - \text{norm Peak OFF}}{\text{norm Peak ON} + \text{norm Peak OFF}}$$

Nonresponsive neurons were identified and moved to the bottom of these plots. Nonresponsive neuron criterion was similar to that used before [45] with only exception that here the entire time window involving both the ON and the OFF responses was taken into consideration.

Angle between the mean ON and OFF projection neuron responses: High dimensional PN response vectors were generated using all recorded neurons. The mean baseline response during a 2 s pre-stimulus period, immediately preceding stimulus onset, was subtracted from all response vectors. The high-dimensional response vectors were averaged over the entire duration of the odor pulse (4 s) to generate the mean ON response template (W_{ON}). Similarly, the high-dimensional vectors were averaged for a 4 s period following the odor pulse termination to generate the mean OFF response template (W_{OFF}). The angle between the mean ON and OFF responses were computed as follows:

$$\text{angular distance} = \cos^{-1}\left(\frac{\mathbf{W_{ON}} \cdot \mathbf{W_{OFF}}}{|\mathbf{W_{ON}}||\mathbf{W_{OFF}}|}\right) \quad (2.1)$$

Different analysis windows (2s and 4 s) were used to ensure that the orthogonal relationship between these two response templates were insensitive with respect to the time bin size (**Fig. 3.1f**).

For **Fig. 3.6d** and **Fig. 3.8e,f**, the comparisons (cosine of the angle obtained from equation (1)) were made either between mean ensemble activities (2s window) during different epochs of a single stimulus (ON vs. OFF), or between the ON and OFF responses evoked by two different stimuli.

Information rate estimation: We estimated the information content carried by the neural spike trains during ON and OFF response windows by computing the mutual information rate between odor stimulus and the neural response[87]. We used the "direct method" approach by finding the difference between the total and conditional entropy rates of the responses.

$$I(S;R) = H_{total} - H_{noise} \tag{2.2}$$

The total entropy rate (H_{total}) was estimated using PN responses to 5 unique stimuli, and the conditional entropy rate (H_{noise}) was obtained from 25 repeated presentations of the same odorant. The unique stimuli used were hexanol 1%, 2-octanol 1%, hexanol 0.1%, 2-octanol 0.1% and the binary mixture of hexanol 1% and 2-octanol 1%.

Cluster analysis for PN responses: For clustering PN responses, we first binned each PN spiking response in 50 ms non-overlapping time bins (smoothed with a five-point average moving average filter). The PN responses over an 8 s period starting at the odor onset (160-dimensional vector) were then trial-averaged. All PNs with a statistically significant response (excitatory or inhibitory) were used for this cluster analysis. Responses recorded for the following four odorants were analyzed: hex, 2oct, iaa, and bzald (at 1% concentration v/v). PN responses were clustered such that the furthest pairwise distance between any two samples assigned to an individual cluster was minimized. A correlation metric was used as a measure of similarity:

$$Corr = \frac{\sum_{i=1}^{160}(x_i - \bar{x})(y_i - \bar{y})}{\sigma_x \sigma_y} \quad (2.3)$$

Where x_i and y_i are ith vector elements of two different PN response vectors, $\bar{x}$ and $\bar{y}$ denote the mean firing rate for each PN over the entire 8 s window, and σ_x, σ_y represent their standard deviations. The optimum number of clusters required to represent the entire dataset was chosen based on the mean-squared error (**Fig. 3.2a–c**). Peak latency was calculated for the ON and OFF responses by finding the time bin with maximum firing rate after baseline subtraction (**Fig. 3.2d**).

Confusion matrix calculation: To quantify variability across stimulus histories, we performed a classification analysis with a leave-one-trial-out cross validation (using the 85-dimensional PN responses). The test trial to be classified was assigned the same class label as the nearest cluster centroid (calculated using training samples that included hex or ger responses for different stimulus histories).

PN response characterization: For analysis in this work, we classified projection neurons as ON-responsive if the spike counts in any time bin during the stimulus presentation exceeded mean + 6.5 s.d. of pre-stimulus activity (2 s window just before onset of any stimulus). Similarly, a PN was regarded OFF-responsive if it met the same criterion in a 4 s window after the termination of the stimulus (0.5 s to 4.5 s after stimulus termination. Note that a 500 ms window immediately after the termination of the odorant pulse was ignored as it confounded both ON and OFF responses. All PNs that did not meet either of these criteria set for ON or OFF responders were regarded as ‘non-responders'.

Response latency for PNs: We defined PN response latency as the first 50 ms time bin when the criterion for the responsive neuron was met (i.e. spike counts exceed mean + 6.5 s.d. of pre-stimulus activity). For sequential presentations, the response latency was determined as the first time bin after the derivative of PSTH became positive.

Support vector machine (SVM): The PN response patterns to solitary introductions of hex, 2oct, iaa, bzald, cit, and app were used as training samples. We regarded this as a binary classification problem, where hex responses were considered as one class, and all other responses were regarded as the second class.

The separating hyperplane was found using an SVM classifier that maximizes the functional margin between the hyperplane and the classes[86].

$$\gamma_i = y_i(v_{svm}^T x_i + b) \tag{2.4}$$

Where γ_i is the functional margin for the data point x_i [85-dimensional PN spike counts in a 50 ms time bin], and y_i is the true class label for the data point [1 for hex-ON and -1 for the rest]. The weight vector v_{svm} (also 85 dimensional; i.e. 85 free parameters to tune the model) plus the bias term b (86th model parameter), was calculated by solving the following optimization problem:

$$min_{\gamma, v_{svm}, b} \ \frac{1}{2}||v_{svm}||^2 + C\sum_{i=1}^{m} \mu_i \tag{2.5}$$

$$\text{s.t. } y_i(v_{svm}^T x_i + b) \geq 1 - \mu_i \ i = 1, \ldots, m,$$

$$\mu_i \geq 0, i = 1, \ldots, m$$

where m is the total number of data points in both the classes and μ_i is the slack variable that help us avoid overfitting while solving this optimization problem. This was done using fitcsvm in MATLAB by taking the box constraint to be 0.01. After determining the optimal weight vector v_{svm}, we classified response patterns generated during sequential stimulus presentations as follows:

$$h(x(t)) = sign(v_{svm}^{T} x(t) + b) \tag{2.6}$$

where *x(t)* is the 85-dimensional PN spike counts in a 50 ms time bin, the sign function results in '1' when the input is classified as 'hexanol present' and '0' corresponded to 'hexanol absent.'

Template matching (multi-class classification): A bin-by-bin, trial-by-trial classification analysis[45, 46] was used to determine the pattern-match between PN responses observed in a particular time bin with the ON and OFF response templates of a particular odorant. Note that the ON and OFF templates were generated using solitary hexanol or benzaldehyde exposures using spike counts in the 2 s time windows immediately following stimulus onset and offset, respectively.

An angular distance metric was used to determine the nearest reference template. Each time bin in a test trial was classified as belonging to one of the following response categories: hexanol ON, hexanol OFF, benzaldehyde ON, benzaldehyde OFF, or as an unclassified response (**Figs. 3.5, 3.8, 3.9**). Those time bins that were not within a certain angular distance threshold (within 63° of the nearest reference template) were categorized as unclassifiable responses. This threshold was chosen such that less than 10% of the ensemble neural activities in the pre-stimulus period were misclassified as being similar to the hexanol or benzaldehyde response templates.

ON minus OFF classifier: PN responses to 4 s long solitary presentations of target stimulus (hex or iaa; **Fig. 5.3**) were used to determine ON responders and OFF responders (using the same criteria discussed in PN response characterization above). For the ON classifier, a binary weight vector was obtained by assigning all ON responsive PNs a weight on '1' and assigning all other PNs a weight of '0.' . PN responses were then linearly combined at each time bin by computing a dot product with the binary vector constructed. The summed activity was then compared to a threshold to classify 'target present' or 'target absent'. Note that the threshold is a free parameter and needs to be determined to minimize false-positives during pre-stimulus period, while maximizing the true-positives during the stimulus. During testing, all the ten trials were used to quantify performance and the trial-averaged classification probabilities were computed as a function of time (shown in **Figure 5.4**).

For the OFF classifier, the same strategy was used to obtain trial-averaged classification using a binary weight vector that assigned only the OFF responsive neurons a weight of '1' (**Fig. 5.4**).

Finally, the difference of the two classifier's output, i.e ON classifier output – OFF classifier output was computed for each timebin and passed through the rectifier (i.e. max(0, x)) and shown as the final result of 'ON-minus-OFF' classification approach.

Granger causality test: We examined whether the results obtained from our classification analysis (physiological data) were Granger causal with the behavioral PORs for the hex-0.5s overlap-bzald stimulus sequence (**Fig. 3.8d,e**). For this time series analysis, we first combined the pattern match probabilities with ON and OFF response templates of hexanol (conditioned stimulus) as follows:

$$\alpha_{ON-OFF}(t) = \alpha_{ON}(t) - \alpha_{OFF}(t) \tag{2.7}$$

We used α_{ON-OFF} as one time series vector and the behavioral POR as the second. In order to have the same sample size for the behavioral POR and the classification template match probability vector, we generated classification results with 200 ms temporal resolution. The significance level was set to 5% and the maximum lag between the two time series was set to 10 samples (i.e. 2 s).

Justification of statistical tests: All statistical significance tests done in the manuscript were two-sided. Bonferroni-corrected *P* values were used in case of multiple comparisons. No statistical methods were used to predetermine sample sizes, but our sample sizes are similar to those reported in previous publications in the field.

For the paired t-tests, normality of the dataset was confirmed using the Jarque-Bera test. The equal variance assumption was tested using the Levene's test. The confidence level was set to 0.05. Wilcoxon signed-rank test is a non-parametric test for comparing the population median responses of matched samples. This test was used to detect when a significant decrease in palp-closing responses occurred.

For the two sample Kolmogorov-Smirnov test, we used a significance level of 5% to check if the two vectors are from the same distribution.

2.4 Modeling

2.4.1 Computational modeling of the locust antennal lobe: orthogonal ON and OFF responses

Odor representation in the antenna was modeled with a repertoire of 50 ORNs. A subset of ORNs was activated by the stimulus as shown in **(Fig. 3.7)**. Note that the sensory neuron response time constants for the rise, adaptation and fall were heterogeneous as found *in vivo*.

Next, the modeled sensory neuron responses (ORN responses) were input to a realistic computational model of the antennal lobe circuits with 50 excitatory projection neurons (PNs) and 25 inhibitory local neurons (LNs). Each PN was modeled as a regular spiking neuron and inhibitory local neuron as a fast-spiking neuron using a reduced Hodgkin-Huxley model[88].

$$\frac{dv}{dt} = 0.04v^2 + 5v + 140 - u + \left(I(t) - v_{thresh}{}^3 \times v_{memory}\right) \quad \text{(fast variable)}$$

$$\frac{du}{dt} = a(bv - u) \quad \text{(slow variable)} \qquad (2.8)$$

if v = 30 mV then v←c, u← u+d

PN model parameters: a = 0.02, b = 0.2, c = -65, d = 8.

LN model parameters: a = 0.1, b = 0.2, c = -65, d = 2.

I is the total input to the each neuron from both sensory neurons as well as summed contributions of other antennal lobe neurons. Note that the adaptive parameters (v_{thresh} and v_{memory}) were limited to PNs only. The update rule for these two parameters is as follows:

$$\frac{dv_{thresh}}{dt} = inc \times \delta(t - t_s) - \frac{(4 + v_{thresh}(t))}{\tau_{thresh}} \qquad (2.9)$$

where inc = 0.3 and τ_{thresh} = 2500 ms for all PNs, t_s is the time when the neuron last fired an action potential, and $\delta(t - t_s)$ is the Dirac delta function. Integration time step is 1 ms.

$$v_{memory}(t) = max\left\{\begin{matrix}0,\\ 2\times\left[\frac{1-exp^{-0.1\times\int_{-\infty}^{t}h(t-s)v(s)ds}}{1+exp^{-0.1\times\int_{-\infty}^{t}h(t-s)v(s)ds}}\right]\end{matrix}\right. \quad (2.10)$$

where *v(t)* is the membrane potential of the neuron at time *t* and h is a one-sided Gaussian kernel with standard deviation uniformly distributed in the range [120 ms, 320 ms].

Model Connectivity: We modeled each PN to receive input from a single sensory neuron. LNs received input from nearly two-thirds of all sensory neurons. Further, since each LNs arborized extensively throughout the antennal lobe [22], each local neuron received excitatory input from roughly 30% of PNs, and provided feedback inhibition to ~30% of non-identical combination of PNs. Note that there were no excitatory lateral interactions between PNs or self-inhibition in the model. These connection probabilities and other network parameters including the type of synaptic currents were constrained based on estimates from locust antennal lobe circuits [22, 58, 89].

The post-synaptic current generated by a pre-synaptic neuron *i* following a spike at time *t* was defined as follows:

$$\frac{dg(i,t)}{dt} = \frac{-g(i,t)}{\tau_{syn}} + z(i,t)$$

$$\frac{dz(i,t)}{dt} = \frac{-z(i,t)}{\tau_{syn}} + g_{norm}\cdot spk(i,t) \quad (2.11)$$

where *z(.)* and *g(.)* are low pass filters of the form $exp(-t/\tau_{syn})$ and $t \times exp(-t/\tau_{syn})$, respectively, τ_{syn} is the synaptic time constant, g_{norm} is the peak synaptic conductance (a constant), and *spk(i,t)* marks the occurrence of a spike in neuron *i* at time *t*. Synaptic parameters used were the following: peak synaptic conductance (excitatory synapse) = 0.1 nS, excitatory synapse response

time constant = 5 ms, peak synaptic conductance (inhibitory synapse) = 0.3 nS, inhibitory synapse response time constant = 6 ms.

Therefore, the total synaptic current received by neuron *k* from all other neurons in the network is given by:

$$I_{syn}(k,t) = \sum_{\forall i \neq k} C_{ik} \cdot g(i,t) \tag{2.12}$$

where C is the recurrent connectivity matrix.

The total input to the neuron *k* taking into account both sensory input and synaptic inputs received through recurrent connections can be written as follows:

$$I(k,t) = W * ORN(t) + I_{syn}(k,t) \tag{2.13}$$

where *W* is the input connection linking ORNs with PNs and LNs, *ORN(t)* is the input vector representing the sensory neuron activity at time *t*.

LFP and sliding-window cross-correlograms: The LFP in the model was computed as the sum of PN membrane potential fluctuations (filtered between 5 and 55 Hz). The pairwise cross-correlations were obtained by averaging LN membrane potential fluctuations in 500 ms time windows (98% overlap between consecutive time segments) and comparing them with LFP during the matching time segment.

Bifurcation analysis: The inhibition was regularized by multiplying a scaling constant (between 0 and 1) to the synaptic weights from LNs to PNs, and the bi-directional adaptation was regularized by multiplying a scaling constant (between 0 and 1) to the update step Δv_{thresh}. For every combination of the inhibition and the bi-directional adaptation, we calculated the total LFP

power in the 5 to 55 Hz frequency range, and the angle between the ensemble ON and OFF responses. The angle between ON and OFF responses was obtained by first binning the data into 50 ms time bins and calculating the response similarity between mean ON response vector and the mean OFF response vector (**Fig. 3.7e**).

2.4.2 Computational modeling of the locust antennal lobe: two LN subtypes facilitate a switch in PN ensembles with intensity

We designed a similar model as shown in the previous section with the following changes (**Fig. 6.5**):

First, the antenna was modeled with 80 ORNs, modeled similarly as shown in the previous section. Next, the modeled ORN responses were input to a computational model with 80 PNs and 30 LNs. PNs and LNs were also modeled similarly as regular spiking neurons and fast spiking neurons respectively. $I(t)$ has not been modified like before.

$$\frac{dv}{dt} = 0.04v^2 + 5v + 140 - u + I(t) \qquad \text{(fast variable)}$$

$$\frac{du}{dt} = a(bv - u) \qquad \text{(slow variable)} \qquad (2.14)$$

if v = 30 mV then v←c, u← u+d

PN model parameters: *a* = 0.02, *b* = 0.21, *c* = -65, *d* = 2.

LN model parameters: *a* = 0.1, *b* = 0.2, *c* = -65, *d* = 2.

Model Connectivity: Both PNs and LNs were divided into two subpopulations (PNs1, PNs2 and LNs1, LNs2). Each local neuron from LNs1 subpopulation received from roughly 30% of PNs,

and provided feedback inhibition to ~10% of PNs in subpopulation PNs2. Similarly, each local neuron from LNs2 subpopulation received from roughly 50% of PNs, and provided feedback inhibition to ~30% of PNs in subpopulation PNs2. peak synaptic conductance (excitatory synapse) for PNs was also changed to 0.2 nS.

2.4.3 Behavioral prediction models

To predict behavioral responses from ensemble neural response data, we used four simple models.

ON model: The ensemble neural activity in a particular time bin *x(t)* became the input to the model. The probability of pattern-match between *x(t)* with the hexanol ON response template was computed as in the classification analysis (red curves from **Fig. 3.5c**). The pattern-match probabilities were thresholded and adjusted for gain to predict behavioral response adjustment *Δy(t)*. The current behavioral response was just a simple linear sum of the behavioral response in the previous time bin *y(t-1)* and the predicted adjustment for the current time bin *Δy(t)*. The entire model can be summarized using the following set of equations:

$$\Delta y_{Open}(t) = \varphi(\alpha_{ON}(t)) \times g_1,\ \varphi(\cdot) = \begin{cases} 1 & \alpha_{ON}(t) \geq thresh_{ON} \\ 0 & \alpha_{ON}(t) < thresh_{ON} \end{cases}$$

$$\Delta y_{close}(t) = Not(\alpha_{ON}(t)) \times g_2 \times y(t-1), \quad Not(\cdot) = \begin{cases} 1 & \alpha_{ON}(t) = 0 \\ 0 & \alpha_{ON}(t) > 0 \end{cases} \tag{2.15}$$

$$\Delta y(t) = \Delta y_{Open}(t) + \Delta y_{close}(t)$$

where $\alpha_{ON}(t)$ is the probability of pattern-match of the average ensemble activity in a given time bin *(x(t))* with the hexanol ON template (same as shown in **Fig. 3.5c**; red curves), $\varphi(\cdot)$ indicates the nonlinear thresholding function, and g_1 = 1 indicates the gain. $Not(\cdot)$ is the NOT gate function, $thresh_{ON}$ = 0.6, g_2 = -0.05 is another gain, and *y(t-1)* is the behavior output at the previous time point.

ON-OFF model: In this model, palp-opening response was solely determined based on the degree of pattern-match with the hexanol ON template (**Fig. 3.5c;** red trace), and the palp-closing was solely determined based on the degree of pattern-match with the hexanol OFF-template (**Fig. 3.5c**; blue trace). This can be summarized as follows:

$$\Delta y_{Open}(t) = \varphi_{ON}(\alpha_{ON}(t)) \times g_{ON}, \qquad \varphi_{ON}(\cdot) = \begin{cases} 1 & \alpha_{ON}(t) \geq thresh_{ON} \\ 0 & \alpha_{ON}(t) < thresh_{ON} \end{cases}$$

$$\Delta y_{close}(t) = \varphi_{OFF}(\alpha_{OFF}(t)) \times g_{OFF}, \ \varphi_{OFF}(\cdot) = \begin{cases} 1 & \alpha_{OFF}(t) > thresh_{OFF} \\ 0 & \alpha_{OFF}(t) = thresh_{OFF} \end{cases} \qquad (2.16)$$

where $\alpha_{OFF}(t)$ is the probability of pattern-match of the average ensemble activity in a given time bin *(x(t))* with the hexanol OFF template, $thresh_{ON}$ = 0.6, $thresh_{OFF}$ = 0, g_{ON} = 1 and g_{OFF} = -0.7. All other variables and constants are the same as in equation (10).

Additionally**,** we recorded and used a new set of neural and behavioral data (neural *dataset4*: hex and bzald). The ON-OFF model parameters in this case were obtained by fitting the predictions to the POR evoked by 6s hexanol puff ($thresh_{ON}$ = 0.36 and g_{OFF} = -0.55).

Active ON model: In this model, a pattern-match with ON template drives both opening and closing of the palps. The model can be summarized using the equation below.

$$\Delta y_{Open}(t) = \varphi(\alpha_{ON}(t)) \times g,\ \varphi(\cdot) = \begin{cases} 1, & \alpha_{ON}(t) \geq 0.6 \\ -1, & \alpha_{ON}(t) < 0.1 \\ 0, & otherwise \end{cases} \quad (2.17)$$

Similarly to the equation (10), $\varphi(\cdot)$ indicates the nonlinear thresholding function, and g indicates the gain. Note that g was assigned two different values depending on whether palp was opening or closing, i.e. if $\varphi(\cdot)$=1 then g = 1.0, alternately if $\varphi(\cdot)$= -1 then g = 300.

Passive ON-OFF model: In this model, a pattern-match with the ON template is sufficient to initiate and sustain the POR responses. However, the mismatch with both ON and OFF response templates triggered the palps to close. The following equations summarize the model:

$$\Delta y_{open}(t) = \varphi(\alpha_{ON}(t)) \times g_1 \quad \varphi(\cdot) = \begin{cases} 1 & \alpha_{ON}(t) \geq 0.6, \\ 0 & otherwise \end{cases}$$

$$\Delta y_{close}(t) = Not\big(\alpha_{ON}(t), \alpha_{OFF}(t)\big) \times g_2 \times y(t-1),$$

$$Not(\cdot) = \begin{cases} 1 & \alpha_{ON}(t) = 0,\ \alpha_{OFF}(t) = 0 \\ 0 & otherwise \end{cases} \quad (2.18)$$

Here, g_1= 1, $\alpha_{ON}(t)$ and $\alpha_{OFF}(t)$ are the probabilities of pattern-match with the ON and the OFF template, respectively, g_2= -0.05, and $y(t-1)$ is the POR at the previous time point.

We fit the models and selected their parameters using the behavioral data observed for hexanol 4 s exposures. The models were tested based on their predictions to behavioral responses to hexanol pulses of other durations and to the overlapping presentation of hex-bzald). Since the models were designed primarily to predict the palp opening and closing dynamics, we rescaled the amplitude of the predicted responses to fit the experimentally observed peak PORs values for each condition. Also, to match the sampling rate of the behavioral data (25 frames per second)

and classification probabilities (50 ms time bins), both neural pattern-match and PORs were re-binned using 200 ms time bins.

To quantitatively compare the performance of different models, we computed the mean squared errors (MSE) between predicted and actual rise time and fall time constants for palp-opening and palp-closing responses **(Fig. 3.8)**. Rise time was defined as the time taken for the median palp-opening response to reach 50% of the peak palp separation distance from odor onset. Similarly, fall time was defined as the time taken for the palp closing responses to reduce to 50% of the palp separation distance after the conditioned stimulus was terminated. The MSE of prediction was computed as follows:

$$\mathrm{MSE} = \frac{1}{4}\sum_{i=1}^{4}(Y_i - X_i)^2 \tag{2.19}$$

Where **Y** represents the set of values predicted by the model and **X** is the measured POR responses. Responses to three different durations of hexanol presentation and to the hexanol-benzaldehyde odor sequence were used for computing MSE.

Chapter 3: Engaging and disengaging recurrent inhibition coincides with sensing and unsensing of a sensory stimulus

3.1 Introduction

Sensory systems can rapidly signal the presence of a visual [90, 91], auditory [92-94], or an olfactory [46, 95, 96] cue encountered by an animal. In addition to being rapid, the stimulus-evoked neural responses are usually elaborate, temporally patterned and tend to outlast the duration of the triggering stimulus[97]. The need for such dynamical neural responses is puzzling, especially considering that the behavioral response initiations can be equally fast, and delayed only by few hundreds of milliseconds after stimulus onset[95]. Further, another bout of strong spiking activities usually occurs after the termination of the stimulus and the behavioral relevance of this 'OFF response' also is not understood. This apparent mismatch between the complexity in the neural encoding and the behavioral decoding raises the following fundamental question: how do neural response dynamics regulate the behavioral responses over time?

A comparison of electrophysiological results reported across sensory systems of different modalities, reveal that there are striking similarities between stimulus-evoked temporally patterned neural responses [44, 97-100]. For example, in the olfactory system, sensory input from olfactory receptor neurons (ORNs) drive spatiotemporal patterns of neural activity in the downstream neural circuits (invertebrate antennal lobe or vertebrate olfactory bulb) that are quite dynamic and information rich at the stimulus onsets and offsets [8, 44, 45, 48, 97]. In between

these transient response epochs, when chemical cues are sustained, the ensemble neural activities in the peripheral and central regions tend to settle down to stable spiking activity patterns, and are often referred to as steady-state responses [97].

In this work, we investigated these questions using an invertebrate olfactory system. We show that the same sensory circuit can use nearly non-overlapping sets of neurons, and different encoding formats (oscillatory vs. non-oscillatory) to represent equivalent information about the identity and intensity of sensory stimulus during different response epochs (at onsets and offsets). Further, our results reveal that switching between distinct neural ensembles over time is important for shaping the behavioral dynamics evoked by a stimulus. Notably, our results reveal that such representations allow sensory neural networks to meet the evolving demands on the behavioral output during these epochs.

3.2 Results

3.2.1 Odor-evoked ON vs. OFF responses

We began by examining stimulus-evoked responses of projection neurons (PNs) in the locust antennal lobe (AL) circuit that receive direct sensory input from the olfactory receptor neurons. We used lengthy pulses of odorants (4 s in duration) in order to decouple and examine the neural responses elicited following the stimulus onset and offset. The stimulus-evoked PN responses could be categorized into two major classes[101, 102] (**Fig. 3.1a**; also refer **Fig. 3.2a–c**): increase in spiking activity limited to the periods of odor presentation (ON response), or excitatory responses that occur only in epochs following stimulus termination (OFF response).

Consistent with previous findings [47, 48], we note that within each PN response category the temporal spiking patterns were heterogeneous.

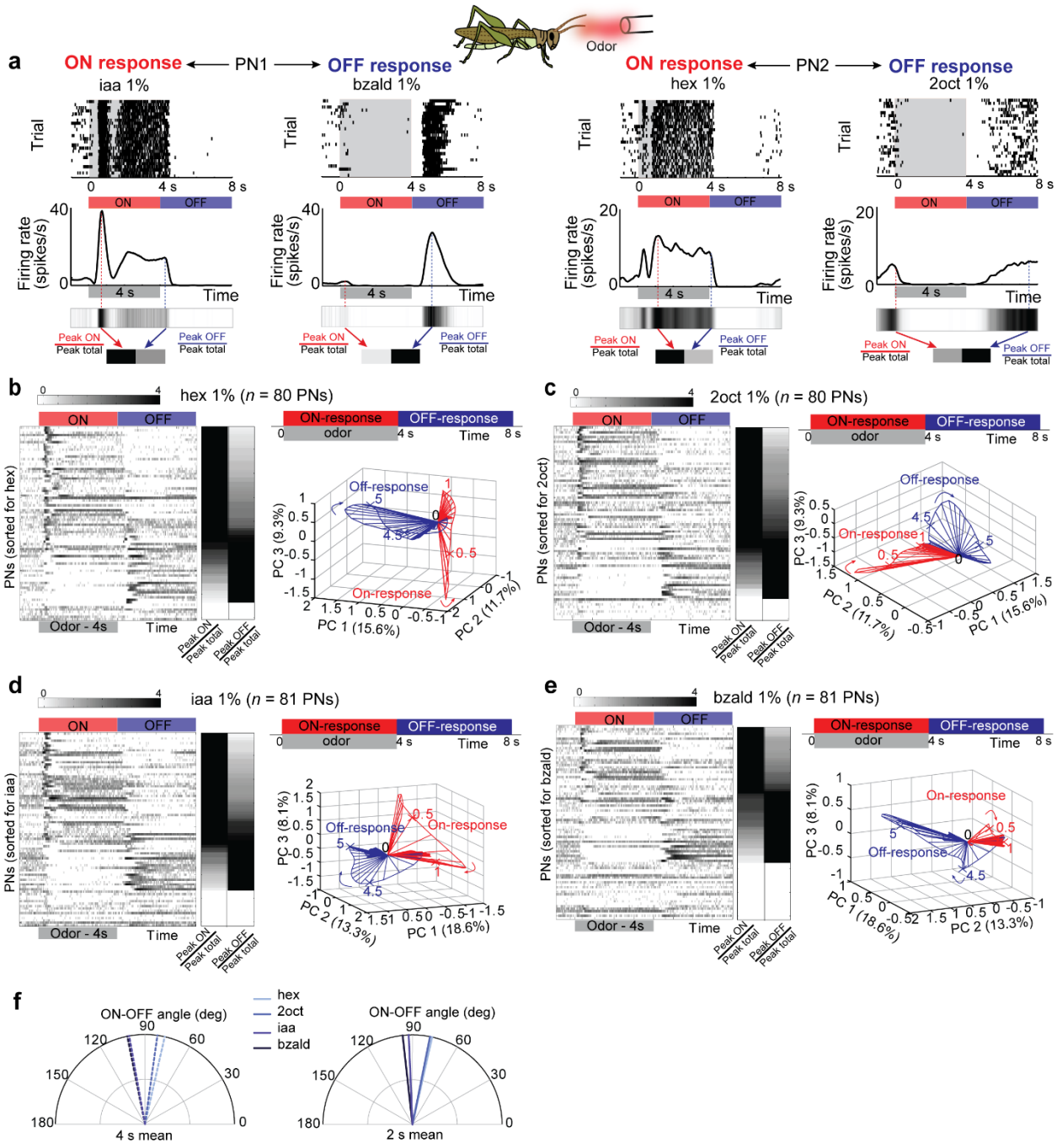

Figure 3.1: Odor-evoked ON vs. OFF neural responses are flexible orthogonal set. (a) Spiking activities of two different olfactory projection neurons (PNs; in the insect antennal lobe) to two odorants

are shown as raster plots. Each row corresponds to a single trial, which includes a 1 s pre-stimulus period, 4 s stimulus exposure (shaded gray region), and a 4 s post-stimulus period. Twenty-five consecutive trials are shown for each PN. Firing rates in non-overlapping 50 ms time bins (with 5 point smoothing) are shown below the raster plot for each PN. Note there are two prominent PN response categories. (i) ON responses: increase in spiking activity that is limited to the period of stimulus exposure (PN1–iaa 1% and PN2–hex 1%), (ii) OFF responses: spiking activity is suppressed during odor presentation period but raises above pre-stimulus levels after odor termination (PN1–bzald 1% and PN2–2oct 1%). Also, note that the same PN can have either ON or OFF response depending on odor identity. The normalized firing rate is shown as a colorbar below each firing rate curve. The peak responses during stimulus exposure (during ON response window) and following its termination (during OFF response window) are identified. 'Peak total' indicates the maximum response taking into account both epochs. **(b)** *Left*, Mean PN firing rates (50 ms time bins; averaged across 25 trials) are shown for hexanol (hex) delivered at 1% dilution (v/v). Each row in the image reveals the mean firing rate activity of one PN during a one second pre-stimulus period, 4s odor presentation period (marked by the red bar on top, stimulus ON) and a 4 s post-stimulus period (indicated by the blue bar on top, stimulus OFF). All recorded PNs are shown. The firing rates are shown on a log scale to allow comparison between neurons. The PNs are ordered based on the difference between the peak firing activities observed during the ON and the OFF response epochs. Neurons that are either non-responsive or with a statistically insignificant response are padded at the bottom. The normalized peak firing rates during the ON and OFF response periods are shown to the right of the panel. Note that darker color indicates higher firing rate and the lighter color indicates lower firing rate. Non-responsive neurons are shown in white. *Right*, Olfactory PN spiking activities pooled across locusts are visualized after dimensionality reduction using linear principal component analysis (PCA; see Methods). Each axis corresponds to one of the three principal directions that best capture the variance in the dataset. The PN responses used for this analysis are same as shown in the left panel. The percentage of variance captured along each principal component is identified along each axis. The trajectory traced by the ensemble neural activities during the 4 s of stimulus exposure ('ON response') is plotted in red. To provide contrast, the 4 s of neural activities following stimulus termination ('OFF response') is plotted in blue. Numbers near response trajectories indicate time in seconds since odor onset, and the arrows indicate the direction of evolution over time. **(c – e)** Similar plots as in **panel b** for three other odorants: 2-octanol (2oct), isoamyl acetate (iaa) and benzaldehyde (bzald). All odorants are at their 1% dilutions (v/v in mineral oil). **(f)** Angular distances between the mean ON and OFF responses of olfactory PNs (high-dimensional vectors of PN spike counts) are shown for all four odorants using two different time windows (4 s and 2 s).

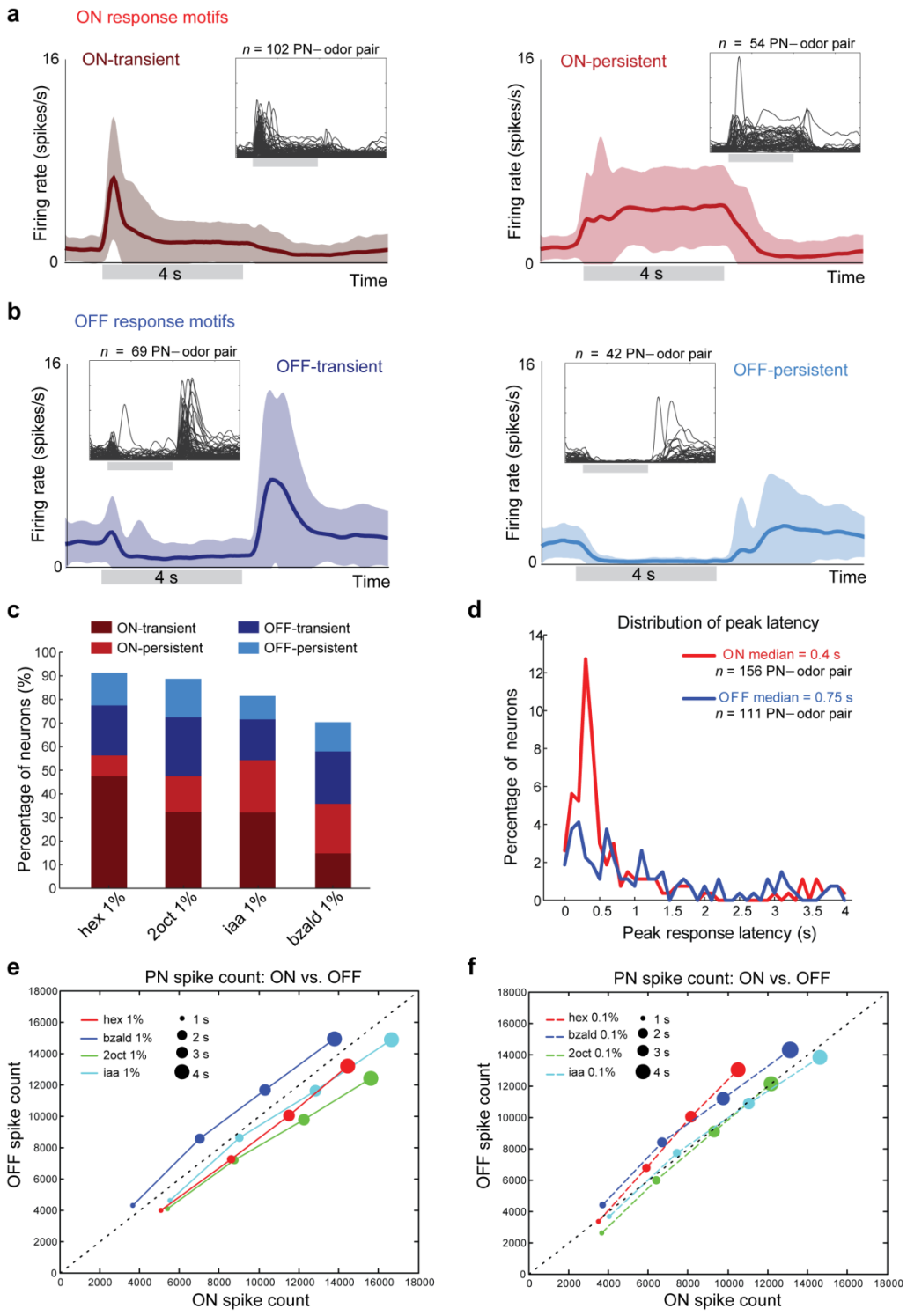

Figure 3.2: ON vs. OFF response features. (a,b) Results from an unsupervised clustering analysis of projection neuron responses are summarized and shown here (see Methods for details). Two predominant response types (ON vs. OFF responses) were identified with two major sub-types for each case. Mean firing rates (± s.d.) averaged across projection neurons are shown as a function of time for each response cluster. Insets show all individual PN responses assigned to a cluster. *n* indicates number of PN responses

assigned to a cluster. **(c)** Percentages of neurons with a particular response motif: ON transient, ON persistent, OFF transient, OFF persistent are shown for four odorants: hex 1%, 2oct 1%, iaa 1%, bzald 1%. **(d)** The time-to-peak-response distributions for ON and OFF PNs are shown here (see Methods). **(e)** Total PN spike count (summed over all neurons recorded, n = 80 for hex and 2oct; n = 81 for bzald and iaa) during stimulus ON and stimulus OFF periods are shown for all four odorants used in the study (at 1% v/v). Comparison between ON and OFF spike counts are provided for the following integration window sizes: 1s, 2s, 3s, 4s (beginning from stimulus onset or stimulus offset). Parity between the ON and OFF responses is shown as a dotted line along the diagonal. **(f)** Similar plot as in **panel e** but shown for the lower concentrations (0.1% v/v) of the same four odorants.

ON and OFF responses have also been reported in both vertebrate and invertebrate visual systems [103-105]. However, a major difference between visual and olfactory ON and OFF responses is worth pointing out. In the visual system, whether a neuron responds with a light ON or light OFF type response is fixed and the 'cell tuning' does not change in a stimulus-dependent manner [104-106] On the other hand, in the antennal lobe circuit, we found that an individual PN can respond with either an ON or an OFF response depending on the odor identity and intensity (**Fig. 3.1a**). Additionally, a comparison of neural firing rates at different processing levels reveals that these OFF responses are weak to non-existent at the level of sensory neurons but become significant and comparable to the ON responses at the projection neuron level (**Fig. 3.3**). Therefore, we conclude that the PN response types are not cell-specific but arise as a result of stimulus-specific circuit interactions within the antennal lobe.

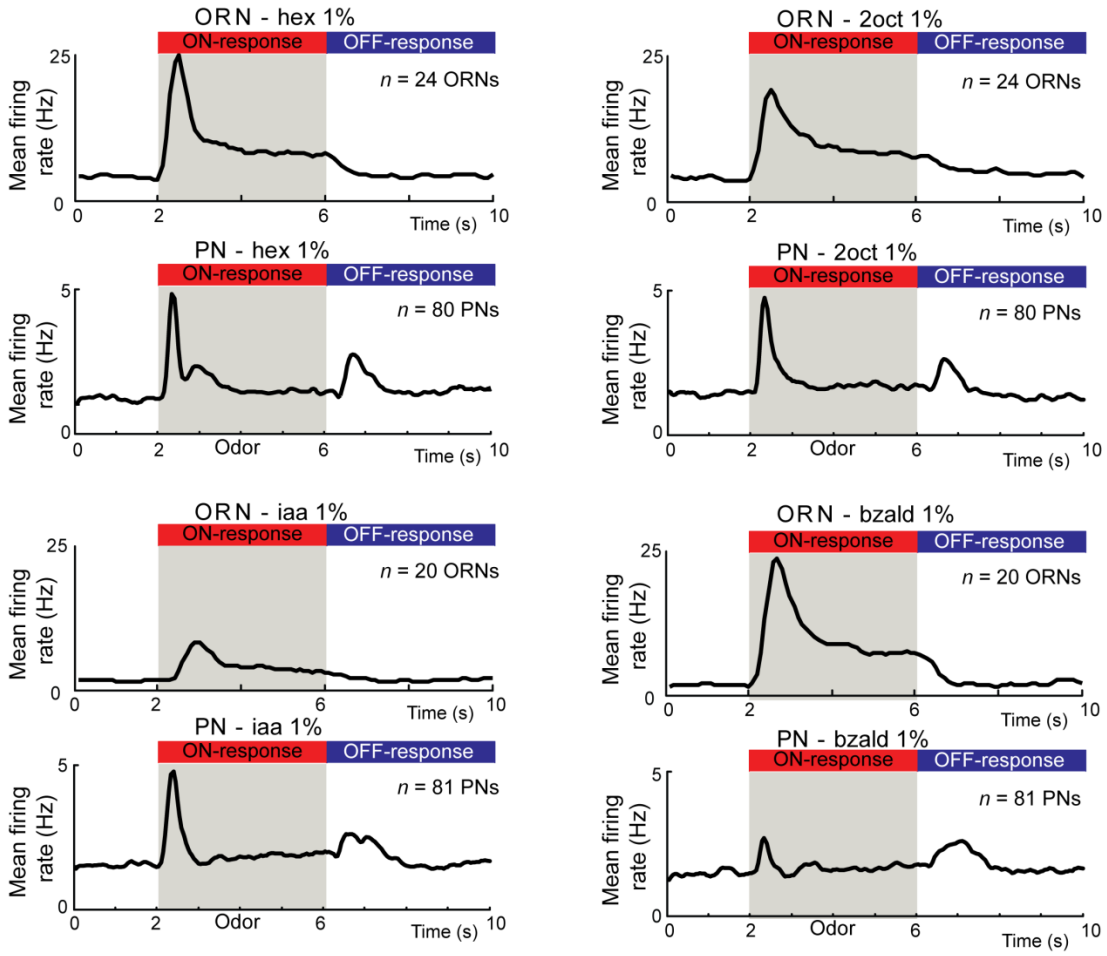

Figure 3.3: OFF responses are stronger in the antennal lobe. Odor-evoked mean ensemble firing rates for both ORNs and PNs to the four odors used in the study are shown. ORN mean firing rates are reproduced from [45]. *n* represents total number of neurons recorded for each odor. Gray box indicates 4 s long odor stimulation window. ON and OFF periods are identified with red and blue bars at the top of each plot.

We examined the relationship between the sets of PNs that were activated during stimulus ON and OFF periods (**Fig. 3.1b–e**). We found that in general, PNs that were activated during stimulus exposure period were inhibited following stimulus termination with the firing activity reaching below baseline levels (**Fig. 3.2a,c**). Similarly, the PNs that were activated following stimulus termination were inhibited during stimulus ON period (**Fig. 3.2b,c**). Therefore, at an ensemble level distinct sets of PNs were activated during odor ON and OFF

periods (**Fig. 3.1b–e**). In addition, we found that the OFF responses were more distributed over time rather than ON responses that had shorter response latencies (**Fig. 3.2d**). However, it is worth noting that both in terms of the total number of spikes (across all PNs), and distribution of information rate across neurons (**Fig. 3.2e,f** and **Fig. 3.4**), both ON and OFF responses were statistically indistinguishable (two-sample Kolmogorov-Smirnov test, $k = 0.1625$, $P < 0.05$).

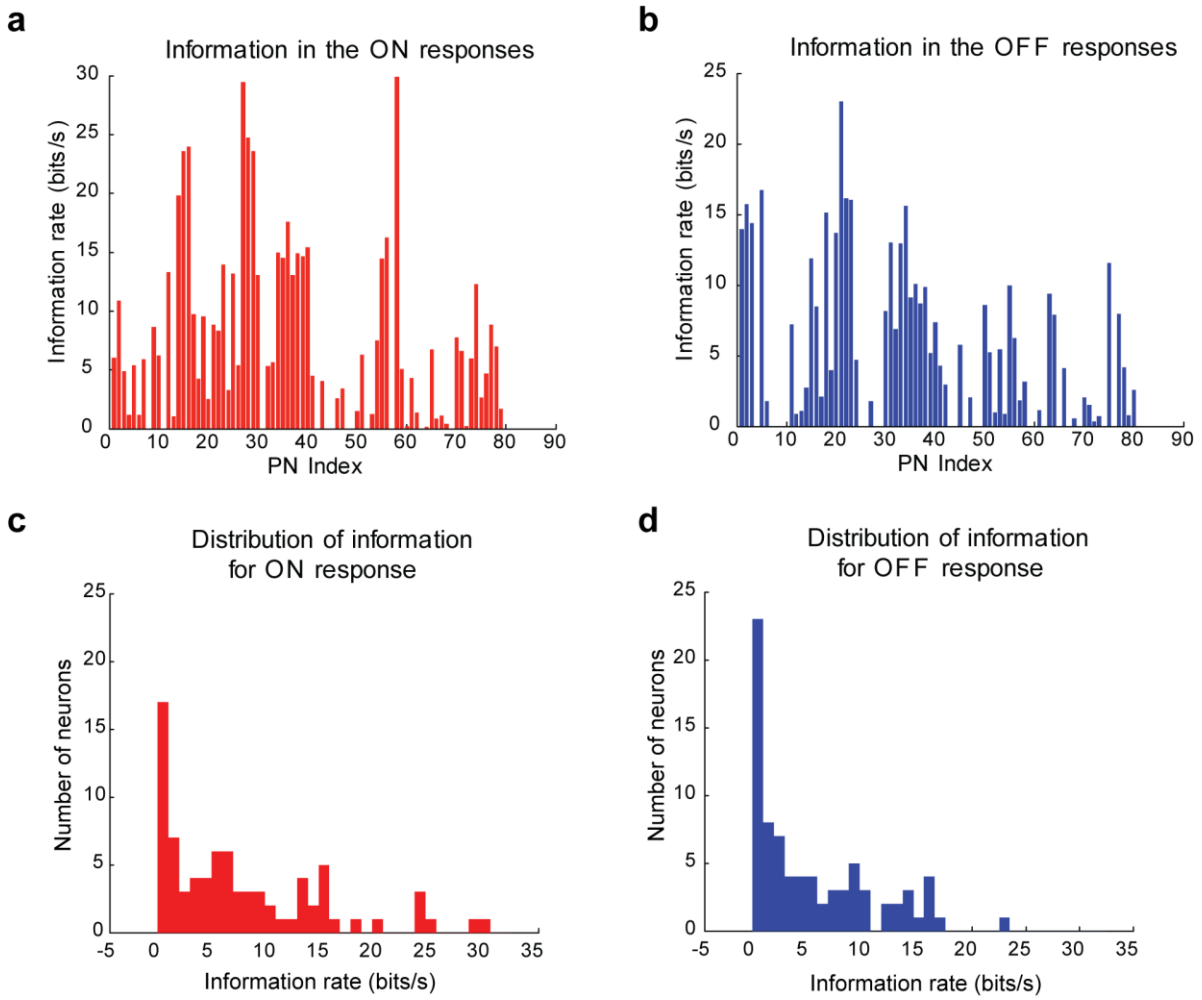

Figure 3.4: Information theoretic analysis of ON and OFF responses. (a) The estimated information rate for ON response is plotted for 80 neurons (hex-2oct odor pair). Responses of each neuron to five unique stimuli were used to estimate the total entropy (see Methods). The variations observed in the twenty five repeated trials of the same stimulus were used to estimate the noise entropy. **(b)** Estimated information rate for the OFF response is plotted for the same 80 neurons. **(c, d)** Histograms of ON and OFF information rate distributions are plotted, respectively.

Next, we visualized odor-evoked neural activities at an ensemble level by pooling neurons across experiments [45, 48, 97]. Responses were aligned and binned with respect to the odor onset. Subsequently, high dimensional response vectors were constructed where each vector element corresponded to the spike count of a single PN in a given time bin (see Methods). To visualize the ensemble neural activity, we performed dimensionality reduction with principal component analysis. We found that each odorant generated two distinct trajectories in the neural response space (**Fig. 3.1b–e**): one during stimulus presentation ('ON response' trajectory), and the other following stimulus termination ('OFF response' trajectory). Plots revealing how these trajectories evolve over time are highlighted in **Fig. 3.5a**. For all odorants examined, we found that the ON and the OFF response trajectories spanned sub-spaces that were nearly orthogonal to each other (i.e. ~90 degrees). These qualitative results were independently confirmed by computing angular distance between high-dimensional response vectors (**Fig. 3.1f**). The generality of these results is shown using a larger odorant panel in **Fig. 3.6a,b**.

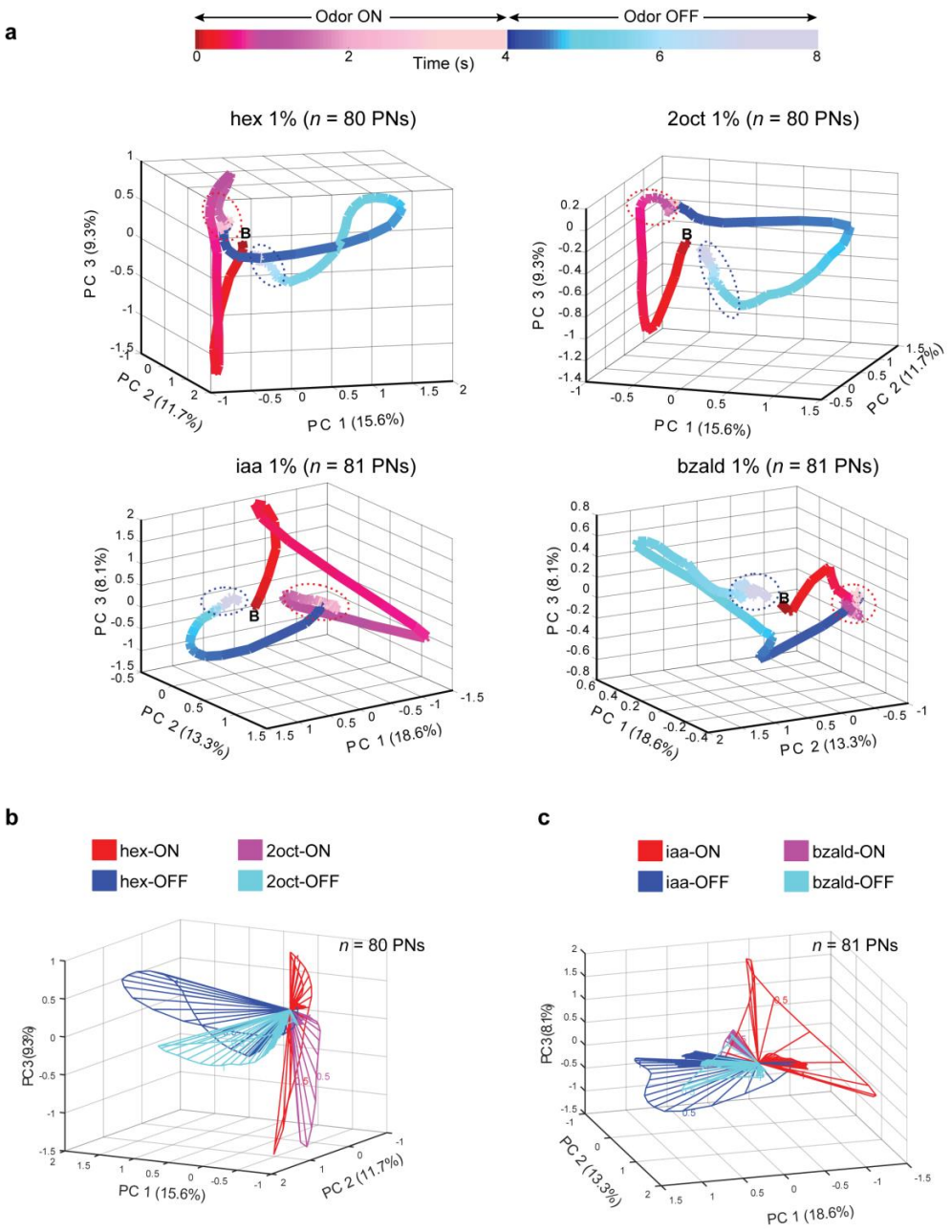

Figure 3.5: Temporal evolution of odor-evoked ON and OFF responses. (a) Ensemble projection neuron responses are visualized after the dimensionality reduction using principal component analysis. Each axis corresponds to one of the top three principal components that best captures the variance in the dataset. Percentages of variance captured are shown along each axis. The color bar shown on top reveals how time since odor onset is represented in these trajectory plots. "B" indicates the baseline or pre-stimulus activity. In all panels, steady-state ON responses and OFF responses are identified using red and blue dotted circles, respectively. PN response trajectories during the ON and OFF durations are plotted for the following four odorants: hex 1%, 2oct 1%, iaa 1% and bzald 1%. **(b)** Population response trajectories of PNs (n = 80) are plotted after the dimensionality reduction using PCA. Both ON and OFF

responses are shown for two odorants: hexanol and 2-octanol. Percentages of variance captured are shown along each axis. **(c)** ON and OFF response trajectories of isoamyl acetate and benzaldehyde are shown.

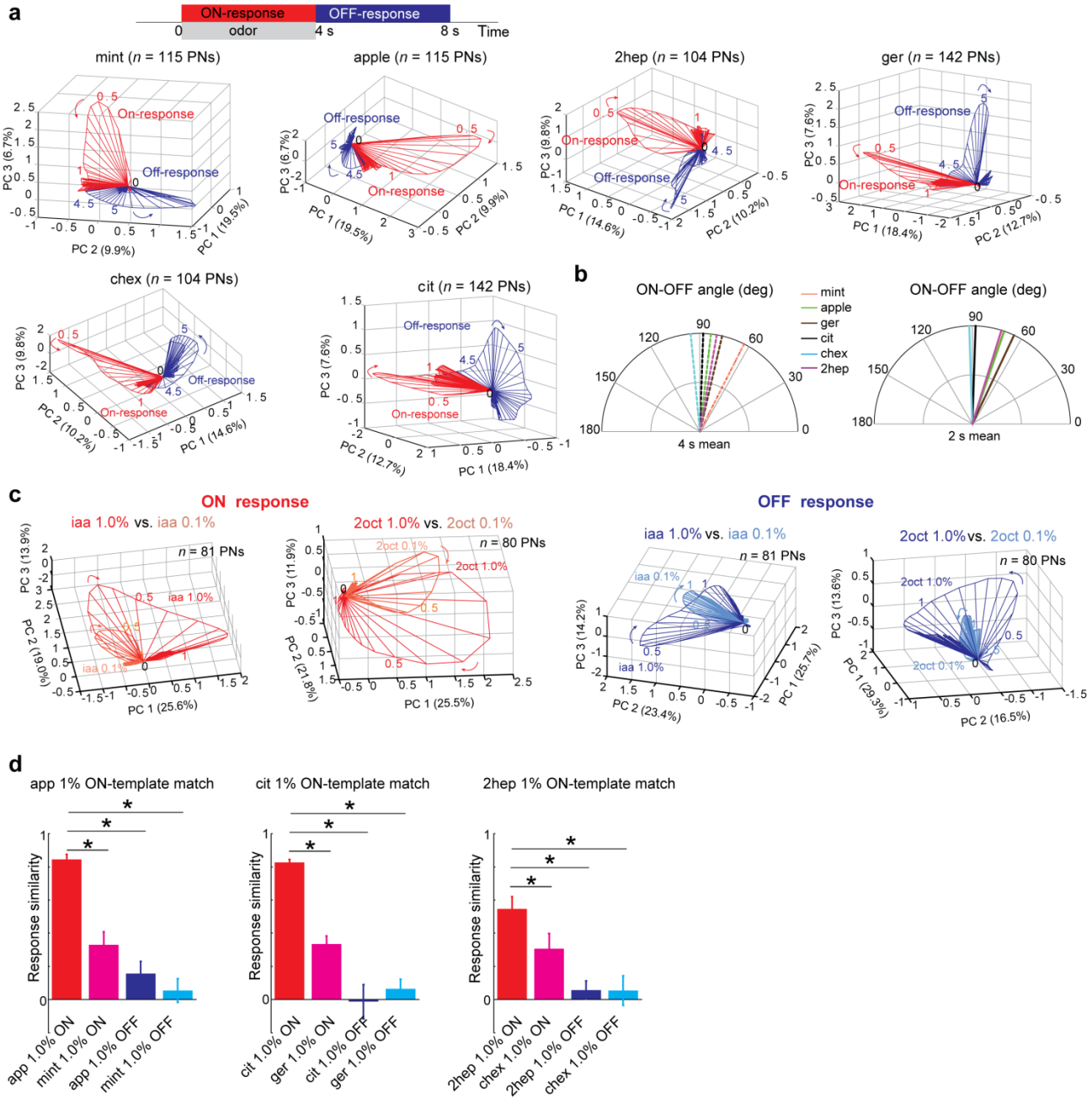

Figure 3.6: Odor-evoked ON vs. OFF neural responses are nearly orthogonal. (a) Odor-evoked ensemble PN response trajectory plots are shown for six additional odors (similar plots as in **Fig. 3.1b**, data re-analyzed from a published study [45]). **(b)** Angular distance between the mean ensemble ON and OFF responses of olfactory PNs is shown (similar to the plots in **Fig. 3.1f**). **(c)** Ensemble PN ON and OFF response trajectories are shown for two different concentrations of 2oct and iaa (1.0% and 0.1% v/v).

Similar odor trajectory plots as shown in **Fig. 3.7b. (d)** Left, the response similarity (see Methods) between the apple 1% ON template with apple 1% ON, mint 1% ON, apple 1% OFF, and mint 1% OFF are shown (mean ± s.d.). Asterisks indicate significant changes in similarity (*P<0.05, paired t-test, n = 10 trials). Similar plots are shown on the right for cit 1% vs. ger 1% and 2hep 1% vs. chex 1%. Data was re-analyzed from a previous study [45]. For comparisons between ON responses of the same odorant (i.e. first bar on each panel), a leave on trial out validation approach was used.

3.2.2 Comparative analyses of stimulus-evoked ensemble responses

Our results clearly indicate that responses following the stimulus onset and termination are quite distinct from one another. Therefore, we next sought to examine whether OFF responses have the same specificity as the ON responses. Consistent with previous results[48, 97], we found that both ON and OFF response trajectories changed directions depending upon odor identity (**Fig. 3.7a**). In comparison, changes in odorant intensity altered the directions of the ON and OFF trajectories only subtly[48], but predominantly lengthened or shrank them (**Fig. 3.7b, Fig. 3.6c**). While both the trajectories' span and length increased as odor concentration increased for some odorants (hex, 2oct and iaa), the opposite was true for bzald. These results are consistent with previous findings that both ON and OFF ensemble responses vary with and therefore contain information about both stimulus identity and intensity[48, 97].

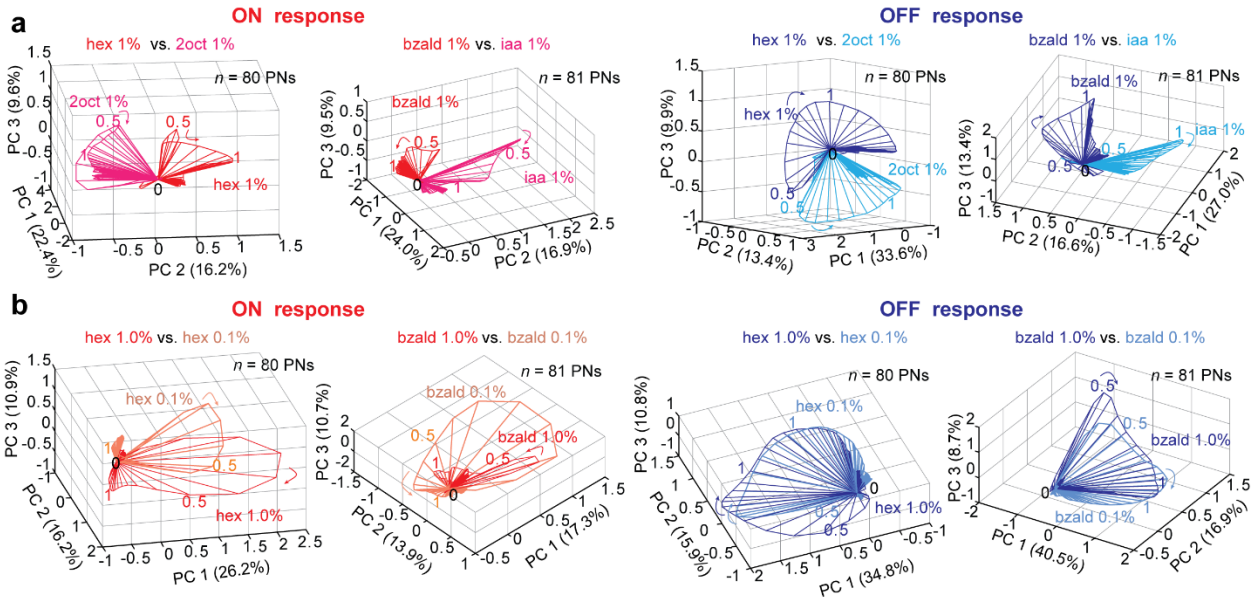

Figure 3.7: OFF responses vary with identity and intensity. (a) Comparison between ON response trajectories evoked by two different odorants is shown after dimensionality reduction for two different odor pairs (left panel; hex vs. 2oct and bzald vs. iaa). Similar comparison between the OFF response trajectories for the same pairs of odorants are shown in the right panel. The ON and the OFF response trajectories were generated and shown separately for clarity. Note that each odorant evoked a distinct response trajectory during both these epochs. **(b)** Similar plots as shown in **panel a** but now comparing responses evoked by the same odorant at two different intensities (hex 1% vs. hex 0.1% and bzald 1% vs. bzald 0.1%).

How different are the PN combinations activated during the ON and OFF epochs of the same stimulus when compared to PN ensembles activated by different odors or the same odor but presented at different intensities? Since these neural circuits have been hypothesized to play a pivotal role in discriminating odorants[35, 107, 108], we expected different stimuli to activate more distinct combinations of neurons. To understand this and quantitatively compare the similarity between ensemble responses generated in different time bins, we performed a correlation analysis[48] (**Fig. 3**). As can be noted, the diagonal high-correlation blocks indicate that the ensemble neural activities evoked during the stimulus ON periods remained highly similar throughout the stimulus ON period. These high-correlation blocks persisted, albeit to varying levels, even when the comparisons were made between ensemble ON responses evoked

by the same odorant but presented at different intensities (**Fig. 3.8c**), or between different odorants (**Fig. 3.8d**). Similarly, the ensemble neural activities evoked during stimulus OFF periods were highly correlated only amongst themselves (i.e. the lower half of the high-correlation diagonal blocks). The off-diagonal blocks, comparing the ON and the OFF responses were the least correlated in all plots (i.e. comparisons between ON and OFF responses of same odorant, different intensities, and between different odorants). Furthermore, our results indicate that the combinatorial variations due to stimulus intensity or identity were less drastic when compared to the differences in the ensemble activities at the onset and termination of the same stimulus (i.e. ON vs. OFF responses; **Fig. 3.8e,f; Fig. 3.6d**). These results, therefore, reveal that the antennal lobe circuit emphasizes difference between stimulus onsets and offsets better than the dissimilarities between odorants.

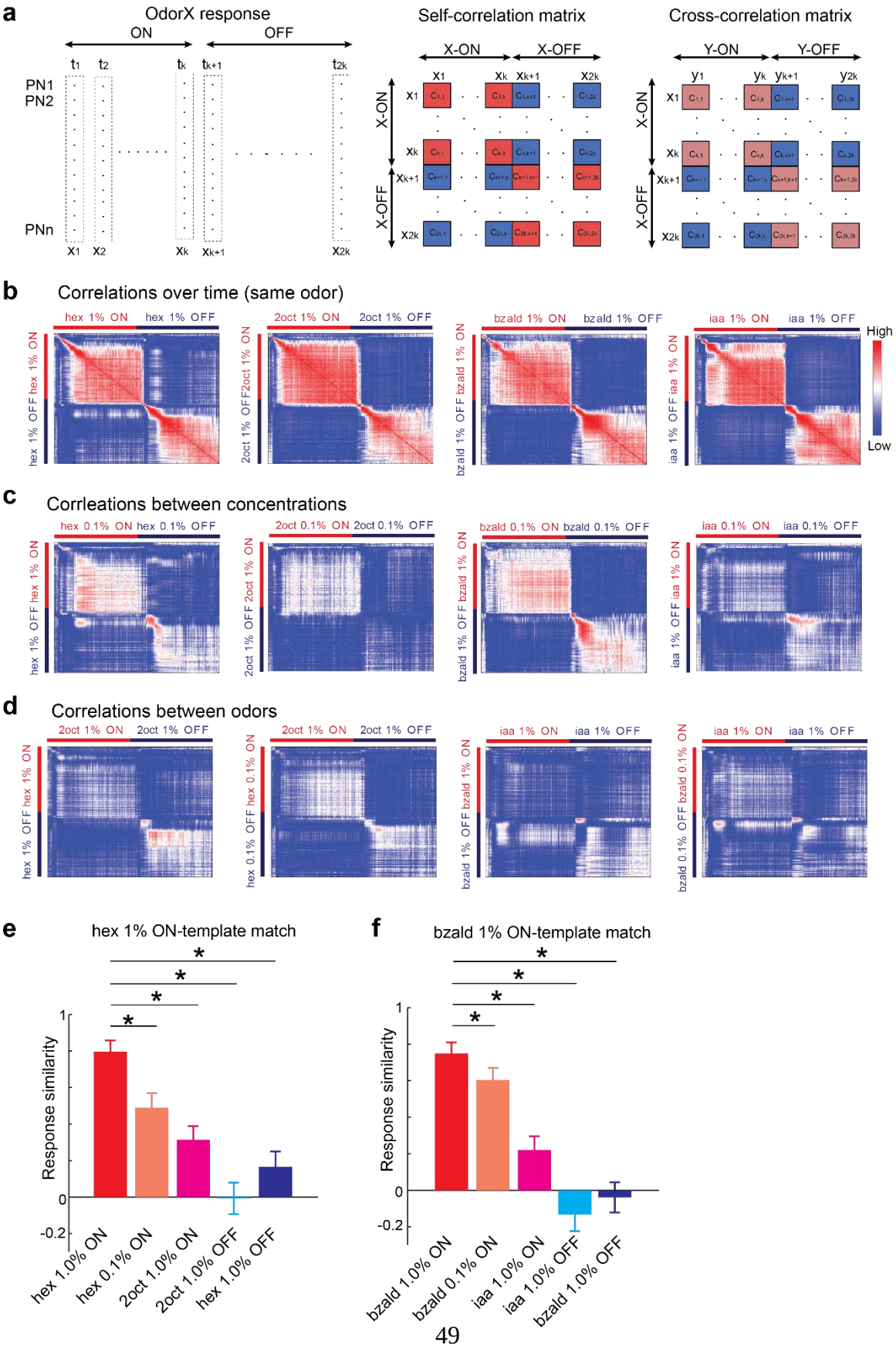
a
OdorX response
ON
OFF
PN1
PN2
PNn
Self-correlation matrix
X-ON
X-OFF
Cross-correlation matrix
Y-ON
Y-OFF
b
Correlations over time (same odor)
hex 1% ON
hex 1% OFF
2oct 1% ON
2oct 1% OFF
bzald 1% ON
bzald 1% OFF
iaa 1% ON
iaa 1% OFF
High
Low
c
Correleations between concentrations
hex 0.1% ON
hex 0.1% OFF
2oct 0.1% ON
2oct 0.1% OFF
bzald 0.1% ON
bzald 0.1% OFF
iaa 0.1% ON
iaa 0.1% OFF
d
Correlations between odors
hex 0.1% ON
hex 0.1% OFF
e
hex 1% ON-template match
Response similarity
hex 1.0% ON
hex 0.1% ON
2oct 1.0% ON
2oct 1.0% OFF
hex 1.0% OFF
f
bzald 1% ON-template match
bzald 1.0% ON
bzald 0.1% ON
iaa 1.0% ON
iaa 1.0% OFF
bzald 1.0% OFF

Figure 3.8: ON vs OFF response similarities. (a) Schematic overview of the analysis approach. Each rectangular column indicates population neuron response vector in a 50 ms time bin. Right, self- and cross correlations between response vectors in different time bins were computed and shown as a color-coded image. **(b)** Correlations between ensemble response vectors evoked by an odorant in different time bins following stimulus onset is shown. The 4 s stimulus ON and 4 s stimulus OFF periods are identified using red and blue bars along the axes. Spike counts were averaged across trials (n = 25 trials) and used for this analysis. Note that each pixel represents correlation between one ensemble vector with another. Similarly, one row or column represents the correlation between one ensemble vector with all other vectors in the identified time periods (80 ON response vectors and 80 OFF response vectors). The color scheme used for representing the correlation values is shown on the right; cooler colors indicate lower correlations; hotter colors represent higher correlations. In general, the diagonal blocks tended to have higher correlations (more red pixels), whereas the off diagonal blocks had pixels mostly of lower correlations (i.e. more blue pixels). **(c)** Similar correlation plots but comparing the ON and OFF response vectors of different concentrations of the same odorants are shown. Comparisons were made between 1% and 0.1% dilutions of the following four odorants: hexanol (hex), 2-octanol (2oct), isoamyl acetate (iaa), and benzaldehyde (bzald). **(d)** Cross-correlations between different odorants are shown. Comparisons were made between the following four odor pairs: hex 1% and 2oct 1%, hex 0.1% and 2oct 1%, bzald 1% and iaa 1%, and bzald 0.1% and iaa 1%. **(e)** A comparison of response similarity (see Methods) between ON and OFF response segments of the same and different odorants are shown. Similarity with respect to hex 1% ON template is shown (mean ± s.d.). Asterisks indicate significant change in similarity (*P < 0.05, paired t-tests with Bonferroni correction for multiple comparisons, n = 25 trials). **(f)** Similar plots are shown but now comparing the response similarity with respect to the bzald 1% ON template.

3.2.3 ON vs OFF responses in odor mixtures

Similar to monomolecular chemicals examined so far, we found that a binary mixture of two odorants also produced ON and OFF responses that were orthogonal to each other (**Fig. 3.9**). Predictably, the mixture trajectories appeared to be some combination of the individual odorant responses, both during the stimulus presentation as well as after the mixture termination. Therefore, the mixture ON trajectories occupied the region between the component ON responses, and the mixture OFF trajectories projected onto the space between the OFF responses elicited by each component. These results combined with the results for complex mixtures, such as apple and mint (**Fig. 3.6**), corroborate our conclusion that these observations regarding ON and OFF responses are general features of odor-evoked neural activities and are not limited to monomolecular chemicals.

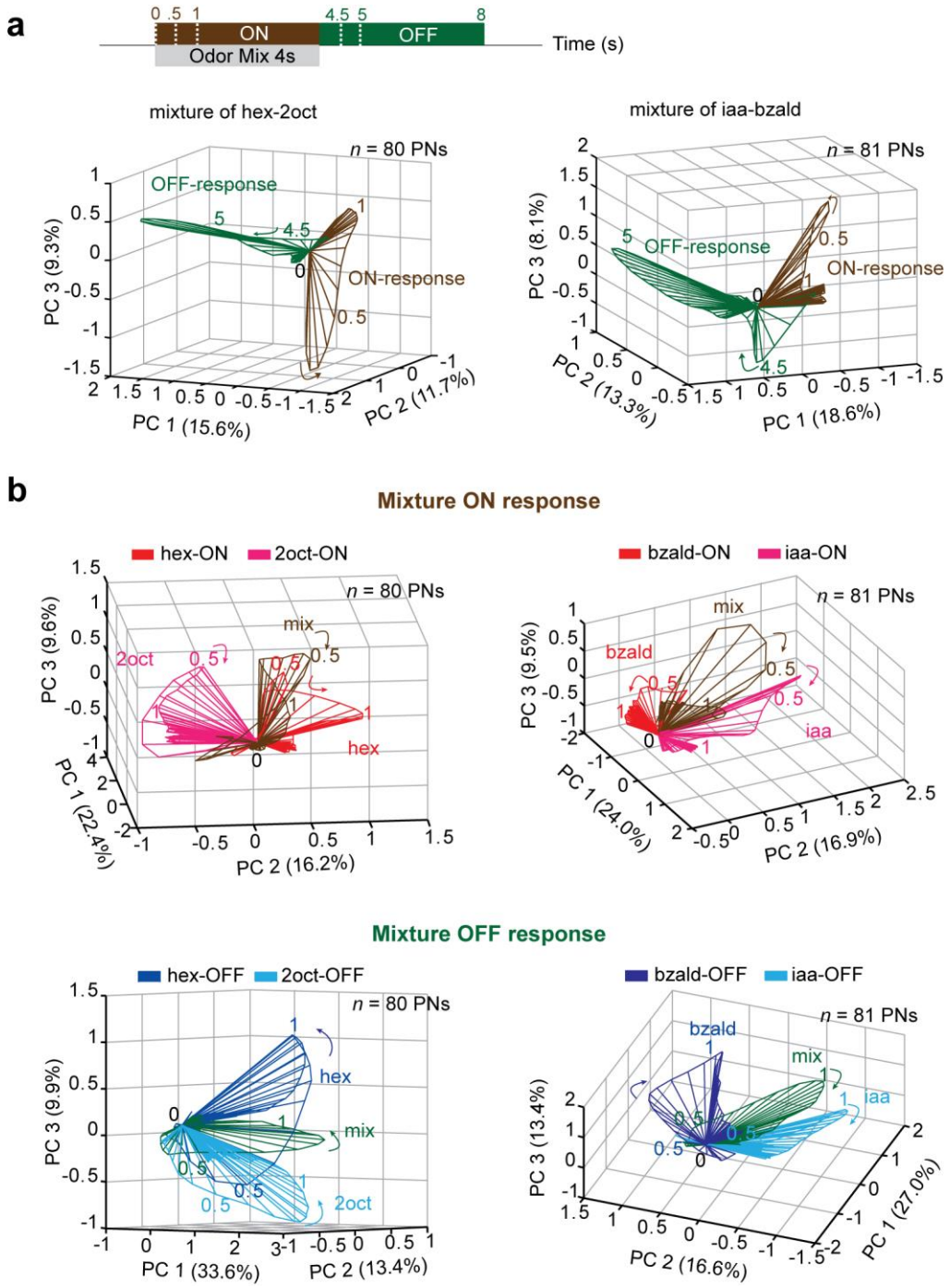

Figure 3.9: Encoding of binary mixtures. (a) Odor trajectories evoked by a binary mixture during ON and OFF epochs are shown after PCA dimensionality reduction. The number of neurons (*n*) used for this analysis and the percentage of variance are shown in each plot. Numbers near response trajectories indicate time in seconds since odor onset. **(b)** Odor trajectories evoked by a binary mixture and its two components are shown after PCA dimensionality reduction. Note, ON responses and OFF responses are compared separately in these plots. Same convention is used as in **panel a**.

3.2.4 Robustness of OFF responses

Apart from identity and intensity, naturally encountered odorant plumes also tend to vary in stimulus length[12]. We next examined how invariant were the OFF responses that followed the same stimulus delivered for different durations. We found that the orthogonal relationship between the ON and OFF responses was maintained independent of the stimulus pulse duration (**Fig. 3.10a**). Furthermore, consistent with prior results[13, 97], the odor response trajectories for different stimulus durations were well aligned during both the response onsets and offsets. Therefore, the ON and OFF response templates obtained for one odor pulse duration (4 s; see Methods), pattern-matched with ensemble neural activities evoked by the same odorant presented for different durations (**Fig. 3.10b,c**). Note that the ensemble response vectors during the entire odor presentation period pattern-matched only with the ON responses, but the response switched and gained similarity with the OFF response template after stimulus termination. On the other hand, different odorants evoked response patterns that were distinct from each other during both ON and OFF response periods (**Fig. 3.10**; hex vs. bzald).

In sum, these results suggest that OFF responses are as consistent as the ON responses, and they actively convey information about the termination of a particular stimulus at a specific intensity. Further, our results also show that neuronal networks can use two minimally overlapping sets of neurons to represent equivalent information about a stimulus during different epochs.

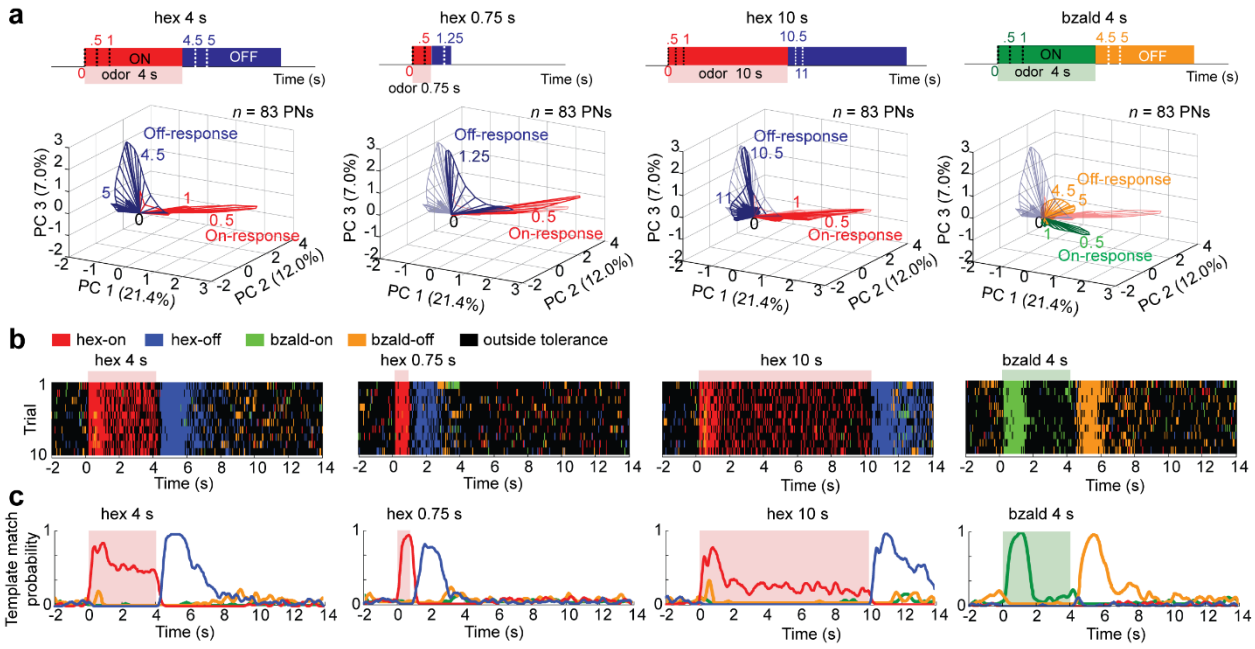

Figure 3.10: Classification analyses of ensemble neural activity. (a) ON and OFF response trajectories evoked by a 4 s hex 1% puff is compared with the response trajectories elicited by a brief (0.75 s) or a lengthy (10 s) presentation of the same odorant, and against a different odorant (bzald 1% delivered for 4 s). For reference, ON and OFF hex (4 s) trajectories are re-plotted in all panels using a lighter shade of red and blue, respectively. *n* represents the total PN number. All other notations and information are consistent with neural trajectory plots shown in **Fig. 3.1b–e**. **(b)** Results from a supervised classification analysis (see Methods) are shown. Each row represents a trial and each tick mark corresponds to the class label assigned to the high dimensional neural activity observed in a 50 ms time bin. Each time bin was labeled based on the closest template with which it pattern-matched: hex ON response template – 'red tick mark', hex OFF response template – 'blue tick mark', bzald ON response template – 'green tick mark', bzald OFF response template – 'orange tick mark', and time bins when the ensemble neural activity differed significantly from all hex and bzald response templates (> 63°) were labeled using a 'black tick mark'. Classification for ten trials are shown for hex presentations of different durations and a 4 s bzald pulse. A leave-one-trial-out validation was followed for classification of hex 4s and bzald 4s conditions. The colored bar on the top indicates stimulus duration. **(c)** The probabilities of pattern-match with different templates (used in **panel b**) are shown as a function of time. The colored box identifies the time period when the stimulus was presented.

3.2.5 ON vs. OFF responses: engaging and disengaging recurrent inhibition

Apart from using different neural ensembles, are there other differences that distinguish the ON and the OFF responses? To understand this, and to gain mechanistic insights, we made intracellular recordings from GABAergic local neurons (LNs) and cholinergic PNs in the

antennal lobe while simultaneously monitoring the local field potential activity in the mushroom body (the neural circuit downstream to the antennal lobe). Although ON and OFF responsive local neurons have been reported in other model systems[109], consistent with published results in locusts[11], we found that most local neuron responses were limited to the odor onset period. We also found that odor exposures entrained oscillatory activity both in individual local neurons and in the local field potential[51] (**Fig. 3.11a,b**). Further, these local neuron and field potential oscillatory responses were limited to the odor presentation period (i.e. only during ON response epochs; **Fig. 3.11b,c; Fig. 3.12a**). Notably, we found that the local neuron activity remained phase locked with field potential activity only when the stimulus was presented (**Fig. 3.11d**). Intracellular recordings from individual PNs were largely consistent with what we had observed in our extracellular datasets and most PN spikes occurred either during or after the stimulus duration (**Fig. 3.11e–g**).

We pondered if the recruitment of inhibition could simply arise due to differences in the strength of the odor-evoked responses observed during these epochs. Therefore, we first compared the average spike counts across all recorded PNs during the ON and OFF epochs (**Fig. 3.11h**). We found that the PN responses had two distinct peaks, one following odor onset and the other following odor offset. PN spiking activity weakened considerably between these two transient response periods (i.e. the sustained/steady-state responses). Interestingly, this weak sustained response was still sufficient to evoke local neuron activity and local field potential oscillations. In comparison, even though the OFF responses were considerably stronger than the neural activity just before the end of the odor pulse, it failed to entrain coherent field potential oscillatory activity (**Fig. 3.11g**). Furthermore, as mentioned before, a comparison of cumulative spike counts during the ON and OFF epochs revealed that the spike counts during these time

periods were comparable (**Fig. 3.2e,f**). Therefore, the overall strength of spiking activities across PNs alone appears to be a poor indicator of whether or not the local field potential oscillations are generated by the AL circuitry.

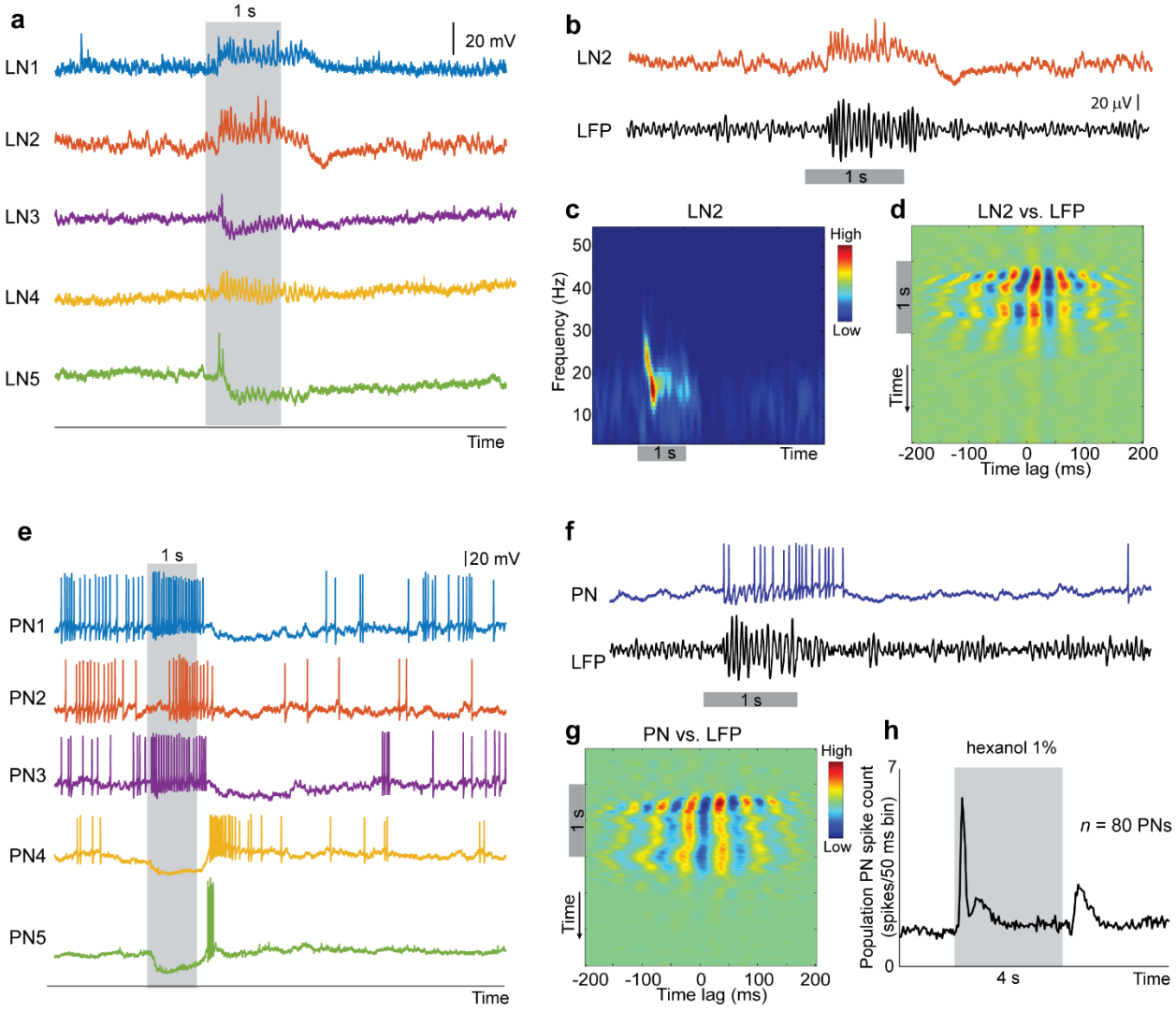

Figure 3.11: Engaging and disengaging recurrent inhibitory network. (a) Intracellular voltage traces of five different local neurons (LNs) are shown before, during and after a short odor pulse (1s duration). Note that consistent with previous reports [51], LNs in the locust antennal lobe do not fire full-blown sodium spikes but rather respond to the stimulus with small calcium spikelets. Also, the response to the odor stimulus deviates from baseline levels only during the period of odor exposure and returns back to baseline levels immediately following the odor termination. **(b)** Intracellular response of a local neuron (LN2) and simultaneously recorded extracellular local filed potential (LFP) are shown for a 1 s long odor stimulation. Note that the LN sub-threshold membrane potential fluctuations and LFP oscillation are both limited to the odor presentation window. **(c)** Evolution of power in different frequencies (see Methods) of

an odor-evoked LN response (LN2) is shown for three different epochs: before, during and after a 1s odor puff. **(d)** Cross-correlations calculated between the local neuron membrane fluctuations (LN2) and the local field potential are shown. The alternating peaks (hot color) /troughs (cool color) correlation bands can be observed only during the ON response period. Note that the time period of the correlation bands is roughly 50 ms (or 20 Hz). **(e)** Odor-evoked projection neuron (PN) intracellular voltage responses are shown for 5 different PNs. Notice that PNs fired spikes either during the ON or the OFF period in a mutually exclusive manner. **(f)** Intracellular response of a PN and simultaneously recorded LFP signals elicited by a 1 s hexanol pulse are shown. **(g)** Similar plot as in **panel d** but cross-correlating the PN response with the LFP signal is shown (same data as in **panel f**). **(h)** Mean spike count across all recorded PNs (n = 80) is shown for hex 1% stimulus. Two stimulus-evoked response peaks, one during the ON and the other during the OFF period of odor presentation (4 s duration), can be observed.

In our earlier work[45], we found that the sensory input from ORNs did not have a strong bout of spiking activities after termination of the odorant as was observed in the PNs. Could this difference in the presence/absence of sensory input alone explain the limited entrainment of field potential oscillations during the odor exposure period? First, we note that the presence of strong input from sensory neurons was a good indicator of whether LFP oscillations were present in the AL. However, consistent with the existing data[11], we found that application of picrotoxin, a $GABA_A$ antagonist, alone can reversibly abolish the field potential oscillations (**Fig. 3.12b–e**). Note that this pharmacological manipulation did not impact the sensory input to the antennal lobe circuits but rather blocked the fast inhibition from the local neurons onto the projections neurons. Combining these two observations, we conclude that input from sensory neurons is necessary for recruitment of inhibition from local neurons that then allow generation of oscillatory field potential activity.

In sum, these results indicate that the ON and the OFF responses significantly differ in their ability to engage the local inhibitory circuits which are necessary for oscillatory synchronization of PN responses. Hence, we conclude that although the ON and the OFF responses have qualitatively similar information content, their neural encoding formats vary significantly.

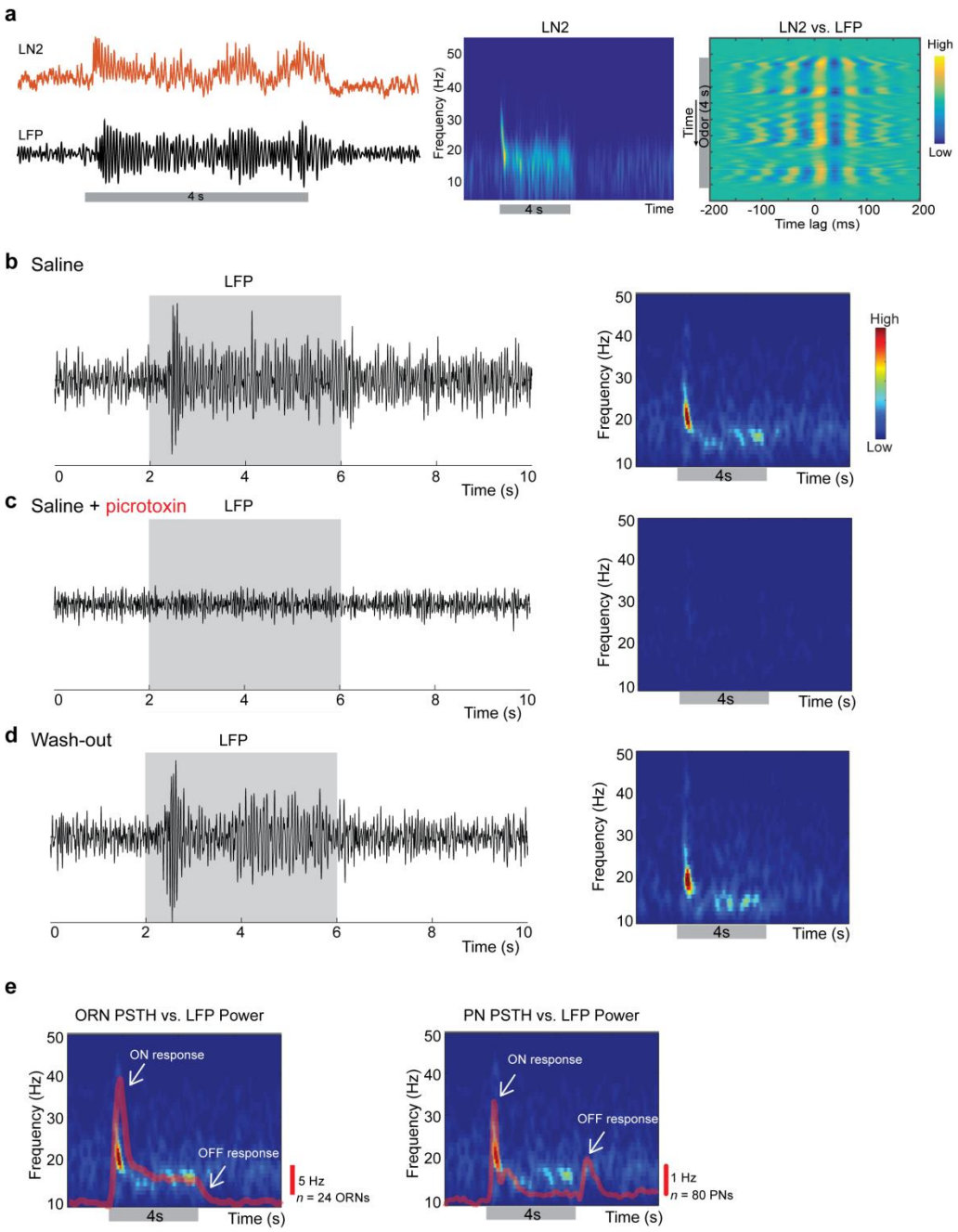

Figure 3.12: Engaging and disengaging recurrent inhibitory network. (a) Left, Intracellular response of a local neuron (LN2) and simultaneously recorded extracellular local filed potential (LFP) are shown for a 4 s long odor stimulation. Middle, power at different frequencies are shown for a LN before, during, and after an odor puff. Right, Cross-correlations calculated between the local neuron membrane fluctuations (LN2) and the local field potentials are shown. **(b)** Left, LFP oscillations are shown for a 4 s hexanol puff (control case; before picrotoxin bath application). Right, trial averaged frequency spectrogram is shown for the same odor stimulation (n = 3 trials; see Methods). **(c)** Same results are

shown when 100 μM picrotoxin was applied in saline bath to block the GABAergic local neurons' input to the PNs. **(d)** The LFP oscillations and the oscillatory power during odor presentation window recover after saline wash. **(e)** Left, mean ORN firing rate plot is superimposed on the frequency spectrogram shown in panel a (*n* = 24 ORNs). Right, same plot as in left panel but with mean PN firing rate superimposed (*n* = 80 PNs).

3.2.6 Mechanistic insights: A simple computation model of the AL circuitry

To further understand the mechanisms, we developed a well-constrained computational model of the early olfactory circuits (see Methods, **Fig. 3.13; Fig. 3.14**). The AL model had the following components: (i) feed-forward input from ORNs onto PNs and LNs (ii) recurrent connections between LNs and PNs (iii) a bi-directional adaptive mechanism in individual PNs. Consistent with published results[47, 110], we found that recurrent inhibition from local neurons was the essential and sufficient component to generate results similar to our *in vivo* observations: 20 Hz field potential oscillations and phase locking of excitatory and inhibitory ensemble activities only during stimulus ON epoch (**Fig. 3.14e,f**). Without these recurrent inhibitory connections from LNs onto PNs, the model did not generate any oscillatory field potential activity (**Fig. 3.13c**). This dependence of local neuron activity on stimulus-evoked input limited the recruitment of recurrent inhibition and therefore entrainment of the field potential oscillations to the duration of the stimulus exposure.

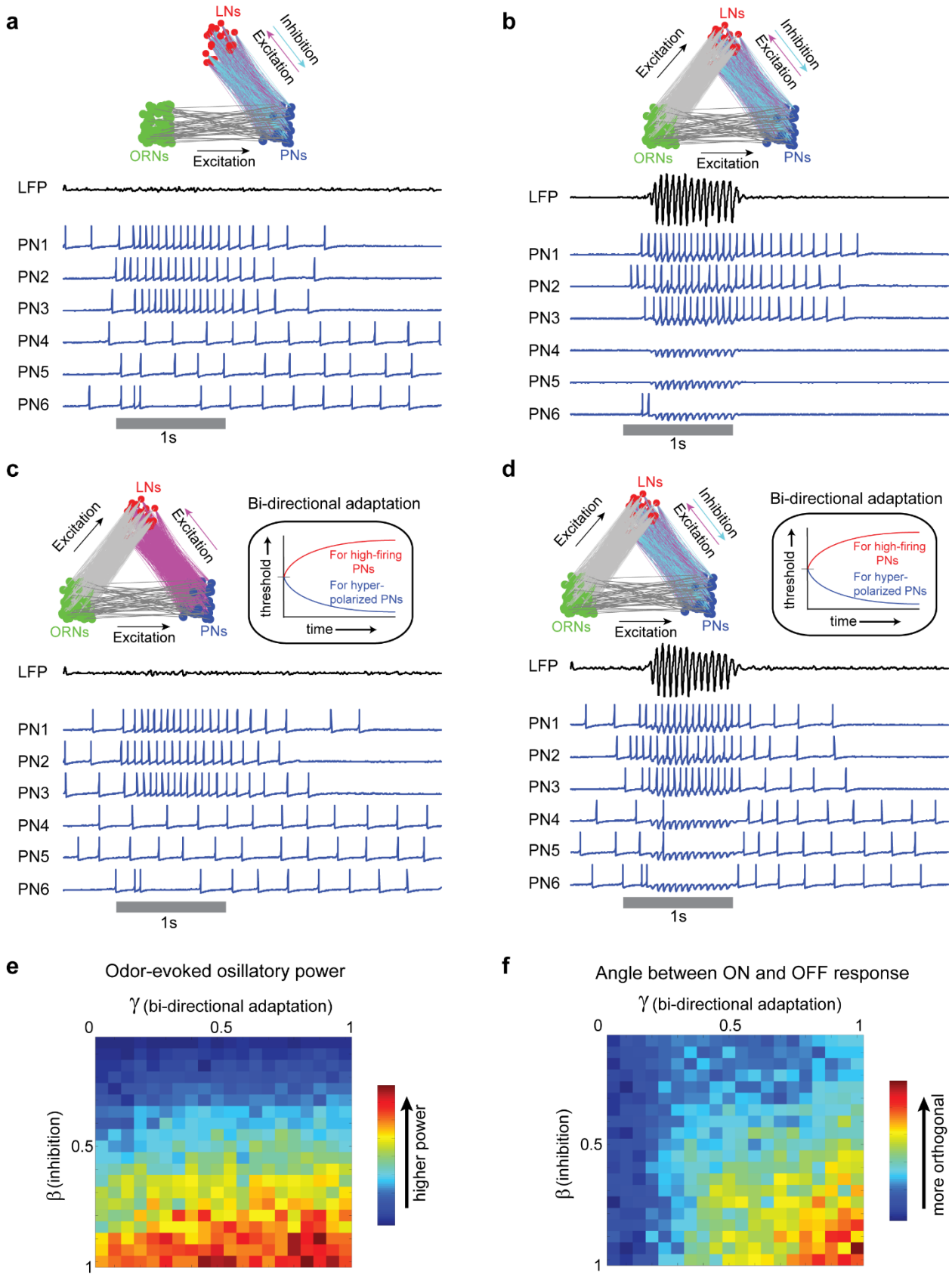
a
LNs
Inhibition
Excitation
ORNs
Excitation
PNs
LFP
PN1
PN2
PN3
PN4
PN5
PN6
1s
b
LNs
Excitation
Inhibition
Excitation
ORNs
Excitation
PNs
LFP
PN1
PN2
PN3
PN4
PN5
PN6
1s
c
LNs
Excitation
Excitation
ORNs
Excitation
PNs
Bi-directional adaptation
threshold
For high-firing PNs
For hyper-polarized PNs
time
LFP
PN1
PN2
PN3
PN4
PN5
PN6
1s
d
LNs
Excitation
Inhibition
Excitation
ORNs
Excitation
PNs
Bi-directional adaptation
threshold
For high-firing PNs
For hyper-polarized PNs
time
LFP
PN1
PN2
PN3
PN4
PN5
PN6
1s
e
Odor-evoked osillatory power
γ (bi-directional adaptation)
0
0.5
1
β (inhibition)
0.5
1
higher power
f
Angle between ON and OFF response
γ (bi-directional adaptation)
0
0.5
1
β (inhibition)
0.5
1
more orthogonal

Figure 3.13: Modelling of ON-OFF neural activity. Local field potential activity (LFP; top trace) and six modeled projection neuron (PN) spiking activities are shown. Four different model architectures were evaluated: **(a)** Model architecture 1: feed-forward ORN inputs to the local neurons (LNs) were removed. This made the total input received by LNs too weak and therefore the LNs were not activated when stimulus was introduced. As a result, PNs did not receive any feedback inhibition. Also note that the stimulus-evoked oscillatory field potentials were not observed. **(b)** Model architecture 2: LNs received inputs from both ORNs and PNs. As a result, LNs were activated and PNs received recurrent inhibition from LNs. Oscillatory field potentials were observed in this model during stimulus exposure period. However, the model did not generate a strong activity following stimulus termination (i.e. no 'OFF' responses). **(c)** Model architecture 3: PN excitability was adapted in a bi-directional manner. LN inputs to PNs were removed. PNs did not receive feedback inhibition. Therefore, the model did not evoke stimulus-evoked LFP oscillations, or strong PN responses following stimulus termination. **(d)** Model architecture 4: PN responses were adapted in a bi-directional manner. LNs received inputs from ORNs and PNs. Therefore, LNs were activated by input stimulus and PNs received feedback inhibition. Therefore, the model produced stimulus-evoked oscillatory field potentials. The strong inhibition to a subset of PNs during the odor input increased the excitability of the inhibited PNs and thereby causing a strong OFF response in this model. **(e)** Bifurcation analysis showing the relative importance of recurrent inhibition from LNs (y-axis) and bi- directional response adaptation (x-axis) for generating oscillatory local field potential in the 5 – 55 Hz frequency range. The horizontal banding reveals that the strength of the feedback inhibition alone is necessary and sufficient for generating LFP oscillations. **(f)** Bifurcation analysis showing the relative importance of recurrent inhibition from LNs (y-axis) and bi-directional spiking threshold adaptation (x-axis) for generating distinct ON and OFF neural activities. Note that both strong recurrent inhibition and bi-directional spiking threshold adaptation are important for generating a distinct ON vs. OFF responses.

While the model with recurrent inhibition alone was sufficient to generate LFP oscillations, as can be noted, the spiking activities in PNs were limited to the epochs when strong ORN input was available (i.e. no OFF responses). Therefore, a bidirectional adaptation mechanism was added to individual PNs that reduced the excitability following high-firing epochs, and at the same time increased the excitability following periods of hyperpolarization. Such adaptive control of neural excitability was necessary to generate orthogonal ensemble activities during stimulus onset and offset (**Fig. 3.13f**). This allowed the model to generate the PN OFF responses even when the sensory inputs were decaying back to baseline (i.e. weak). We note that to keep the simulations simple and consistent with our electrophysiology data (see **Fig.**

3.3), we did not include any OFF-responsive ORNs in the simulations shown here. Also note that the LN inhibition was absent during these periods as a strong ORN input was necessary in the model to recruit recurrent inhibition. Therefore, the PN OFF responses in the model were also desynchronized, thereby reducing power in the oscillatory field potential activity (**Fig. 3.13d**). Bifurcation analyses (**Fig. 3.13e,f**) indicate that the strength of local neuron inhibition is the only parameter that controls the power of the entrained field potential oscillations in the model, whereas a strong inhibition from local neurons and the bi-directional adaptation of PN excitability were both necessary for generating distinct ON and OFF responses.

Hence, our modeling study suggests that stimulus-dependent engagement and disengagement of recurrent inhibition in the antennal lobe circuits provides a simple mechanism for generating distinct ON and OFF neural activities with differing response formats (oscillatory vs. non-oscillatory).

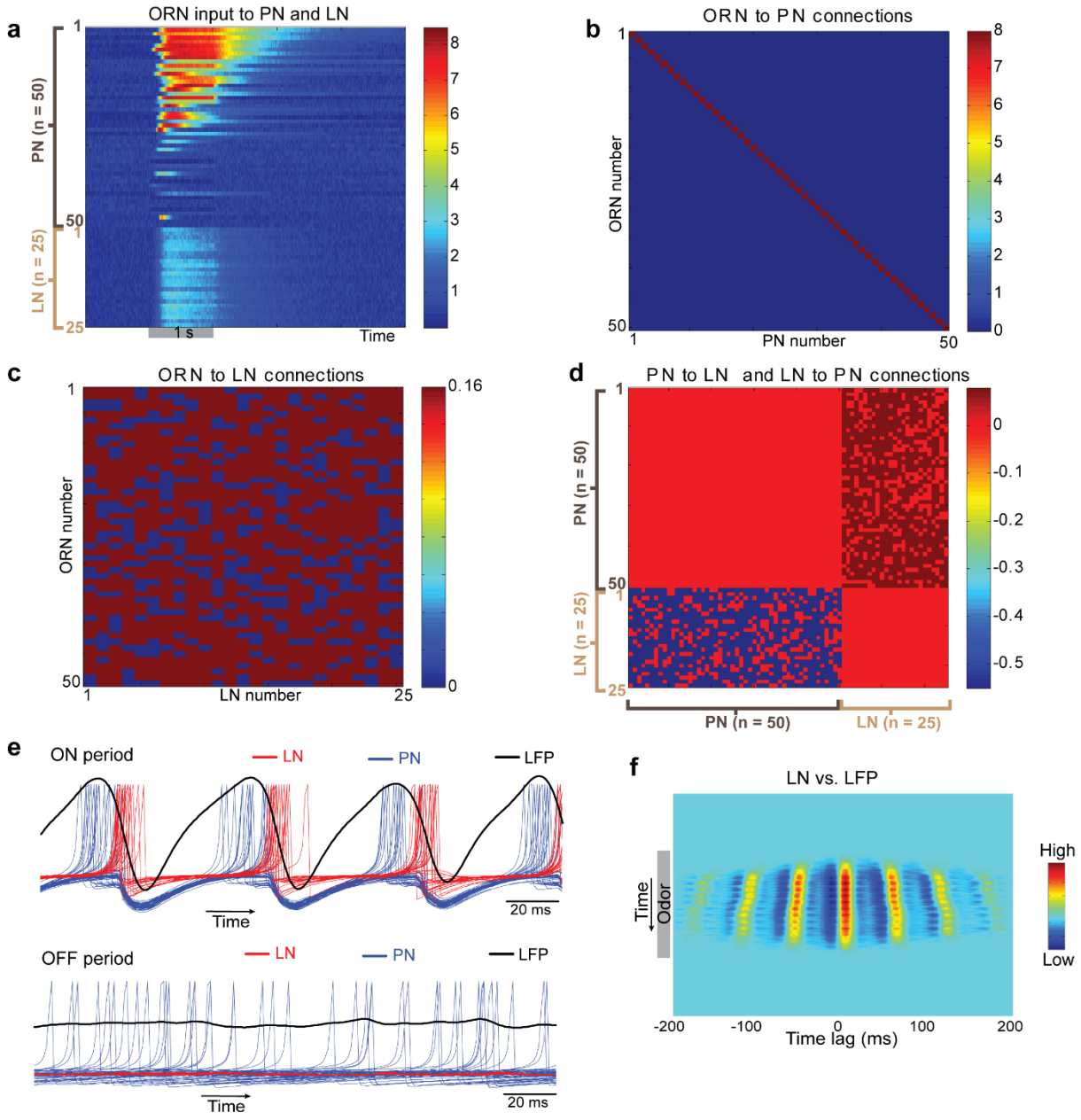

Figure 3.14: Characterization of the antennal lobe computational model responses and connectivity. **(a)** Modeled ORN activity that were input to the PNs and LNs is shown. **(b)** Connectivity matrix between the modeled ORNs and PNs is shown. **(c)** ORN to LN connectivity matrix is shown. **(d)** Connectivity matrix between the PNs and the LNs is schematically shown. **(e)** Top, stimulus-evoked PN (n = 50) and LN (n = 25) spikes are shown along with the LFP (black) during a 200 ms time window during stimulus exposure. Note that the PN and LN spikes are phase-locked with the LFP. Bottom, similar plots as in top panel but now showing PN, LN spikes and LFP responses during OFF period (after odor termination). Note that both LN spikes and LFP oscillations are absent during this time window although PN spiking activity persists. **(f)** Cross-correlations between LN activity (averaged across all LNs in the antennal lobe model) and the LFP signal are shown. As can be noted, the LN activity transiently phase locked to the

LFP during odor presentation window. The red and blue banding patterns indicate the peaks and troughs of the cross-correlation, respectively.

3.2.7 Behavioral relevance of ON and OFF responses

Are the response patterns observed at the odor onset and offset relevant to odor-evoked behavior? Earlier studies in rodents and insects have shown that odor recognition can be rapid and usually happens within a few hundred milliseconds of stimulus onset[45, 96, 111]. Based upon these results, the early portions of only the ON responses can be expected to play a role in stimulus recognition. What then is the need for another round of stimulus-specific neural activity after odor termination? We sought to examine this issue using an appetitive-conditioning assay. During the training phase, starved locusts were presented with an odorant (conditioned stimulus) followed by a reward (wheat grass; see Methods). We found that locusts reached their asymptotic performance levels after six training trials[45, 76]. Following training, locusts were tested in an unrewarded test phase. Locusts that learned the association between the odorant and the reward opened their maxillary palps following the presentation of the conditioned stimulus in anticipation of the reward. Consistent with previous studies, locusts retained the learned association even when tested multiple times in the unrewarded test phase[45, 76]. To quantify the behavioral palp-opening response, we painted the distal end of the locust palps with a non-odorous green paint and tracked their whereabouts with fine spatial and temporal resolution (**Fig. 3.15a**; see Methods).

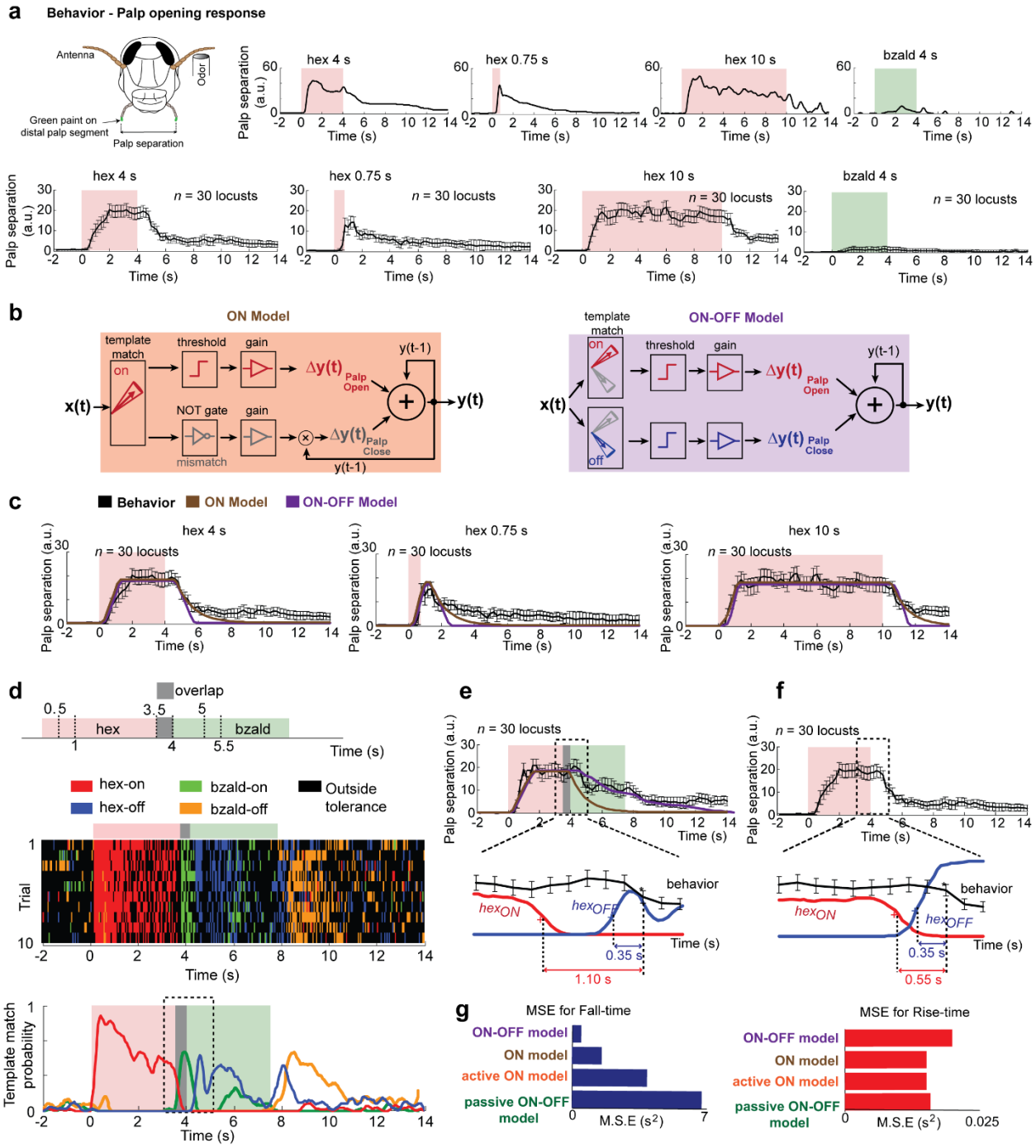

Figure 3.15: Stimulus-evoked OFF responses are required for behavioral reset. (a) *Top left panel*, schematic of the palp-opening response (POR) behavior observed in trained locusts following presentations of the conditioned stimulus. Separation between the maxillary palps of the locusts was used to quantify behavior with fine temporal resolution. *Top right panels* reveal the POR of a single locust to the conditioned stimulus (hexanol) for three different durations and to an untrained stimulus (4 s pulse of bzald). *Bottom panel*, the median distance between palps (± s.e.m.; across all trained locusts, n = 30 Locusts) is shown for presentations of the conditioned stimulus (hex) for three different durations and to

an untrained odorant (bzald). *n* indicates the number of locusts used in the behavioral assay. **(b)** Two plausible models to translate ensemble neural activity to palp opening and closing responses. **ON model** (*left panel*)**:** pattern-match or lack thereof with the ON responses of the conditioned stimulus, after thresholding and gain adjustments, is used to predict both palp-opening and palp-closing. **ON-OFF model** (*right panel*)**:** pattern-match with ON responses of the conditioned stimulus translates to palp-opening response, whereas pattern-match with OFF responses of the conditioned stimulus determines the palp-closing. **(c)** Comparison between observed behavioral responses with the predicted responses from ON model and ON-OFF model are shown for hexanol presentations of three different durations (PORs are re-plotted from **panel a**). Note that the models were fit only using the 4 s POR data (see Methods). Both models can predict the opening and closing of palps for solitary odor presentations of different durations. **(d)** *Top*, to test the two models, an overlapping sequence of hexanol (hex) and benzaldehyde (bzald) was presented. Note that the first stimulus (hex) is also the conditioned stimulus in the behavioral assay. The distractant cue (bzald) was introduced 0.5 s before the termination of the hex to perturb the neural response pattern-match with the hexanol ON responses. *Middle*, classification analysis for the ensemble neural activities generated by the hex-bzald overlapping sequence are shown. The ON and OFF responses observed during solitary hex and bzald introductions were used as templates to be pattern-matched (same templates as used in **Fig. 3.10b)**. *Bottom*, the probabilities of pattern-match with different response templates are shown as a function of time. Boxed region identifies a small time segment starting just before the distractant (bzald) onset and ending after the termination of the conditioned stimulus (hex). **(e)** POR (median $\pm$ s.e.m., $n = 30$ Locusts) when the trained locusts were presented the same overlapping sequence of hex and bzald (in black) is shown. The behavioral responses predicted from the ensemble neural activities by the ON- and the ON-OFF models are also shown (same color code as in **panel c**). The inset magnifies the epochs before, during and after hex-bzald overlap to facilitate comparison between POR and pattern-match probabilities during these time segments (magnified view of the dotted region in **panel d**). Note that the palps closed not when the pattern-match with the ON response of the conditioned stimulus was lost (i.e. red curve returns to baseline), but when similarity with the OFF responses was gained (i.e. blue curve ramps up from baseline). A Wilcoxon signed-rank test was used to detect the time bin when the first significant reduction in palp-opening response occurred (black star; $P < 0.05$ and Bonferroni corrected for multiple comparisons). For classification results (blue and red curves obtained from the boxed region in **panel d**), the peak derivative of pattern-match probabilities was used to determine when a mismatch with ON responses (red cross) or a match with OFF responses began (blue cross). **(f)** To allow comparison, the behavioral response to solitary presentations of the conditioned stimulus (hex) and the evolution of neural response pattern-match over time are shown. It is worth noting that the latency with which the palps closed following loss of pattern-match with the hexanol ON responses doubled for the hex-bzald overlapping stimulus sequence. Importantly, the time from the pattern-match with the OFF responses to the onset of palp-closing behavior was constant across conditions. **(g)** A quantitative comparison of the four different models explored is presented. The mismatches of rise and fall time constants predicted by these models with actual behavioral results for different hexanol presentations are quantified as mean-squared errors (see Methods).

We found that the palp-opening responses were quick to start and the palps were kept open as long as the conditioned stimulus persisted (**Fig. 3.15a**). The behavioral responses generalized independent of the duration of the conditioned stimulus (note only a 10 s hexanol pulse was used to train the locusts; see Methods). More importantly, we found that the periods during which the ensemble neural activities pattern-matched with the ON responses corresponded to epochs when the palps were opened and usually kept open (**Figs. 3.10c** and **3.15a**). In contrast, time segments when the palps closed correlated with those epochs when neural activity gained similarity with the OFF responses (**Figs. 3.10c** and **3.15a**). In sum, these results suggest two possible models for translating population neural activity into palp-opening and palp-closing responses: (i) *ON model:* gaining or losing pattern-match with ON responses underlies palp-opening and palp-closing responses, respectively; and (ii) *ON-OFF model:* pattern-match with the ON responses triggers behavioral response onset, whereas pattern-match with OFF responses is necessary for terminating the behavioral responses. We found that both the ON and the ON-OFF model could generate predictions consistent with the observed palp opening and closing responses for hexanol presentations of different durations (**Fig. 3.15b,c**). Note that we also explored two other model variants for completeness (**Fig. 3.16a,b**).

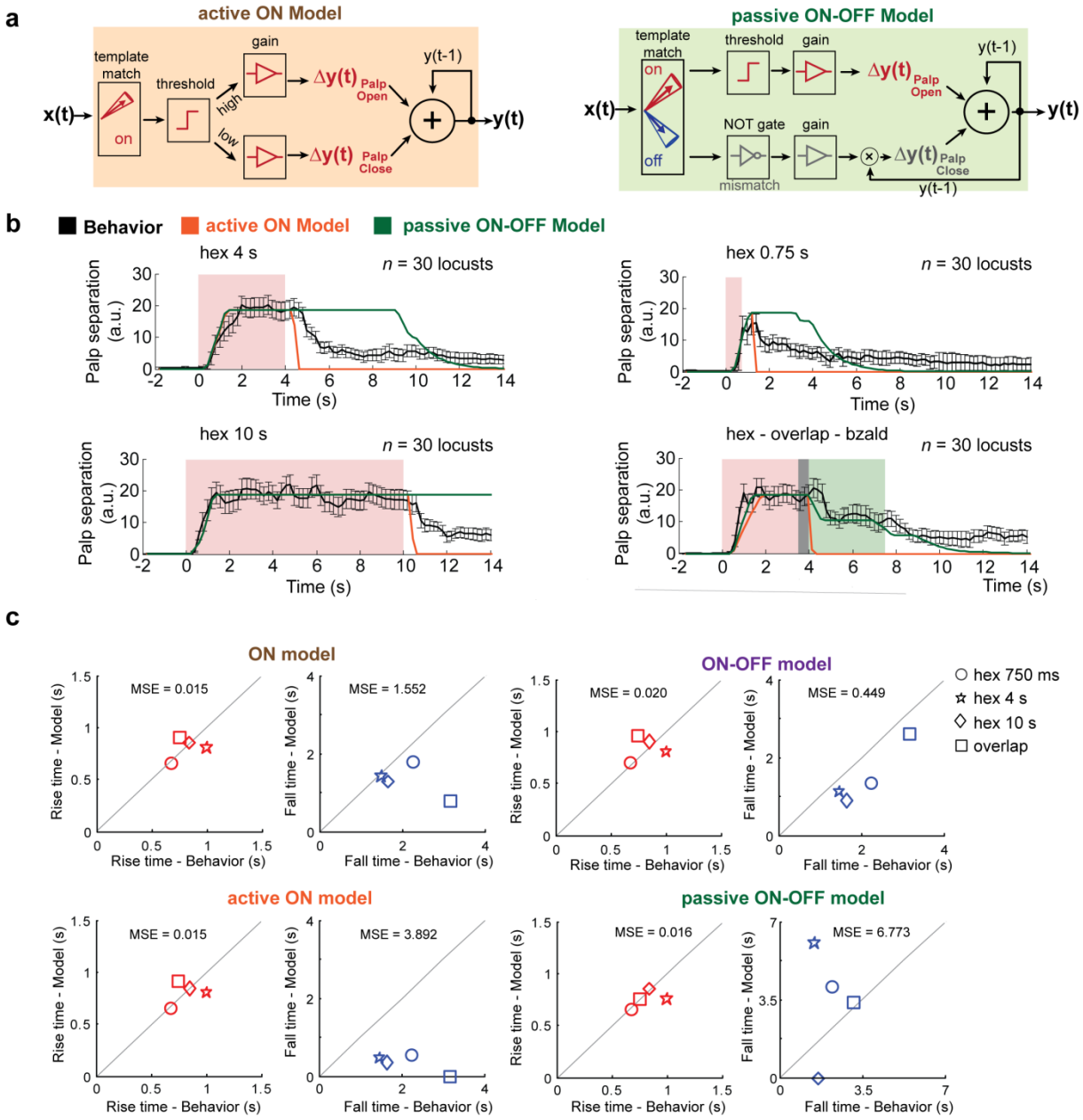

Figure 3.16: Behavioral relevance of ON vs. OFF responses. (a) Two variants of the models shown in **Fig. 3.15b** to translate ensemble neural activity to palp opening and closing responses. **Active ON model** (*left panel*)**:** A strong pattern-match with the hexanol ON response template initiates and sustains palp-opening response, whereas a weak pattern-match with the ON response template causes a palp-closing response. **Passive ON-OFF model** (*right panel*)**:** Pattern-match with ON response template opens and sustains the palps and a lack of pattern-match with both the ON and the OFF responses are necessary to close the palps. **(b)** Comparison of the observed behavioral responses in four different stimulus conditions with the responses predicted by the active ON model and passive ON-OFF model are shown (see Methods). **(c)** Comparisons between the rise-time and the fall-time constants obtained using the responses

predicted by each model (y axis) and the actual POR responses obtained from behavioral experiments (x axis) are shown.

3.2.8 ON-OFF model is a better predictor of behavioral output

We sought to test these models for translating neural activity to behavioral output by perturbing the pattern-match with the ON responses. To achieve this, we first presented the trained odorant (hex) and a distractant (bzald) as a binary mixture whose components were delivered synchronously (**Fig. 3.17**). We found that the PN response to this mixture stimulus was dominated by a single component (hex), however, the pattern match with hex ON response templates (solitary presentations) was diminished (**Fig. 3.17a,b**). Matching these classification analyses results, we found that locusts trained with hex, responded to the binary mixture of hex and bzald with a similar reduction in POR (**Fig. 3.17c**). These results clearly demonstrate that reduction of pattern match with the ON response template of conditioned stimulus diminishes the behavioral POR responses.

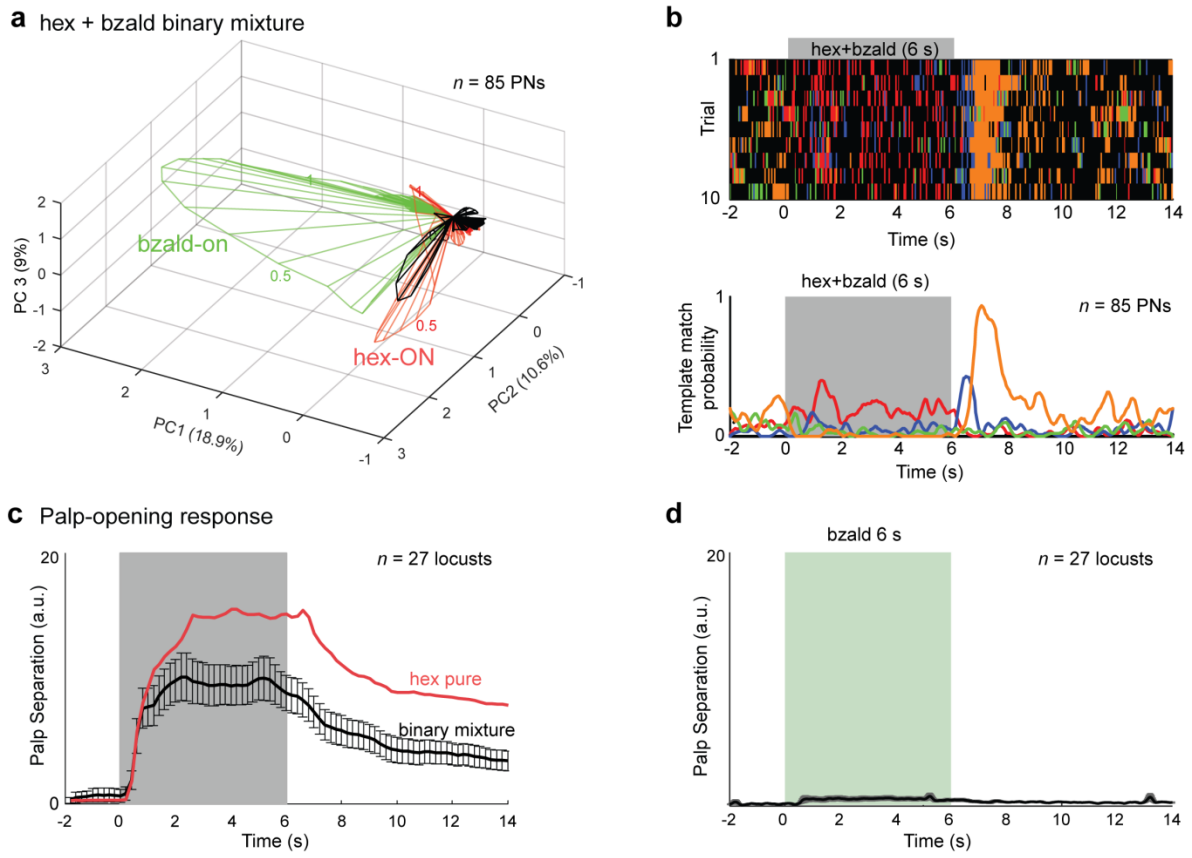

Figure 3.17: Neural and behavioral responses to a binary mixture and its components. (a) Neural trajectory for the mixture of hex and bzald where both components were introduced simultaneously (note only ON responses are shown for clarity). The synchronous binary mixture of hex-bzald generated population neural responses that were aligned more with the hex-ON response alone. This new data was collected from a different PN population as compared to **Fig. 3.10**. **(b)** Results from a bin-by-bin, trial-by-trial classification analysis are shown for the synchronous mixture of hex and bzald. The ON and OFF responses observed during solitary hex and bzald introductions were used as templates to be pattern-matched. Bottom, the probabilities of pattern-match with different response templates are shown as a function of time. **(c)** Median palp-opening responses are shown for a 6 s hexanol presentation (CS, in red) and the synchronous binary mixture (hex+ bzald, in black). Error bars represent s.e.m. Total of 27 locusts were tested for this study. **(d)** No significant palp opening response was observed when a 6 s bzald odorant was puffed solitarily.

Next, we presented the same two odorants in series such that onset of the distractant (bzald; untrained odorant) happened 500 ms before the termination of the conditioned stimulus (hex; **Fig. 3.15d)**. Consistent with previous findings[45], and unlike the synchronously presented binary mixture case, the neural activity remapped to gain pattern-match with the second odorant

in the sequence (i.e. bzald) following its onset. However, following the termination of the conditioned stimulus (hex), we found that the ensemble neural activity again remapped to gain similarity with the OFF response of the first odorant (i.e. hex; **Fig. 3.15d, Fig. 3.18a**). Interestingly, we found that the palp-opening response to hexanol (the conditioned stimulus) did not end when a distractant was introduced (**Fig. 3.15e**). Rather, the closing of palps began after the termination of the conditioned stimulus following epochs when pattern-match with hexanol OFF responses was observed (**Fig. 3.15e**). Therefore, the amount of time it took for closing palps following a mismatch with the ON responses doubled across the two conditions tested (**Fig. 3.15e,f**).

Two other observations are worth pointing out here. First, the distractant presented solitarily did not evoke a significant palp-opening response (**Fig. 3.15a**). So the prolongation of the POR after introduction of bzald cannot be explained based on the ongoing PN activity during this epoch as it pattern matched with the bzald ON template (**Fig. 3.15d**). Second, it is worth noting that in the overlapping sequence, the degree of pattern match with the hex OFF response template was diminished due to the presence of the distractant. Matching this physiological result, we found that the POR response termination was also slower than that observed in the case of solitary hex presentations (**Fig. 3.18b,c**). Therefore, these results suggest that after the palps have been opened, a pattern-match with the ON responses may not be necessary for sustaining the behavioral response. More importantly, gaining pattern-match with the OFF responses of the conditioned stimulus is a good indicator of the palp-closing response dynamics. This interpretation is supported by the modeling results, which revealed that only the ON-OFF model was able to generate consistent palp-closing behavior across conditions (**Fig. 3.15g, Fig. 3.16c**). Furthermore, we found that POR to the hex-0.5s overlap-bzald stimulus sequence can be

better predicted using results from the classification analysis than those directly made using the POR data. In other words, the time series of ensemble neural activities was Granger causal with the behavioral POR evolution over time ($f_{Neural->POR} = 7.37$, $P < 0.05$; see Methods).

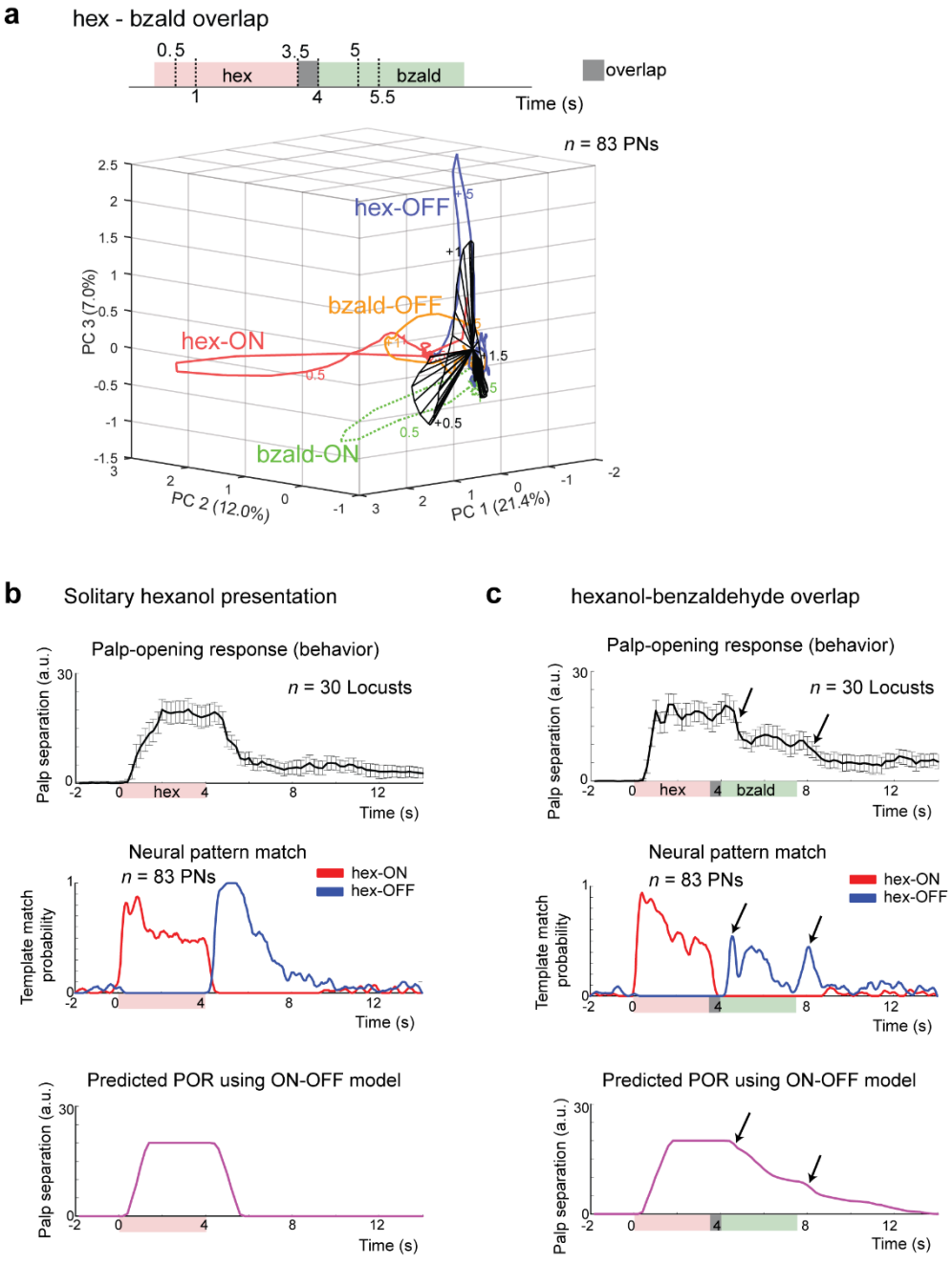

Figure 3.18: ON-OFF model a better predictor of POR. (a) Neural response trajectory evoked by the overlapping sequence of hex-bzald is shown. The black trajectory shows the 4 s period following bzald application. The response trajectories elicited by solitary presentations of hex and bzald are also shown to facilitate comparisons. Color-coded numbers on the plot indicate time since introduction of a particular odorant. *n* represents the number of neurons used for this analysis. **(b)** Top, the median palp opening response is plotted (± s.e.m; $n = 30$ Locusts) in the case of 4 s duration hexanol presentation. Middle, the ensemble neural response match with the hex-ON and hex-OFF template are shown during the odor onset and offset periods. Bottom, the predicted POR using the ON-OFF model (see Methods) is shown for 4 s hexanol solitary presentations. **(c)** Same format as in **panel b** but results are shown for the hex-0.5s overlap-bzald odor sequence.

Finally, to further confirm this hypothesis, we presented the conditioned stimulus (hex) in a pulsatile fashion (**Fig. 3.19**). We found that the ON and OFF responses precisely encoded the presence and absence of the hexanol puffs. As can be predicted, trained locusts opened or closed palps during epochs when hex ON and OFF responses were observed, respectively. Taken together, these results validate our hypothesis that orthogonal neural activities cause opposing behavioral responses in this olfactory system.

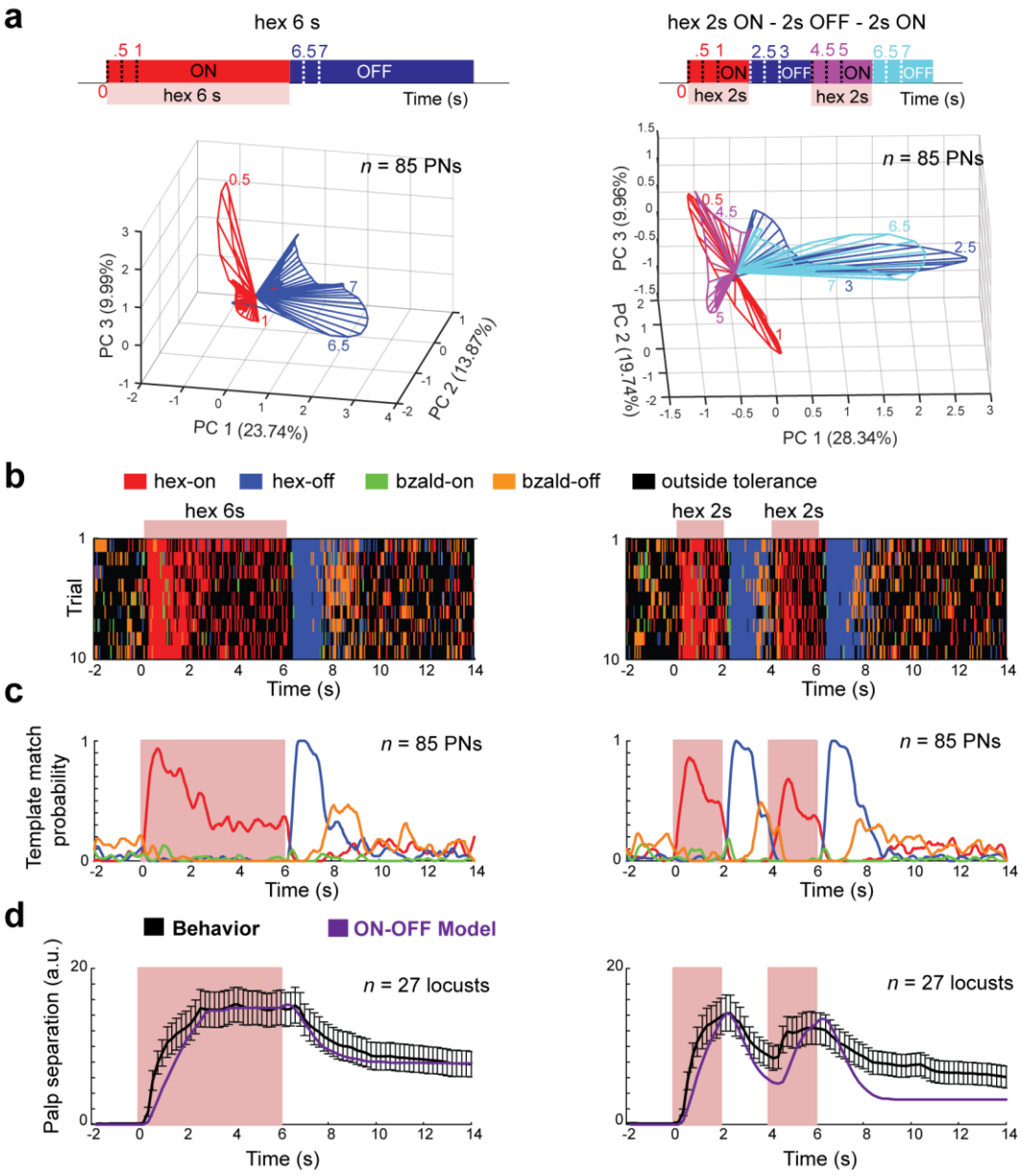

Figure 3.19: Neural and behavioral responses to odor pulses. (a) Left, ensemble PN response trajectory is shown for 6 s long hexanol pulse. ON and OFF trajectories are identified using red and blue colors, respectively. Right, PN response trajectory is shown for 2s ON–2s OFF–2s ON hexanol pulse. Red and purple portions of the trajectories indicate the ensemble ON activity during the first and second hexanol pulse (ON responses), and the blue/cyan trajectories trace the PN ensemble responses following the termination of the first and the second hexanol pulse. **(b)** Results from a classification analysis are shown in a bin-by-bin, trial-by-trial fashion. Based on the closest template, a class label has been assigned for each 50 ms time bin. hex ON response template – 'red tick mark', hex OFF response template – 'blue tick mark', and time bins when the ensemble neural activities that differed significantly from both hex ON and OFF response templates were labeled using a 'black tick mark'. Classification for ten trials are shown for 6s hex pulse and 2s ON–2s OFF–2s ON hexanol pulse. A leave-one-trial-out validation was

used for generating these results. The colored bar on the top indicates stimulus exposure periods. **(c)** The probabilities of pattern match with hex-ON and hex-OFF templates are plotted as a function of time for a uninterrupted 6s hexanol pulse and a 2s ON–2s OFF –2s ON hexanol pulses. **(d)** Behavioral palp opening responses are plotted (median ± s.e.m, n = 27 Locusts) for hex 6s and hex 2s ON–2s OFF–2s ON pulses. The prediction from the ON-OFF model (purple trace) is also shown for comparison.

3.3 Discussion

A behavioral response initiated by any sensory stimulus must be reset after its termination. In most cases, the response onset (deviation from baseline) following the stimulus introduction, and the reset (return to baseline) following its termination are by necessity opposites of one another. Is the behavioral response reset actively brought about by the neural circuitry, or is it a result of a passive return of stimulus-evoked activity to the spontaneous level? Two lines of evidences appear to suggest that a more direct representation of the stimulus absence will be necessary in most sensory systems. First, sensory memory following stimulus encounters may persist even after the termination of the stimulus [47, 112-114]. Second, in natural settings, sensory cues are mostly encountered in overlapping sequences, and a passive return to baseline may not happen until after all of the succeeding stimuli terminate. Furthermore, in sensory systems, absence of a stimulus can be as informative as their presence (light vs. dark [115, 116] or heat vs. cold in temperature sensing [117, 118]). Taking into account that most sensory stimuli generate another round of transient activity following stimulus termination [8, 97, 98], it would appear that an active signal regarding the absence of stimulus is available in many sensory systems.

For the OFF responses to encode stimulus absence, the neural activities during this epoch must be different from the ON responses and exclusively encode for each stimulus. Our results indicate that the ensemble neural activities at sound and odorant offsets were nearly orthogonal to (i.e., independent from) the ON responses. Nevertheless, both these neural activities during

stimulus onsets and offsets were able to uniquely encode for identity and intensity of a sensory cue. Importantly, while the onset responses were necessary for the initiation of the behavioral response ('the palp-opening response'), our results reveal that the offset responses are necessary to actively terminate it ('the palp-closing response'). Thus, orthogonal neural activities encoded for presence and absence of a stimulus, and were translated to generate behavioral responses that were opposites of one another (start/onset vs. stop/reset). Such mapping of distinct neural activities to generate behavioral responses that are opposites of one another have indeed been shown in a number of neural systems [103, 117-124]. Our work is the first to show that a single sensory stimulus can activate unique and independent sets of neurons during and after its presentation in order to meet opposing behavioral output demands during these epochs.

3.4 Author Contributions

Part of the work described in this chapter has been published as: D. Saha, W. Sun, C. Li, S. Nizampatnam, W. Padovano, Z. Chen, A. Chen, E. Altan, R. Lo, D. L. Barbour, B. Raman. Engaging and disengaging recurrent inhibition coincides with sensing and unsensing of a sensory stimulus. *Nature communications* (2017).

B.R. conceived the study. D.S. and B.R. designed the olfaction experiments. C.L. and B.R. designed the analysis methods. Z.C. and B.R. developed the computational model. D.S., C.L., S.N., and B.R. performed the experiments and the analysis. W. P. performed the behavioral experiments and their analysis. S.N., A.C., E. A., R.L., performed portions of additional experiments and analyses that were necessary to address the reviewers' comments. B.R. wrote the paper, incorporating inputs and comments from all authors. B.R. and D.L.B. provided overall supervision.

Chapter 4: Dynamic contrast enhancement and flexible odor codes

4.1 Introduction

The key task of a sensory system is to transduce and represent information about environmental cues as electrical neural activities so that the organism may generate an appropriate behavioral response. The precise format in which neural activities represents stimulus-specific information i.e. 'the neural code' has been a topic of great debate in neuroscience [32-37]. Both patterns of spiking activities distributed across an ensemble of neurons [14, 38, 52, 125-128] (i.e. 'the spatial code'), and the temporal features of these neural spike trains such as their synchronicity [11, 41], relative response latencies [42, 43, 129], dynamics [12, 35, 44, 45, 48, 82, 107, 130] (i.e. 'the temporal code') have been shown to be important for sensory coding. While stimulus-specific information exists in both spatial and temporal dimensions, what is not understood is the stability or constancy with which these neural coding schemes allow recognition of the same stimulus encountered in a variety of different ways. We examined this issue in this study.

Alternately, flexibility in sensory representation will be necessary for carrying out certain computations. Often, sensory cues encountered by an organism change dynamically, and the same sensory cue can be encountered in a variety of different contexts (for example, coffee beans in a coffee shop or in a perfume shop). Therefore, emphasizing novelty/uniqueness or suppressing/masking redundancies becomes necessary for detecting changes in the environment. Previous electrophysiological [45, 55, 131-133], imaging [134], and psychophysical [135] studies do indeed reveal such interactions exists particularly when sensory cues are dynamically encountered. Can certain aspects of the neural responses be adapted to allow the flexibility

needed for adaptive computations, while at the same time maintaining stable recognition of stimulus identity?

We examined this issue in the locust olfactory system. The insect olfactory system has been widely used for studying odor coding [11-14, 41, 45, 46, 48, 52, 54, 82, 97]. In this system, an odor stimulus is detected by olfactory receptor neurons (ORNs) in the antenna and the transduced electrical signals get relayed downstream to the antennal lobe (analogous to the olfactory bulb in the vertebrates). In the antennal lobe, cholinergic projection neurons (PNs) and GABAergic local neurons (LNs) interact to reformat the sensory input received from the ORNs. The spatiotemporal activity patterns of the PNs are thought to represent odor identity and intensity [8, 45, 46, 48, 52, 130]. In this work, we examined how the spatial and temporal aspects of neural responses are altered when a target stimulus is delivered in several non-overlapping distractors–target odor sequences. Our results suggest a surprisingly simple neural encoding solution that provides an adequate trade-off between the representational stability needed for robust recognition and flexibility needed for adaptive sensory computations.

4.2 Results

4.2.1 PN responses vary depending on stimulus history

We began by examining how stable or variable were odor-evoked individual PN responses when the same stimulus was delivered with different stimulus histories. Variations in stimulus histories were introduced by delivering the same odorant (‘target stimulus’) in various distractor–target odor sequences. A 500 ms inter-stimulus interval was used to separate the two stimuli delivered. Five different odorants were used as distractor cues and two target stimuli were used in all our experiments (**Fig. 4.1a,b**). It is worth noting that the distractor odorants comprised of

four odorants belonging to different functional groups (2octanol (2oct) – an alcohol, isoamyl acetate (iaa) – an ester, benzaldehyde (bzald) – an aldehyde, citral – a terpene), and a complex blend (apple). The target odorant comprised of an odorant that has been shown previously as suitable for associative conditioning (hexanol), and an innately attractive odorant (geraniol) [45].

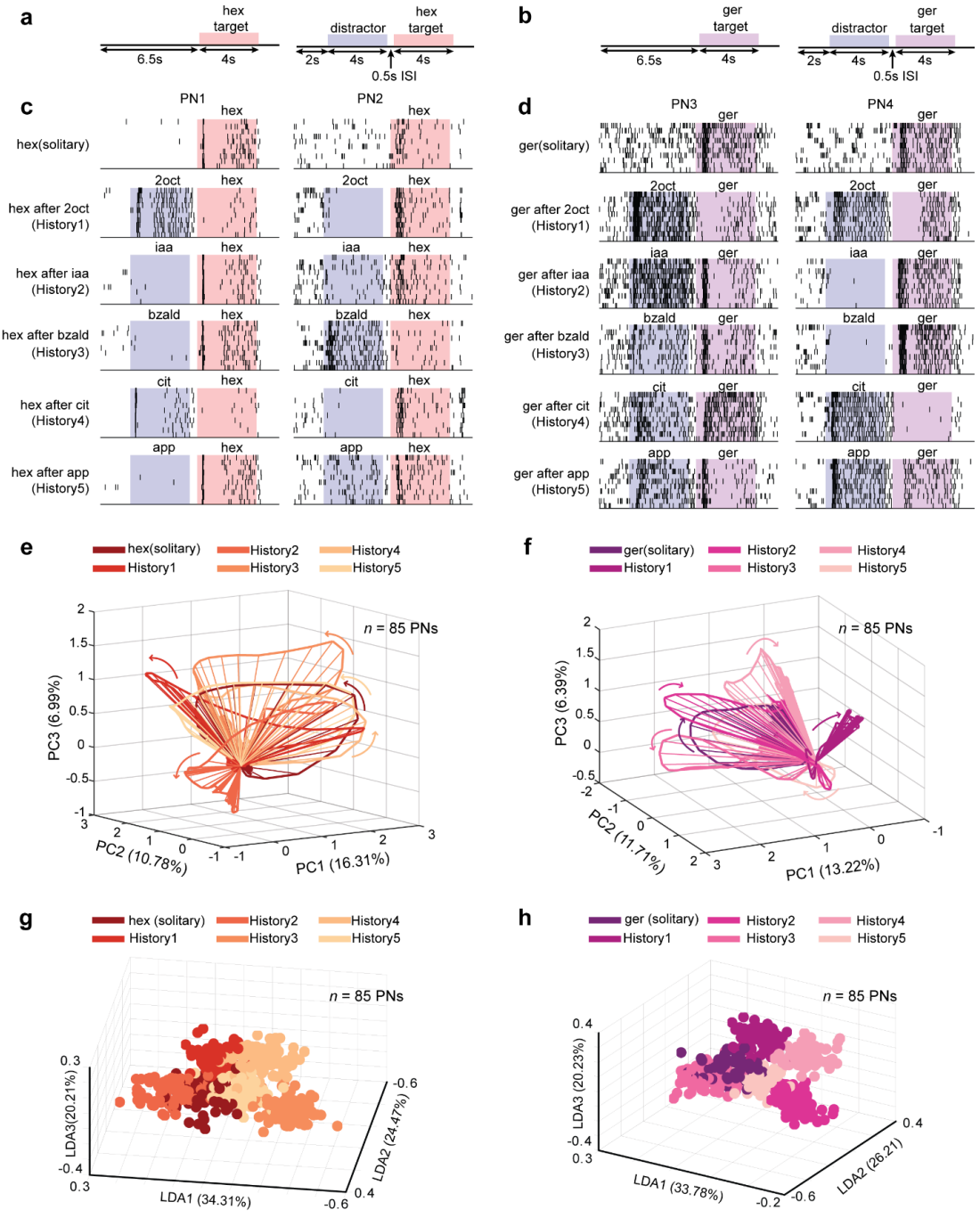

Figure 4.1: Projection neuron responses vary in a stimulus-history dependent manner. (a, b) Distractor-target sequences used in this study are shown. A target stimulus (hexanol – hex or geraniol – ger) was presented solitarily or in a non-overlapping sequence with a distractor cue. All target and distractor stimuli were presented for 4 s. The time interval between the termination of the distractor stimuli and the onset of the target stimulus was 500 ms. **(c)** Spiking responses of two different projection neurons (PNs) in the locust antennal lobe are shown. Each tick mark represents an action potential fired by the PN. Each row corresponds to one trial and PN responses in ten consecutive trials are shown for assessing the repeatability of observed spiking response patterns. The duration when the distractor (blue) and target (red) stimuli were presented are shown using colored boxes. As can be noted, the target stimulus (hex) can be presented solitarily (top panel) or following one of the five different distractor cues: history1 – 2octanol (2oct), history2 – isoamyl acetate (iaa), history3 – benzaldehyde (bzald), history4 – citral (cit) and history5 – apple (app). **(d)** Similar plots as in **panel c** but showing responses of two more PNs to presentations of geraniol (ger) with different stimulus histories. **(e)** Responses of eighty-five PNs projected onto the first three principal components are shown. Each spoke represents the ensemble neural activities in a 50 ms time bin after PCA dimensionality reduction. Arrows indicate direction of evolution of the stimulus-evoked responses over time. The six trajectories shown correspond to PN responses observed following the introductions of the target stimulus either solitarily or in one of five stimulus sequences. **(f)** Similar trajectory plots as in **panel e** but visualizing ensemble PN responses evoked by introductions of geraniol (ger) with different stimulus histories. **(g)** Population PN responses are shown after linear discriminant analysis dimensionality reduction (n = 85 PNs). Each 3D-sphere represents an eighty-five-dimensional PN activity vector in a 50 ms time bin. Eighty data points corresponding to ensemble neural activities evoked during 4 s of hexanol exposure with a particular stimulus history are assigned the same color. **(h)** Similar plot as in **panel g** but showing responses elicited during geraniol exposures.

We found that although responses of individual PNs during solitary introductions of the target stimulus were reliable across trials, they were altered when the same stimulus was delivered with different stimulus histories (**Fig. 4.1c,d**). When compared to the solitary target odor responses, the number of spikes increased for some stimulus histories (e.g. PN2 2oct-hex vs. PN2 hex) but reduced for others (PN2 bzald-hex vs PN2 hex). Further, note that increase/decrease in target stimulus response was not based on the chemical similarity between the two cues delivered in the sequence. Our results indicate a simple rule for cross-talk: if a PN responded strongly to the first cue in the sequence (i.e. the distractor) then its response to the second stimulus (i.e. the target) was likely to be reduced. Alternately, if the spiking activity reduced below baseline levels during exposure to the distractor cue, then its response to the

following target increased in most cases (all comparison made with respect to the response evoked by the solitary target stimulus; **Fig. 4.2a,b**).

Next, we examined how the variations observed at the individual PN level affected the ensemble neural representation of the target stimuli. To visualize odor-evoked population PN responses, we used a dimensionality reduction analysis. Individual PN responses were aligned with the odor onset and binned in 50 ms time windows. The spike count per time bin of each PN became a vector component, and the spike counts of all recorded PNs in that same time bin were regarded as the high-dimensional neural response. The time series of high-dimensional PN responses during the entire target stimulus presentation (4 s duration) was then projected along three principal component axes (see Methods). We found that introduction of the same stimulus generated not one ensemble neural response trajectory but a family of trajectories, one for each stimulus history. Further, consistent with the earlier studies [8, 45, 54, 97], we found that all introductions of the target stimuli generated ensemble neural trajectories that included a fast-transient response component (~1 – 1.5 s from odor onset) that subsequently stabilized into steady state responses. Notably, the direction of the high-dimensional vectors (indicates variation in the set of PNs activated), and the direction of their evolution (variation in spatiotemporal patterning) during the target stimulus presentation varied in a history dependent manner. This can be clearly noted from the misalignment between the family of neural response trajectories generated during the exposure to the same target stimulus (**Fig. 4.1e,f**).

How distinct or separable are these responses generated by the same stimulus? To examine this, we used a supervised dimensionality reduction technique (linear discriminant analysis or LDA) that seeks to capture the differences between the ensemble neural responses evoked by the target odorant. Projecting the data along the LDA axes, we found that the target

stimulus-evoked PN responses created multiple, separable clusters, one for each stimulus history with which it was presented (**Fig. 4.1g,h**). This qualitative observation was further quantified using a classification analysis (**Fig. 4.2c,d;** see Methods). Therefore, we conclude that both at the individual and population levels, PN responses that are thought to mediate identification of an olfactory stimulus in the insect olfactory system can vary significantly when the same stimulus is encountered with different histories.

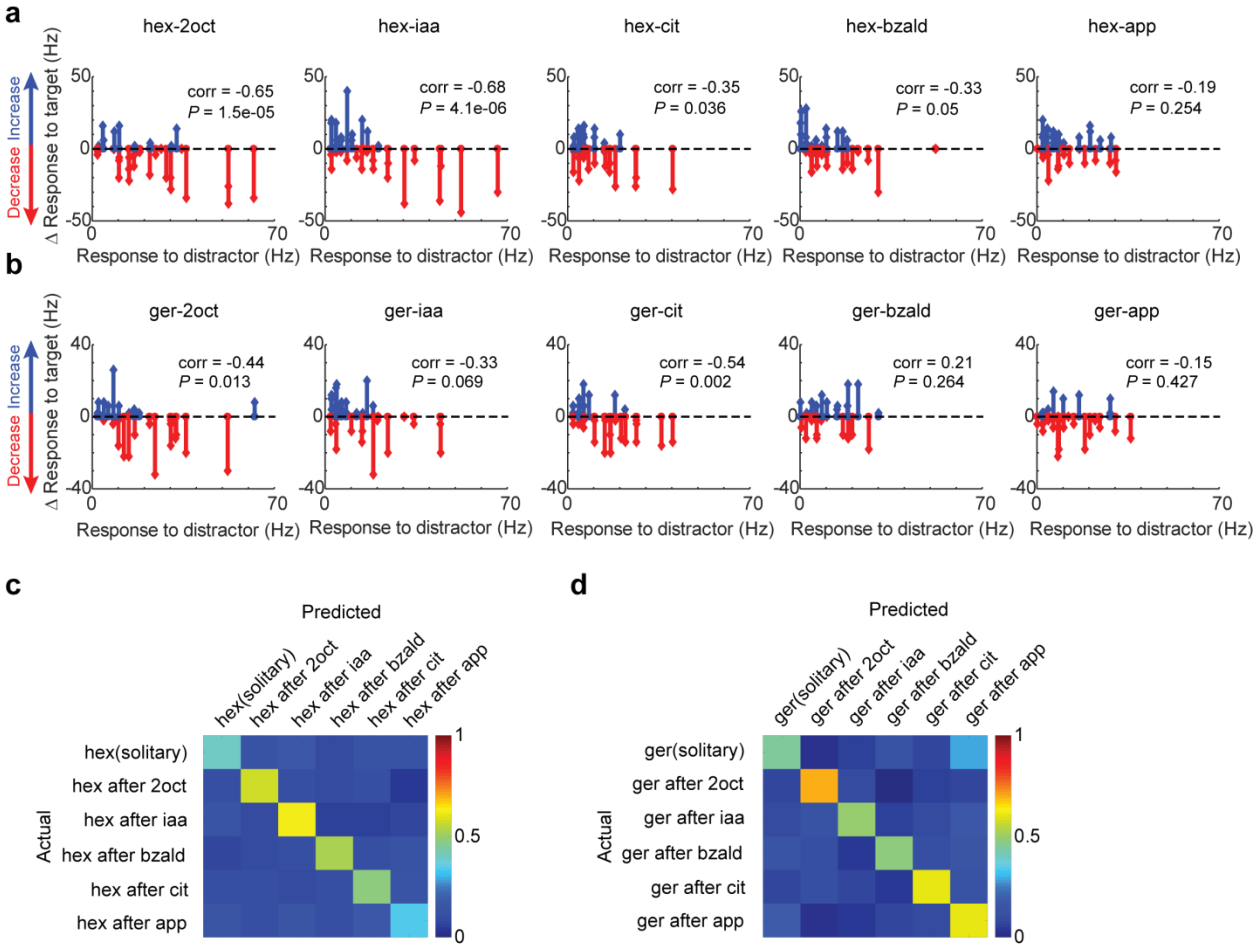

Figure 4.2: PN responses of a stimulus become separable following distracting stimuli. (a) Change in PN responses to the target odorant (y axis) vs. response to distractor (x axis) is plotted for five distractor-target pairs (the target odorant is hex in all cases). The maximum spike rate in a 50 ms time bin during the first 1 s of odor presentation is shown for all PNs that were excited by hex (n = 36 PNs for solitary hex; see Methods for PN response categorization). Zero represents identical response to both solitary and sequential presentation of the target odorant. Red lines indicate that the response to target after distractor

is less than the response to target alone (i.e. negative values). Blue lines indicate increase in the response for target after distractor when compared to target alone (i.e. positive values). A very small uniform random noise has been added to jitter the points with same x-values and reduce overlap between colored lines. Correlations between the change in target odor response and response to distractor odor (corr values) and their significance levels are shown on each panel. **(b)** Similar plots as **panel a** but plotted when the target odor was ger (n = 30 excitatory PNs for solitary ger). **(c)** The separability of the PN responses (six categories: hex(solitary) and five sequential conditions of hex) is quantified and shown as a confusion matrix. Rows correspond to the actual stimulus identity and the columns indicate the predicted stimulus identity. A nearest centroid method with leave-one-out cross-validation in 85-D space was used for generating these classification results (see Methods). Note that the confusion matrix is mostly diagonal indicating that the PN responses evoked by the same stimulus presented with different histories are distinct. **(d)** Similar plot as in **panel c** but the confusion matrix analyzing the response separability of the solitary and sequential geraniol presentations is shown.

4.2.2 Stimulus-history dependent contrast enhancement

Are these variations in odor-evoked ensemble neural responses random? To examine this issue, we compared the neural responses evoked by solitary and sequential presentations of the target stimulus with the distractor cue (**Fig. 4.3a,b; Fig. 4.4a,b**). Our results indicate each olfactory stimulus evoked a closed-loop trajectory that evolved in a unique direction. As can be expected from our earlier analysis, the solitary and the sequential introductions of the same target stimulus generated two different neural response trajectories. As a rule, compared to the solitary target stimulus response, when presented following the distractor cue, the ensemble response trajectory shifted further away from the responses evoked by the distractor cue. This is consistent with individual and ensemble PN response analyses (**Fig. 4.1c,d** and **Fig. 4.5**) where we found that during sequential presentations of the target stimulus, common neurons were suppressed (i.e. responds to both target and the preceding distractor stimulus), whereas those that responded uniquely to the target odorant tended to increase.

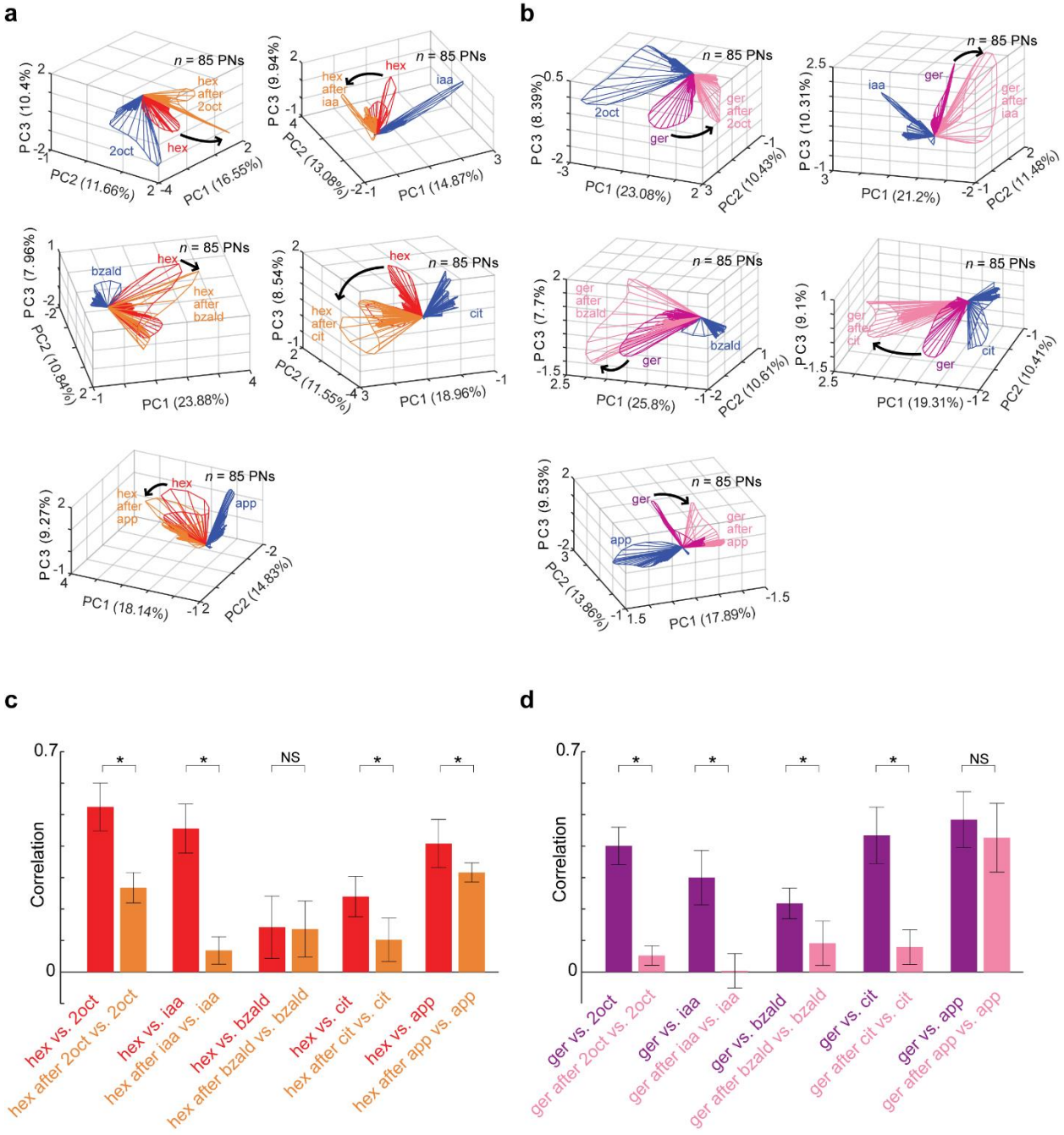

Figure 4.3: Dynamic contrast enhancement of odor-evoked ensemble responses. (a) Similar trajectory plots as shown in **Fig. 4.1e** but comparing the population PN responses generated during solitary presentations of the distractor odorant (blue trajectory) and target odorant (red trajectory) with responses elicited by the same target odorant presented after the termination of the distractor cue (orange trajectory). Five plots are shown corresponding to hexanol introductions in the same five stimulus sequences shown in **Fig. 4.1a,c**. Note that compared to the red trajectories, the orange trajectories are more distant from the blue trajectories in every panel. **(b)** Similar plots as in **panel a** are shown for five sequential presentations of geraniol. It is worth noting again that compared to the solitary geraniol responses (purple trajectories), the responses observed during sequential presentations (pink trajectories)

are more distant from the distractor cue evoked responses (blue trajectories) in every panel. **(c)** The mean of correlation values between the ensemble PN responses (n = 85 PNs) evoked by hexanol and the five distractor cues are shown as bar plots. Error bars indicate ± s.d across ten trials. The mean odor-evoked responses during the initial 1 s after stimulus introduction was used for computing these correlations. Red bars quantify similarities between solitary distractor cue and solitary hexanol presentations. Orange bars indicate similarities between the solitary distractor cue and sequential hexanol presentations. Asterisks indicate a significant decrease in the correlation (*P < 0.05, NS: P > 0.05, paired t-tests, n = 10 trials). **(d)** Similar plots as in **panel c** but geraniol is used as the target odorant.

As a direct consequence, the angular separation between neural response trajectories between the target and distractor cues increased, which can be expected to enhance discriminability between these two odorants (i.e. contrast enhancement). To quantify this, we used a correlation analysis where we compared the similarity between ensemble PN activities evoked by the target stimulus and the distractor cue. We made this comparison for both the solitary exposure of the target stimulus and the sequential presentations (**Fig. 4.3c,d;** similar analysis but for later response segments shown in **Fig. 4.4c,d**). As can be noted, the correlation between the distractor cue and the target stimulus significantly reduced during sequential presentation of the target stimulus. Further, the shift in the ensemble responses were predictable using a linear approximation where the target odor response was added with the target minus distractor response (i.e. uniqueness; see **Fig. 4.6**). Hence, our results indicate that alterations in the ensemble neural responses allow the antennal lobe circuit to enhance the uniqueness of the target stimulus with respect to the preceding cue i.e. dynamic, history-dependent contrast enhancement.

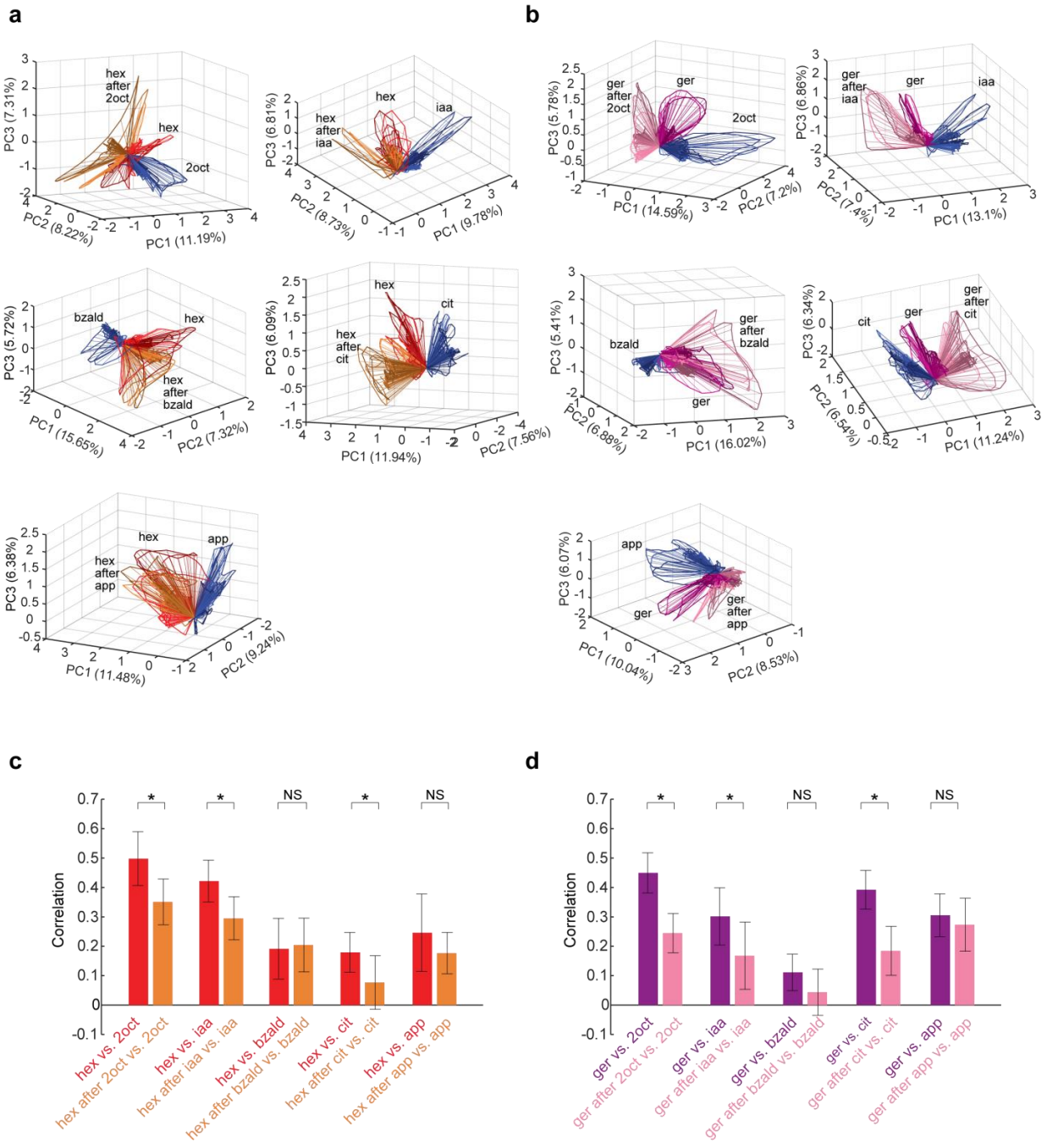

Figure 4.4: Contrast enhancement is more prominent than trial-to-trial variations. (a) Similar trajectory plots as shown in **Fig. 4.3a,b** but trial-to-trial variations are included. Population PN responses evoked by the distractor odorant, hex, and the sequential presentation of hex are shown for three sets of trials: mean of trials 1-3, mean of trials 4-6, and mean of trials 7-10. The darker colored traces correspond to the earlier set of trials. **(b)** Similar plots as in **panel a** but shown for five sequential presentations of geraniol. **(c, d)** Similar plots as in **Fig. 4.3c,d**, but the correlations are now computed using the mean odor-evoked response during the last 1 s of stimulus presentation window.

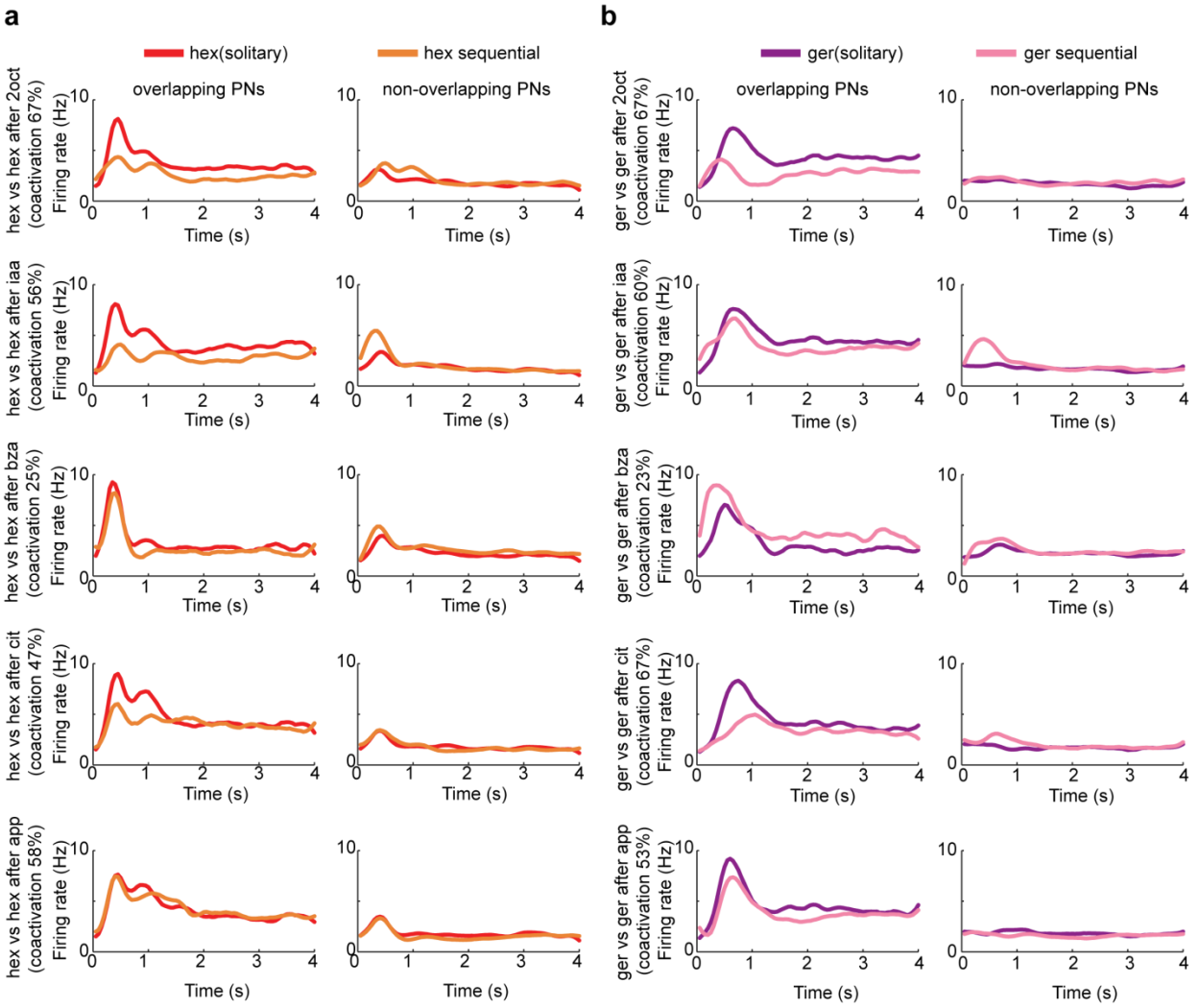

Figure 4.5: Common neurons get suppressed and unique ones get enhanced. (a) Comparison between the mean firing rates averaged across two distinct sets of PNs is shown for the solitary (red trace) and sequential presentations (orange traces) of hex. Overlapping PNs correspond to the set of PNs that were responsive to both the target (hex) and distractor odorant. 'Non-overlapping PNs' correspond to the remaining set of PNs that were not 'overlapping PNs'. Left panel shows the firing rate of overlapping PNs averaged across trials (n = 10). Right panel shows the firing rate of non-overlapping PNs averaged across ten trials. The percentage of overlapping PNs (i.e. co-activation) for each distractor odorant is shown. **(b)** Similar plots as in **panel a** but comparing the mean firing rates of overlapping and non-overlapping PNs during solitary and sequential geraniol presentations.

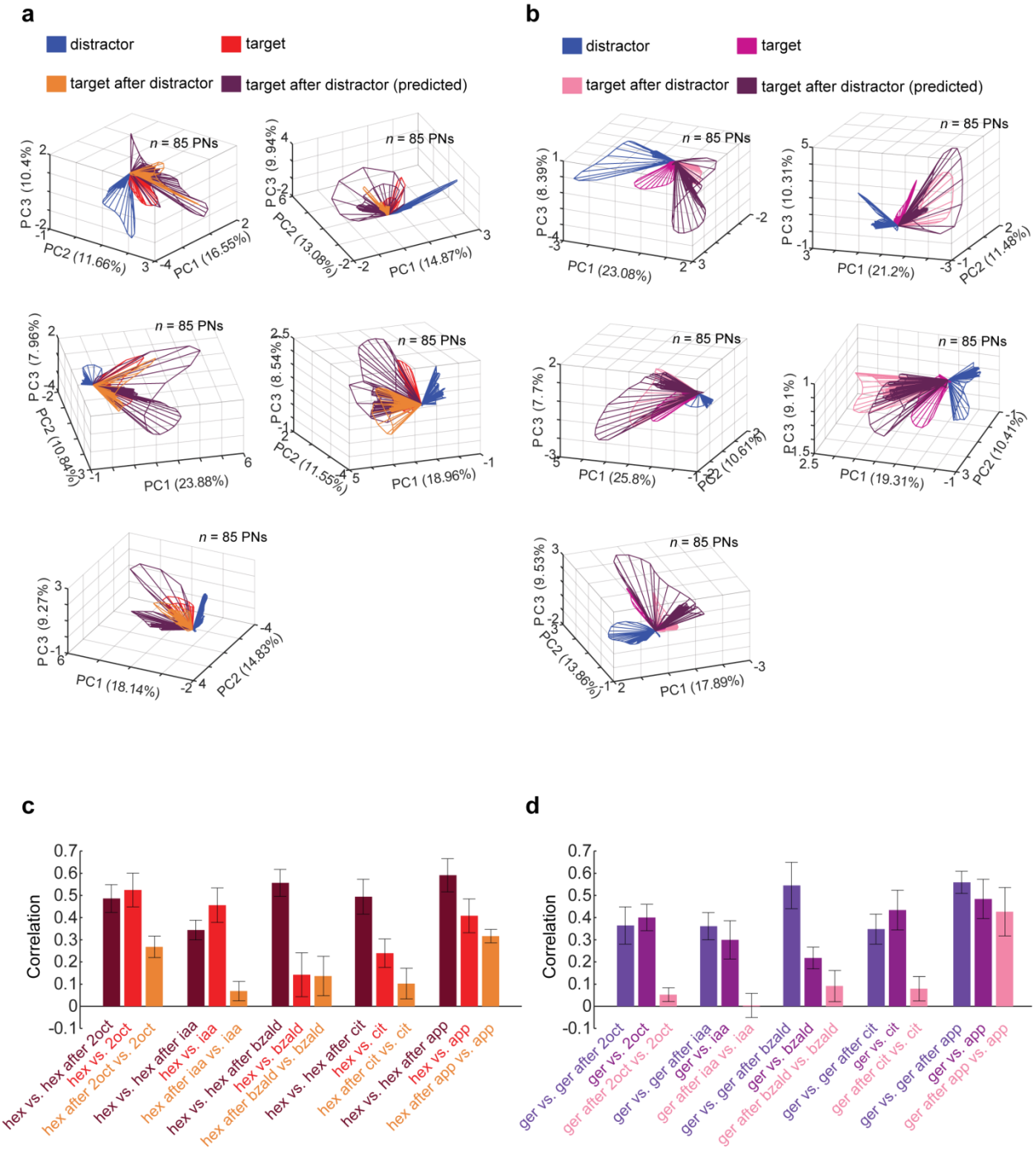

Figure 4.6: PN response variations can be predicted using a linear combination. (a, b) Similar plots as in **Fig. 4.3a, b.** Predicted response trajectory is shown in each panel along with response trajectories for distractor, target, and target after distractor. The predictions were made for each target after distractor by taking a sum of target vector and (target vector - distractor vector) at each time bin. **(c, d)** Similar plots as in **Fig. 4.3c, d**, but correlations between target alone and target after distractor are also shown for comparison.

4.2.3 Same stimulus can activate varying combinations of neurons

To enhance contrast with different distractor odorants, the same target stimulus must activate a different subset of the PNs. So, we wondered if there exists a unique set of neurons that is activated during all the target stimulus presentations to allow stable recognition. To understand this, we classified the PN responses into 'responsive' or 'non-responsive' categories (see Methods). We found that the percentage of neurons activated and the composition of the set of responding neurons varied when the same target stimulus was presented with different histories (**Fig. 4.7a,b**). Further, the percentage of PNs that consistently responded to all introductions of hexanol and geraniol (the two target stimuli) was a smaller fraction of the set that responded to the solitary introductions of these two target stimuli.

To represent the identity of the target stimulus, the set of neurons must be consistent as well as unique. So, we examined how many of these consistent neurons were also unique responders i.e. respond to target stimuli alone (**Fig. 4.7c,d**). Surprisingly, we found that there was not a single PN that responded uniquely and consistently to hexanol in all the conditions. Only 2% neurons responded uniquely and consistently to geraniol presented with different stimulus histories. Therefore, our results indicate that combinatorial code involving a consistent and unique set of neurons may not be a suitable approach for achieving stable recognition of a sensory stimulus encountered with varying stimulus histories.

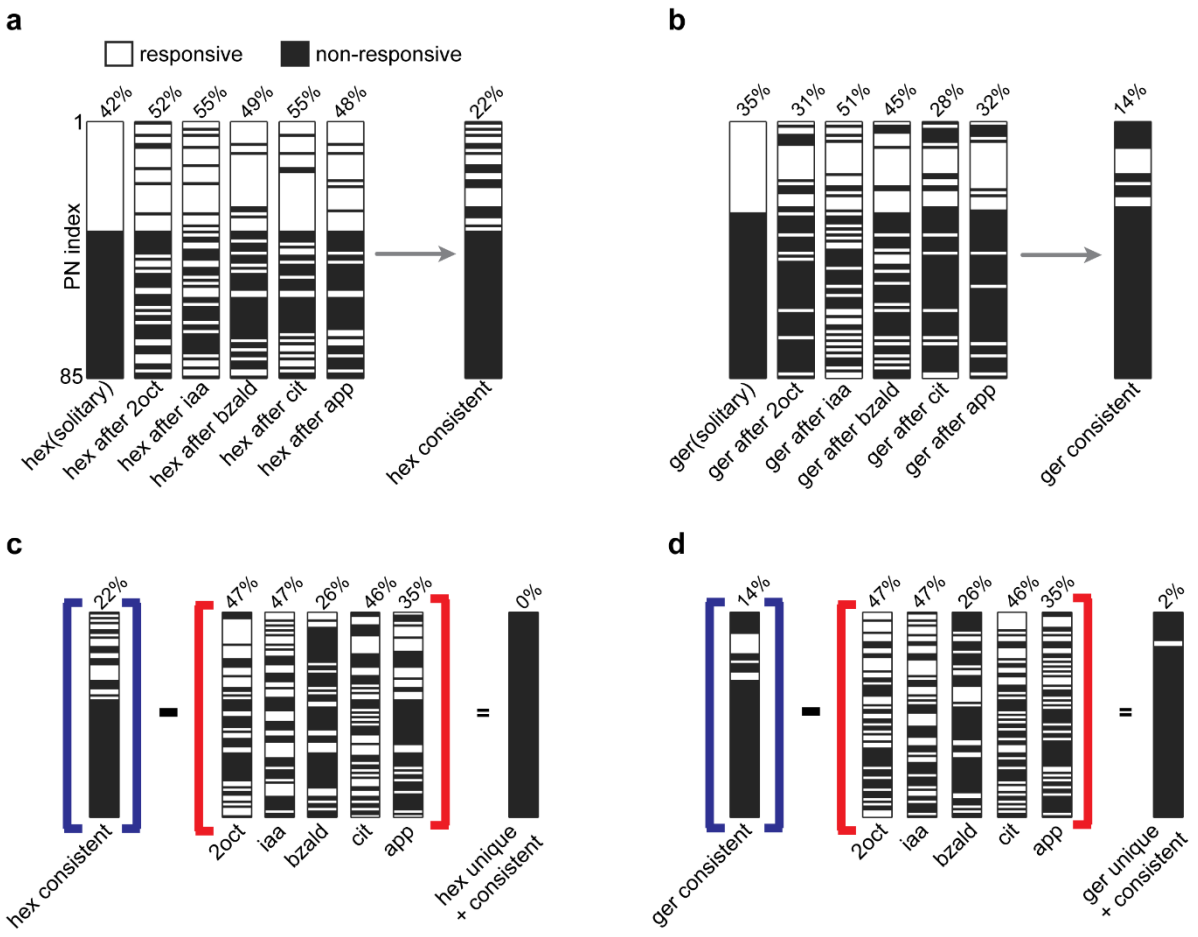

Figure 4.7: Evaluating the stability of the combinatorial code. (a) Each projection neuron was classified as being 'responsive' or 'non-responsive' to the target stimulus (see Methods) and the classification of all eighty-five neurons are shown as a barcode. This binary classification was done for solitary and sequential introductions of hexanol. Note that all barcoded PNs are identically sorted and displayed to facilitate comparison. The percentage of PNs classified as being responsive during each hexanol presentation is shown above the barcode. The set of PNs classified as being responsive for all hexanol introductions is identified as the 'consistent set' and is also shown as rightmost barcode. **(b)** Similar plot as in **panel a** but comparing geraniol responsive and non-responsive set of PNs is shown. **(c)** Barcodes identifying responsive and non-responsive PNs for the five different distractor stimuli are shown. These PNs were removed from the set of neurons activated during all introductions of hexanol i.e. 'the consistent set', to identify those PNs that were both consistent and unique responders to hexanol (the rightmost barcode). As can be noted, this is an empty set for hexanol. **(d)** Similar plot as in **panel c** but identifying the unique and consistent set of PNs that responded to geraniol. For geraniol, this set consisted of only 2% of the PNs.

4.2.4 Temporal response features also vary with stimulus history

How robust are temporal features such as response latency and pattern of stimulus-evoked spike trains in allowing stable odor recognition? To examine this, we defined the response latency as the first time bin when a neuron's response exceeded a certain threshold value (see Methods; **Fig. 4.8a,b**). We then classified neurons as early responders (latency < 600 ms) or late/non-responders (latency > 600 ms). Note that the early responders were PNs that responded before behavioral response onset (median ~600 ms [45, 46]). For visualization, we represented this classification of the response latency across the ensemble of PNs as a color bar **(Fig. 4.9a,b**). The response latency vector was generated for different introductions of the target stimulus and shown as a color bar to allow comparisons. Our results indicate that depending on the stimulus history, some of the early responding projection neurons to the solitary presentations of the target stimulus became late/non-responsive in the sequential presentations, while some of the late/non-responders became early-responders. Furthermore, only a small subset of neurons consistently responded early to the target stimuli. Similar to the combinations of PNs activated (**Fig. 4.7**), the sets of consistent early responders that were also unique responders to the target stimuli were empty or near empty sets (**Fig. 4.9c,d**).

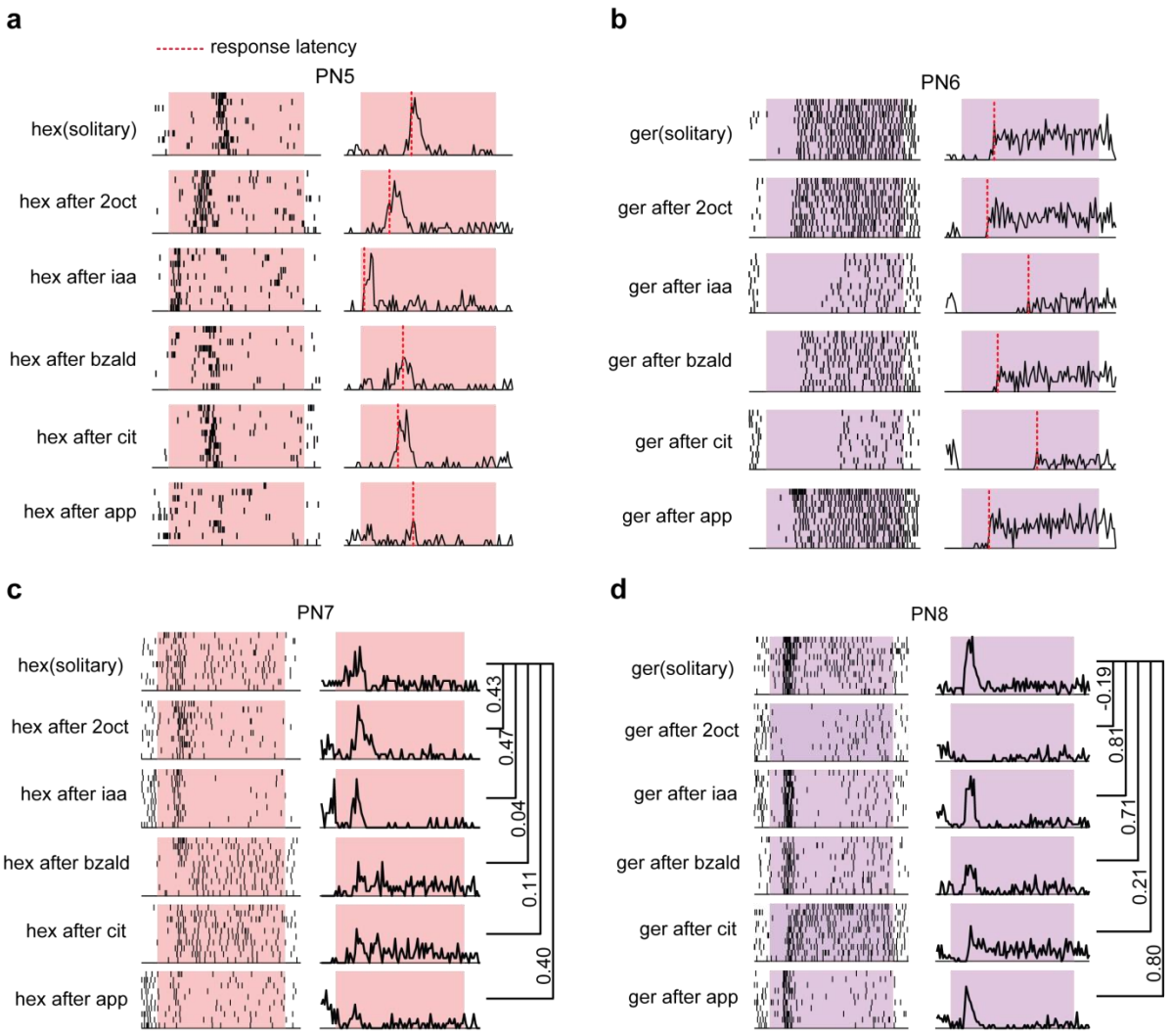

Figure 4.8: Response latency and temporal response patterns vary with stimulus history. (a) Left panel, raster plots showing spiking response of a PN to solitary and sequential introductions of hexanol. Same conventions as **Fig. 4.1c**. Right panel, mean spike counts in 50 ms time bins across trials are plotted as a function of time. The first time bin when the firing rate exceeds a fixed threshold was defined as its response latency and is identified using a dotted vertical line in each panel. **(b)** Similar plots as in **panel a** but showing the response of a different PN to solitary and sequential introductions of geraniol. The evolution of firing rates over time and the response latency for each geraniol presentation are shown. **(c)** Left panel, raster plot showing a representative PNs spiking responses to different hexanol introductions. Right panel, mean spike counts plotted as a function of time. Correlations between firing rate patterns observed during different sequential hexanol introductions with solitary hexanol presentations are shown. **(d)** Similar plot as in **panel c** showing the spiking response variations for different geraniol introductions.

How robust are other features of PN responses such as the pattern of their stimulus-evoked spike trains? To examine this, we considered the evolution of trial-averaged PN spike

counts over time (during the 4 s of target stimulus presentation) as the temporal response vector. We computed the correlation between the PN temporal response vectors generated by the same target stimulus presented with different stimulus histories (**Fig. 4.8c,d**). The distribution of this temporal pattern similarity metric for each target-history combination revealed that more correlation values were closer to a value of ‘zero’ rather than ‘one’ (**Fig. 4.9e,f**). This indicated that the temporal patterns of PN spiking activities also change considerably with stimulus history.

Taken together, these results indicate that temporal features of PN responses are also highly variable and may not allow robust recognition of a stimulus when it is encountered with different stimulus histories.

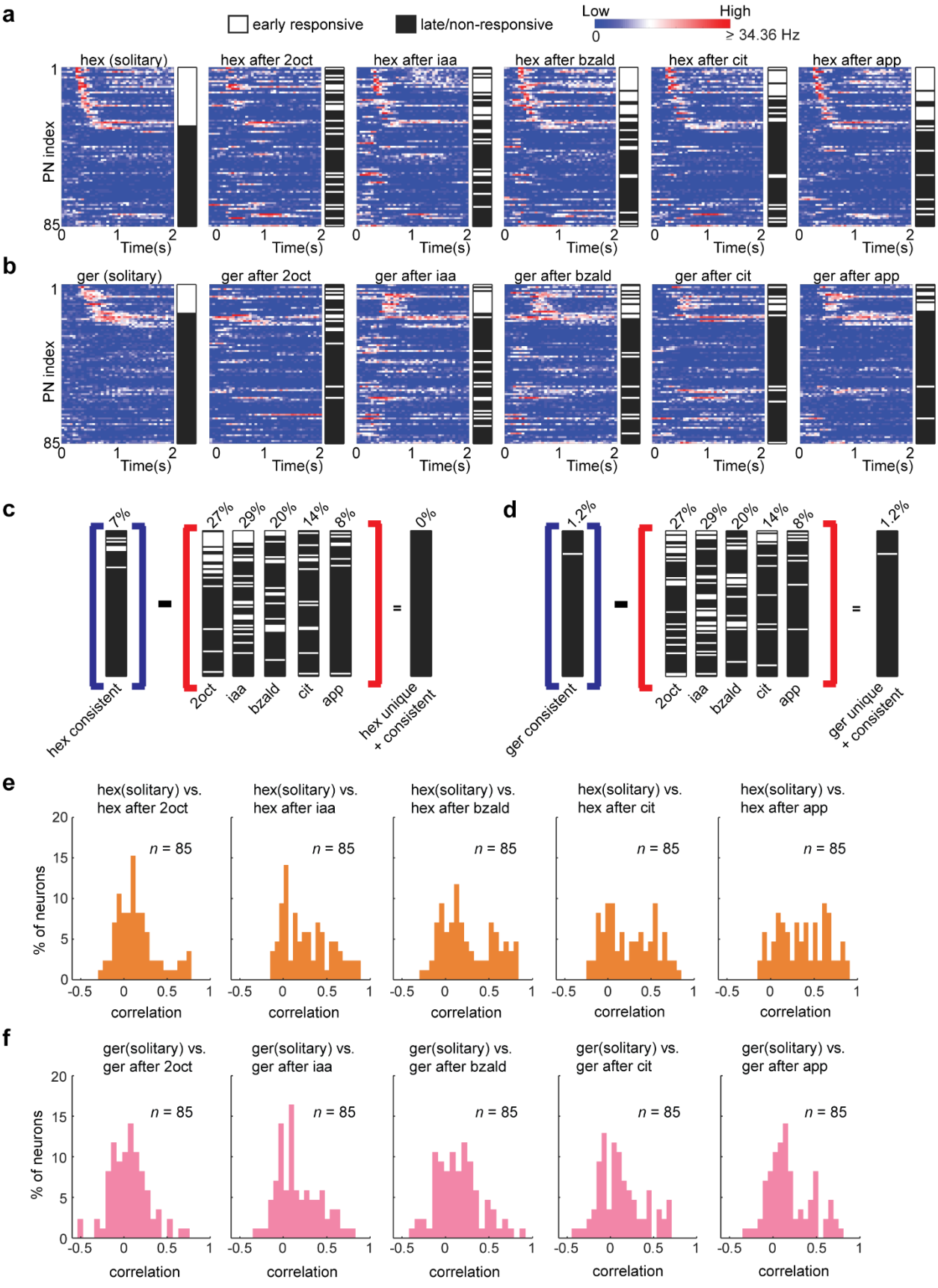
a
early responsive
late/non-responsive
Low
High
0
≥ 34.36 Hz
hex (solitary)
hex after 2oct
hex after iaa
hex after bzald
hex after cit
hex after app
PN index
Time(s)
b
ger (solitary)
ger after 2oct
ger after iaa
ger after bzald
ger after cit
ger after app
c
7%
27%
29%
20%
14%
8%
0%
hex consistent
2oct
iaa
bzald
cit
app
hex unique + consistent
d
1.2%
ger consistent
ger unique + consistent
e
hex(solitary) vs. hex after 2oct
hex(solitary) vs. hex after iaa
hex(solitary) vs. hex after bzald
hex(solitary) vs. hex after cit
hex(solitary) vs. hex after app
n = 85
% of neurons
correlation
f
ger(solitary) vs. ger after 2oct
ger(solitary) vs. ger after iaa
ger(solitary) vs. ger after bzald
ger(solitary) vs. ger after cit
ger(solitary) vs. ger after app

Figure 4.9: Temporal response features vary with stimulus histories. (a) Firing rates of eighty-five neurons during the 2 s following hexanol introductions are shown. A log scale was used to allow comparison between different PNs. Firing rates in 50 ms time bins were averaged across trials and are shown as a function of time. Note that the PNs were sorted based on their response latency to solitary hexanol introductions with early responders at the top and late/non-responders at the bottom. The color bars next to the firing rate plots reveal the response latency category of each PN: early responders in white and late/non-responders in black. Firing rates of the PN ensemble and the response latency vector are shown for solitary and sequential introductions of hexanol. **(b)** Similar plots as in **panel a** but now showing PN responses and their latencies to solitary and sequential introductions of geraniol. **(c)** Same analysis as in **Fig. 4.7c,d**. Barcodes identifying the set of PNs that responded consistently early during solitary and sequential hexanol introductions is identified. The early responsive and late/non-responsive PNs for the five different distractor stimuli are also shown. The set of PNs that were both consistent and unique early responders to hexanol is identified (the rightmost barcode). As can be noted, this is an empty set for hexanol. **(d)** Similar plot as in **panel c** but identifying the unique and consistent set of PNs that responded early to geraniol. For geraniol, this set consisted of only 1.2% of the PNs. **(e)** Distributions of correlation values between PN spike trains for each sequential introduction of hexanol with solitary hexanol responses are shown. **(f)** Similar plots as in **panel e** but analyzing PN responses to solitary and sequential introductions of geraniol.

4.2.5 Robust behavioral recognition

Our electrophysiological results indicated that combinations of neurons and their temporal response features changed when the same stimulus was presented with different histories. Therefore, we wondered if locusts can behaviorally recognize a conditioned stimulus if it is presented in a similar fashion. To determine this, we trained locusts using an appetitive-conditioning paradigm. Briefly, during the training phase, starved locusts were presented a conditioned stimulus (hexanol; also target stimulus in electrophysiology experiments) followed by a food reward (wheat grass) with significant stimulus-reward overlap (see Methods). Six such training trials were sufficient for the locusts to learn the association between the olfactory cue and the reward. In an unrewarded test phase, locusts that learned this association between the stimulus and reward opened their sensory appendages close to their mouths called maxillary palps in anticipation of the reward. The distance between the palps was tracked using a custom-written software and used as a metric for successful recognition (see Methods). Notably,

responses of the trained locusts to the conditioned stimulus were consistent even when the same stimulus was presented multiple times without reward during the test phase. Therefore, we assayed the palp-opening responses of the trained locusts to the conditioned stimulus presented with varying stimulus histories (**Fig. 4.10a–f**).

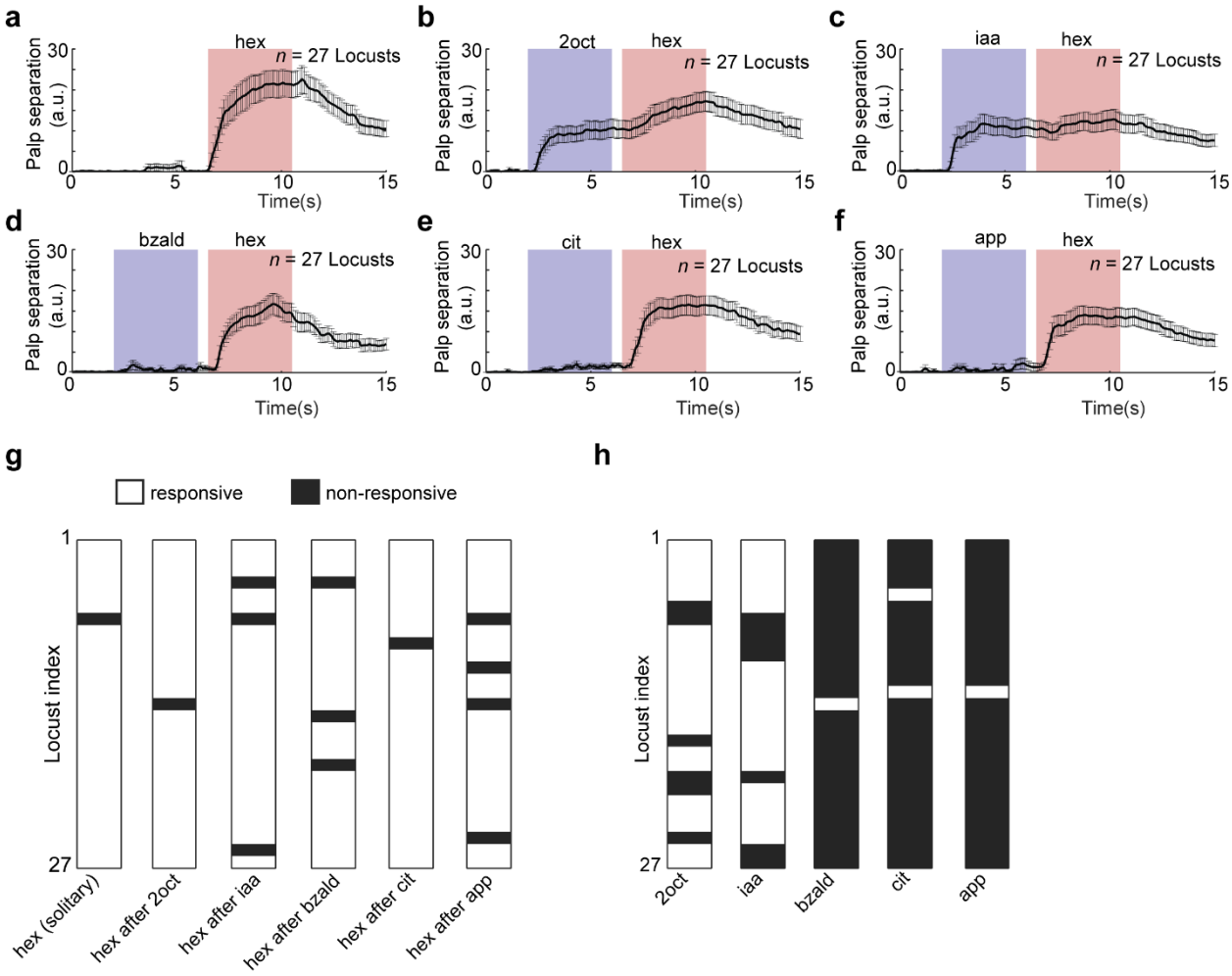

Figure 4.10: Robust behavioral response to a conditioned stimulus. (a) Locusts were trained to associate an odorant with a food reward. Trained locusts subsequently responded to the conditioned stimulus presentations by opening their sensory appendages close to their mouths called maxillary palps. The distance between the palps was tracked and plotted as a function of time. Mean palp-opening response of locusts trained to recognize hexanol (conditioned stimulus) is shown. Error bar represents standard error across locusts (n = 27). **(b–f)** Palp opening responses to five different sequential presentations of hexanol (i.e. the conditioned stimulus) are shown. Note that these stimulus sequences are identical to the ones used in our physiology experiments. **(g)** PORs of each locust to hexanol were classified as responsive and non-responsive and shown for solitarily and each sequential presentation of

the conditioned stimulus. **(h)** PORs of each locust to the five distractor odorants: 2oct, iaa, bzald, cit, and app are shown.

We observed that trained locusts responded to the conditioned stimulus (hexanol) irrespective of whether it was presented solitarily or in a sequence following a distractor cue (**Fig. 4.10g**; see Methods). While three of the five distractor cues did not elicit a palp-opening response (POR), two odorants (2oct and iaa) evoked POR responses that were weaker than those observed during solitary presentations of the conditioned stimulus (**Fig. 4.10h, Fig. 4.10b–f**). It is worth noting that both 2oct and iaa elicit PN responses that have considerable overlap with those evoked by hexanol[46]. So, there is some generalization of the learned POR response to these 'similar' odorants. Such olfactory generalizations have been reported in other invertebrate models[136, 137] and are consistent with our prior neural/behavioral results (2oct-hex odor pair [45, 46]). Evaluation of POR responses to an expanded odor panel with five additional distractor-target odor sequences indicates that the behavioral responses of locusts are indeed highly selective to the trained odorant (**Fig. 4.11**).

In sum, our behavioral data reveal that trained locusts were able to robustly recognize the conditioned stimulus.

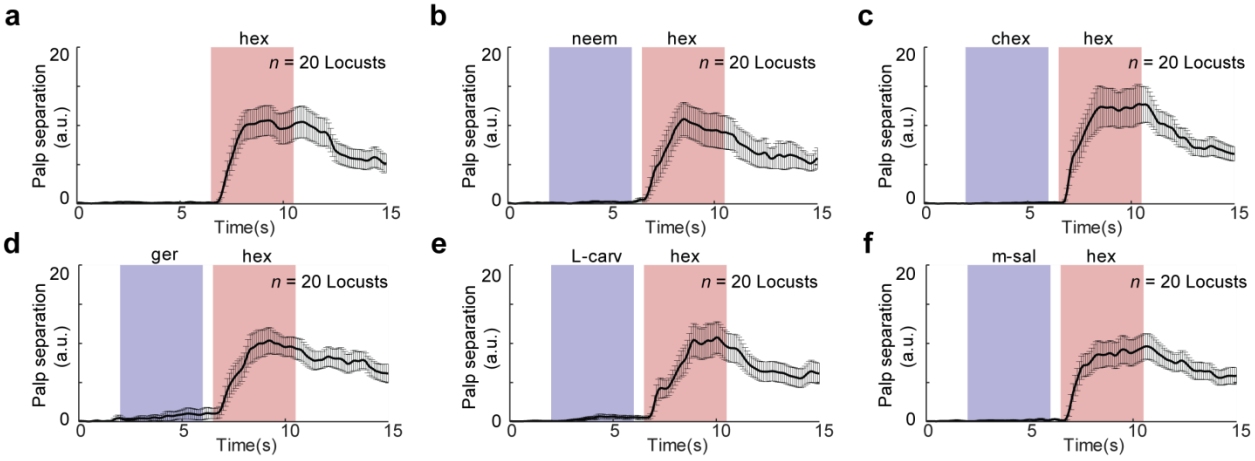

Figure 4.11: Robust behavioral response is more generalized. (a-f) Palp-opening responses (POR) to additional distractor-target odor sequences are shown. The distance between the palps was tracked and plotted as a function of time. Error bar represents standard error across locusts (n = 20).

4.2.6 Decoding with an optimal linear classifier

Can the behavioral responses to distractor-conditioned stimulus sequences be predicted from the ensemble PN neural activities? To understand this, we first sought to determine whether the target can be robustly recognized in a distractor-target sequence (i.e. pairwise odor classification). For this approach, we used a linear optimal classifier (linear support vector machine[86, 126]) to separate the target odorants from all five distractor stimuli (**Fig. 4.12a**). Surprisingly, we found that this was indeed feasible and the target stimulus can be robustly discriminated and recognized (**Fig. 4.12b**). Note that for '*n*' neurons this approach would require '*n+1*' free parameters (*n for the weight vector* v_{svm} *and 1 bias term).* The PN responses to target odor and all the distractor odorants must be known to determine the right set of parameters. Furthermore, even though the classification results show that robust recognition of the target stimulus is feasible from the ensemble PN activities, it still does not match well with the behavioral POR observed for these stimuli. Particularly, it is worth noting that this approach did

not generate the false positives for 2oct and iaa even though these odorants generated false PORs in the behavioral assay.

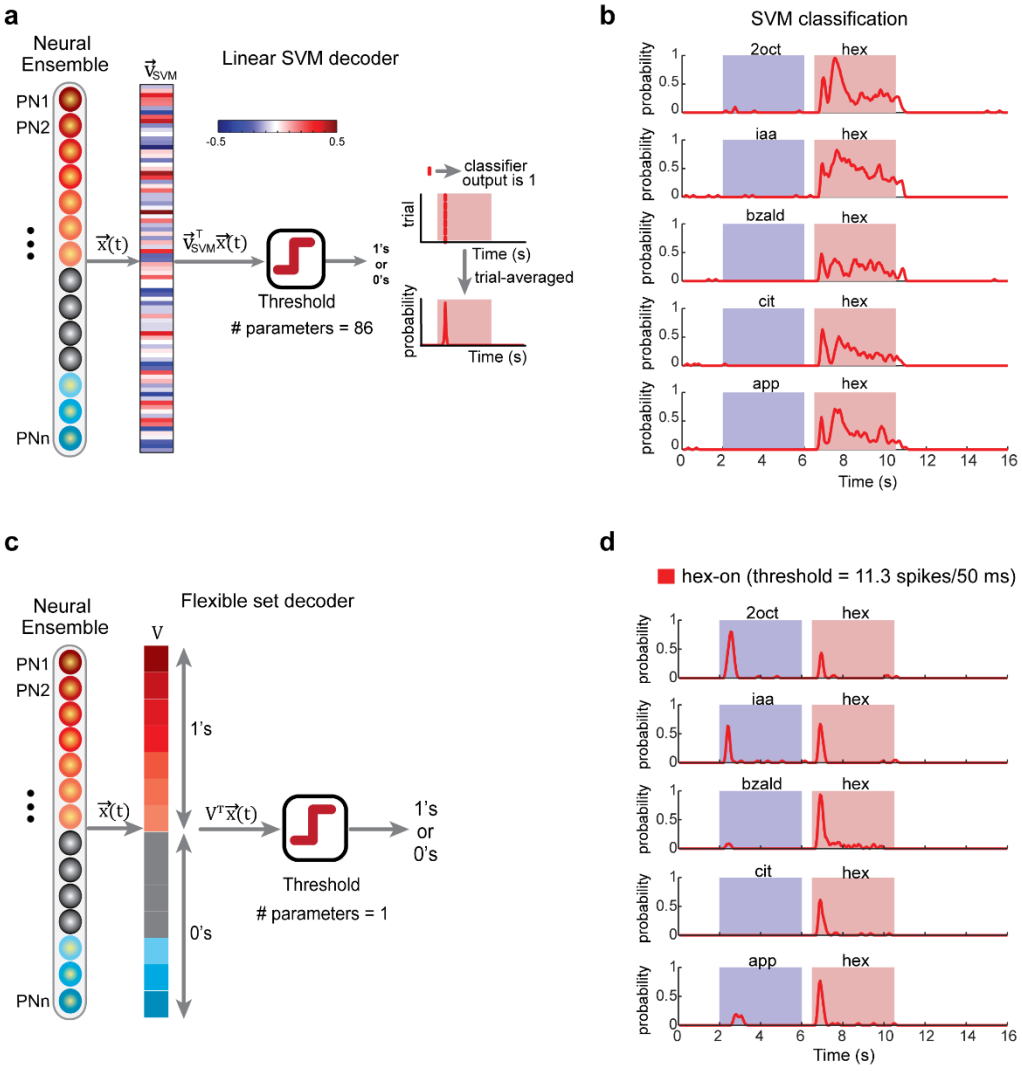

Figure 4.12: Linear neural decoding of ensemble neural activities. (a) A schematic of the multi-class linear support vector machine (SVM) classifier is shown. Here again the input to the classifier was an eighty-five-dimensional ensemble PN activity vector in a 50 ms time bin ($x(t)$). The optimal weight vector that separates hexanol responses for all other odor-evoked and baseline activities was determined and is shown as a color bar (v_{svm}). Contribution of each PN was weighted based on the corresponding weight-vector component ($v_{svm}{}^{T} x(t)$) and thresholded to produce a binary classification output: 'hexanol present' or 'hexanol absent'. Note that the number of parameters here are 86 (number of neurons and threshold). Probability of classification in each time bin was determined by averaging classification results across trials. **(b)** The probabilities of hex classification using the linear SVM classifier, across trials are plotted as a function of time for different hexanol presentations. **(c)** A schematic of the flexible set decoder is shown. Ensemble PN activity vector in a 50 ms time bin ($x(t)$) was the input to the classifier. The weight

vector *v* had the same number of components as x(t). A vector component of '1' was assigned corresponding to PNs that were responsive to the solitary hexanol introductions, and '0' was assigned corresponding to non-responsive PNs. A dot product of *x(t)* and *v* resulted in summation of all hexanol responsive PNs. This scalar value was subsequently thresholded to determine the classifier output. The threshold to be exceeded was set to allow flexible subsets of neurons to contribute towards reaching the cutoff value. A digital version of the classifier when input vector *x(t)* was also binarized and is shown in **Fig. 4.13**. **(d)** Classification probabilities for the flexible set decoder are shown. Same convention as in **panel b**. The value of the only free model parameter, i.e., the classification threshold, is also reported.

4.2.7 Flexible neural decoder: OR–of–ANDs

We sought to determine the simplest approach to transform ensemble PN responses into behavioral PORs. To design this decoder, we exploited the observation that for pairs of target stimulus presentations with varying histories there was a substantial overlap in the set of neurons activated (**Fig. 4.7a**). However, when all stimulus histories were considered simultaneously, the set of consistent and unique PNs reduced significantly. Therefore, we reasoned that a decoder capable of exploiting information distributed in a flexible subset of neurons would allow robust recognition of the target stimulus.

To design the flexible classifier, we summed the contributions of all neurons activated by solitary introductions of the target stimulus and disregarded the contributions of all other projection neurons (i.e. weight of '*1*' for each neuron activated by solitary introductions of the target stimulus, and '*0*' for all others). Next, the classification threshold (*m*) was set to a value less than the number of neurons (*n*) assigned a weight of '*1*' (i.e. $m < n$). It is worth to note that the classifier becomes analogous to an OR-of-ANDs logical operation: *m-1* ANDs and *n choose m* ORs (or combinations) can generate an output of '*target present*' from the classifier (**Fig. 4.12c**). Any *m*-out-of-*n* neurons that respond to the solitary introductions of the target stimulus are sufficient for robust recognition of the target stimulus. Also, note that the composition of the *m* neurons is allowed to vary across stimulus histories under this scheme.

We examined performances of both analog (PN firing rates were retained) or digital (binarized into 'responsive' and 'non-responsive') versions of this linear classifier (**Fig. 4.12d** – analog classifier**, Fig. 4.13** – digital classifier). In both cases, the classification results from the OR-of-AND classifier revealed robust recognition of all presentations of the target stimulus. Interestingly, misclassifications were made for 2oct, iaa, and apple. It is worth noting that both 2oct and iaa evoked POR in locusts trained for recognizing hexanol. However, any further manipulation of classifier's free parameter (i.e. threshold or value of *m*) to reduce misclassification for apple, resulted in overall recognition performance degradation.

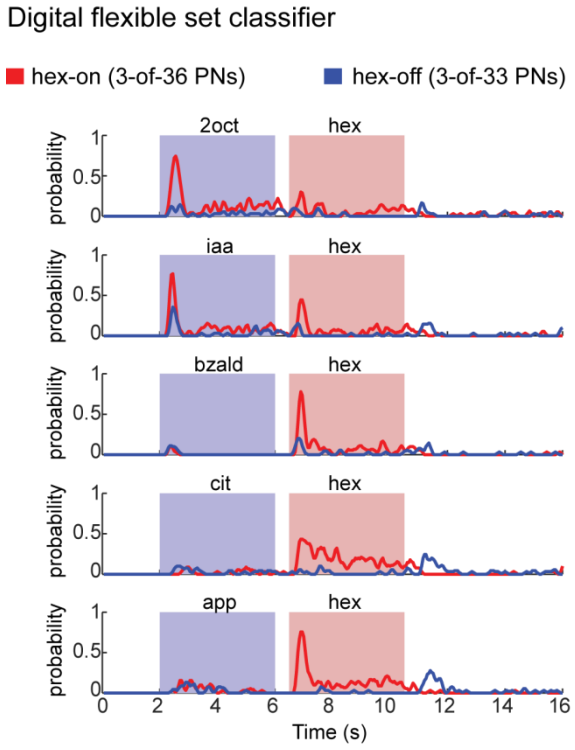

Figure 4.13: Flexible decoding using OR-of-ANDs. Classification results for the digital version of the flexible set decoder are shown. For any 50 ms time bin, the threshold for ON classification was set to be 3–of–36 PNs must be responding to the stimulus presentation (i.e. firing rate > 6.5 s.d. of pre-stimulus activity). The threshold for OFF classification was also set to be 3–of–33 PNs. The 36 hex-ON PNs and 33 hex-OFF PNs were determined based on solitary hexanol presentations alone. Note that these classification results are very similar to the analog version that we presented in **Fig. 4.14b**.

An earlier work showed that following termination of an odor pulse, a nearly non-overlapping set of neurons are activated(OFF ensemble neural response)[82]. These odor-evoked OFF responses are stimulus-specific. More importantly, a pattern-match with the ON neurons allowed prediction of palp-opening response and a pattern-match with the OFF neurons were better indicators of palp-closing. Therefore, we modified the decoding scheme to include two OR-of-AND classifiers, one for monitoring similarity with the set of hex-ON neurons, and the other to track the similarity with the set of hex-OFF neurons. Note that the weight vectors used for the hex-ON and hex-OFF classifiers were highly non-overlapping (or orthogonal; **Fig. 4.14a,b**). Our results indicate that the performance of this ON-OFF flexible decoder (**Fig. 4.14c–i**) was comparable to the ON response model except for one important difference. We found that unlike 2oct and iaa, distractor cues that evoked POR, apple alone activated comparable pattern-matches with both hex-ON and hex-OFF neurons. When the classifier outputs were transformed into behavioral responses (**Fig. 4.14i**), these contributions cancelled each other out (palp-opening vs. palp-closing). Therefore, the ON-OFF flexible decoder predicted mean POR trends that tightly matched with those observed in our behavioral experiments for all distractor-target odor sequences.

In sum, we conclude that a decoding scheme based on flexible combinations of neurons would allow stable recognition of an odorant while allowing the antennal lobe circuits to adapt their ensemble responses in a stimulus-history dependent manner.

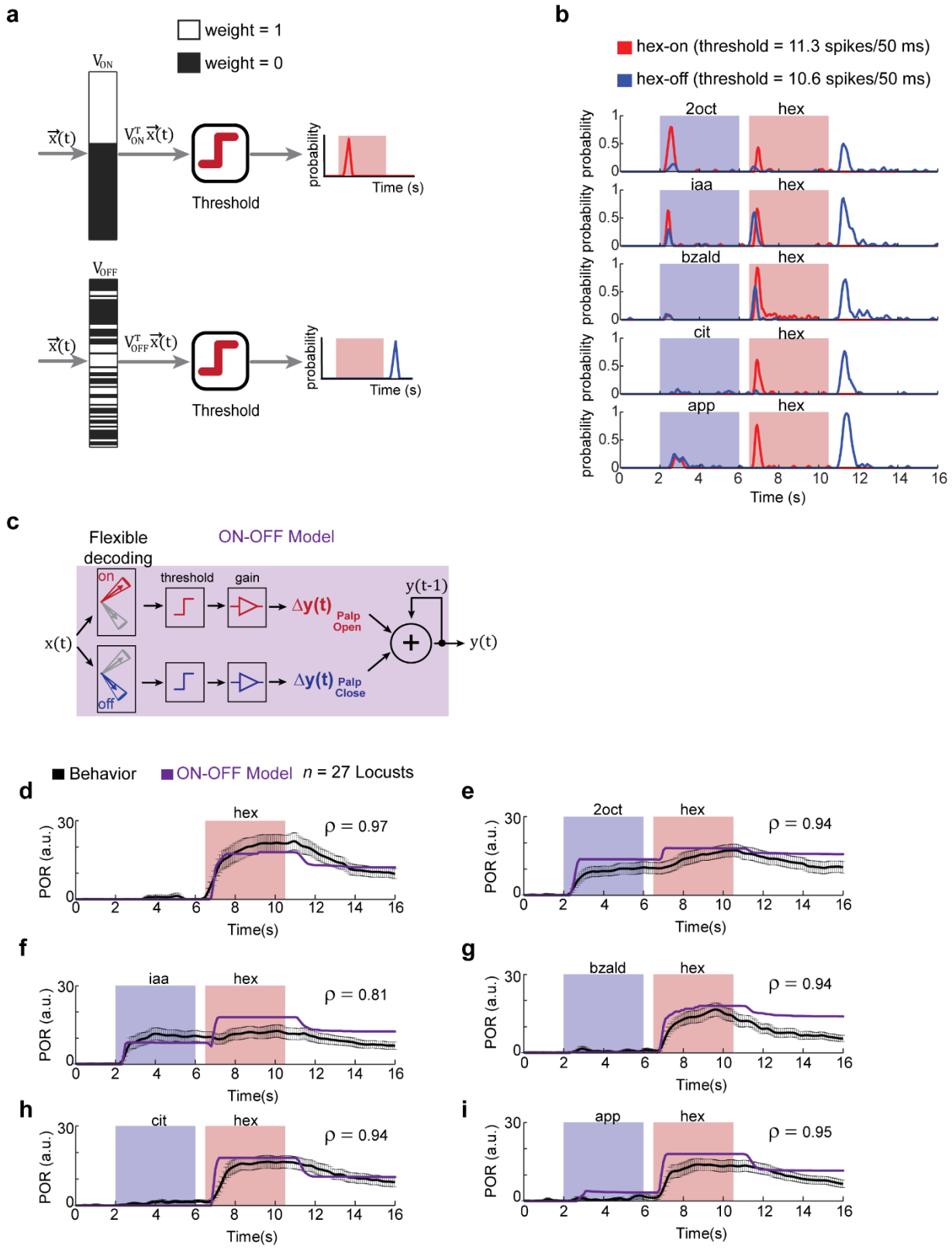

Figure 4.14: Predicting behavioral responses from neural activities using flexible decoding. (a) V_{ON} and V_{OFF} weight vectors used for generating classification results are shown. Vector component with a

value ‘1’ (i.e. responsive PN) are shown in white and the vector component corresponding to the non-responsive PNs is shown in black. Note that the set of PNs activated during and immediately after hexanol presentations are nearly non-overlapping. **(b)** Results from two flexible set decoders using weight vectors V_{ON} and V_{OFF} are shown. V_{ON} was a binary weight vector with a vector component *‘1’* corresponding to PNs responsive during hexanol presentation (i.e. stimulus ON epochs). V_{OFF} was also a binary weight vector but with a vector component *‘1’* corresponding to those PNs that were activated after the termination of the hexanol presentation (i.e. stimulus OFF period – a 4 s time window that began 500 ms after stimulus termination). Probability of classification for hex-on (shown in red) and hex-off (shown in blue) over time are shown for the odor sequences. **(c)** A schematic of the *ON-OFF* model for translating the classification results from the flexible set decoder using V_{ON} and V_{OFF} weight vectors into behavioral PORs. The classification probabilities (i.e. red and blue traces shown in **panel b**) were appropriately thresholded and scaled to generate the PORs. Note that pattern match with ON responses were used to generate palp-opening responses, whereas pattern match with OFF responses were used to generate palp-closing responses. **(d–i)** Observed PORs to various presentations of hex (same as in **Fig. 4.10a–f**) are shown in black. The predicted PORs generated from the *ON-OFF* model are shown in purple. The correlation coefficient between the actual (mean trend; i.e. the black trace) and predicted PORs are shown on each of the six panels. The model parameters were set based on PORs to solitary hexanol presentation.

4.3 Discussion

What is the neural code for a sensory stimulus is a fundamental question in sensory neuroscience. Several encoding schemes that depend on a unique set of neurons activated (‘the combinatorial or spatial code’), or the temporal features of neural electric discharges (‘the temporal code’), or their combination (‘spatiotemporal schemes’) have been proposed for representing stimulus-specific information in sensory circuits. While it is well established that stimulus-specific information can indeed exist in both spatial and temporal dimensions, how robust are these schemes to extrinsic (for example, stimulus history[46, 55] or ambient conditions[138]), or intrinsic (for example, plasticity[47] or internal-state such as hungry vs. satiated[139]) perturbations? This is what we sought to determine in this study.

We examined the stability of neural representations to odorants when only the stimulus history was systematically varied. Surprisingly, this manipulation was enough to induce variations in spatial, temporal and spatiotemporal features of neural responses elicited by an

odorant. Nevertheless, locusts trained to recognize a conditioned stimulus could robustly recognize and respond to the same. This mismatch between the lack of stability in the neural representation and robustness in behavior necessitated a re-examination of potential mapping schemes between neural inputs and behavioral outputs.

We used multiple decoding schemes to quantitatively examine whether robust odor recognition could be achieved when the same odorant was encountered with different stimulus histories. First, we used a linear support vector machine classifier that used $n+1$ free parameters (where n is the number of neurons) to recognize the target odorant. Results from this approach revealed that although PN responses evoked by an odorant varied depending on the preceding stimulus, there was sufficient information to robustly recognize its identity. However, the behavioral predictions generated by this scheme mismatched with actual behavioral responses observed (**Fig. 4.10**). The false positives that we observed in the behavioral responses were not predicted using this decoding method.

Having determined that robust odor recognition was indeed possible, we next sought to determine the simplest possible decoding approach that would generate predictions consistent with the observed POR responses. For this purpose, we used a flexible decoding scheme (with ON responses only; **Fig. 4.12d**) that used only one tunable parameter. This simple scheme generated predictions that better matched with the actual behavioral responses including the false positives. The only mismatch observed was the response to app. Although this scheme predicted a POR response to app, none were observed in the actual experimental data.

In a previous work[82], we showed that the ensemble activity during (ON response) and immediately after (OFF response) odor exposure were orthogonal and highly non-overlapping in nature. Notably, we showed that the ON responses were a better indicator of when the locusts

opened their palps, and the OFF responses were a better indicator of when the locusts closed their palps. So, we combined the outputs from two flexible decoding classifiers (i.e. flexible decoding with ON and OFF responses; uses two free parameters; **Fig. 4.14b**). One used the pattern match with the ON-response template of the conditioned stimulus, the other did the same with the OFF-responses elicited by the conditioned stimulus. Notably, for the app odorant, the output of the flexible ON decoder and the flexible OFF decoder canceled each other out, thereby generating more accurate predictions of PORs elicited in our behavioral assay. In sum, our results indicate that a linear scheme that decodes information from flexible subsets of neurons was sufficient to transform variable neural responses to robust behavioral outputs.

a

b

Object \ Feature	4 Legs	Seat	Back support	Arm rest
Chair 1	✓	✓	X	X
Chair 2	✓	✓	✓	✓
Chair 3	X	✓	✓	✓
Chair 4	✓	✓	✓	X
Chair 5	X	✓	✓	X

✓ → 1

X → 0

c

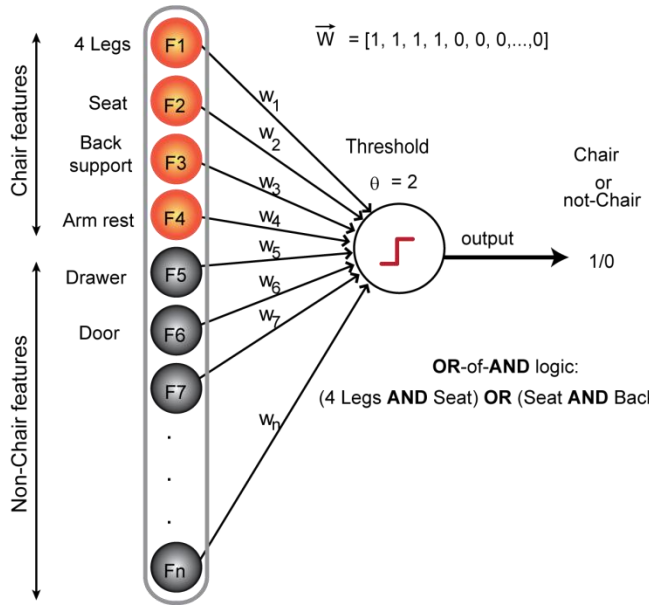

OR-of-**AND** logic:

(4 Legs **AND** Seat) **OR** (Seat **AND** Back support) **OR** … (4 Legs **AND** Seat **AND** Back support **AND** Arm rest)

d

Flexible object recognition	Flexible odor decoding
Chair	Target stimulus (hex or ger)
Different chairs	Different presentations of the same target stimulus
Feature present	PN responding
Feature absent	PN not responding
Chair recognition	Stimulus identification

Figure 4.15: Object recognition using Flexible decoding. (a, b) A schematic illustration of the flexible set decoder is shown. Here the problem is cast as one of object recognition (i.e. chair recognition). Images of different chairs and their features are tabulated. **(c)** A schematic of an OR-of-ANDs or disjunction-of-conjunction classifier is shown. Input features are binary 'feature present' or 'feature absent'. The weight vectors are constant and set based on an ideal object (Chair 2 in **panel a**): the weight vector component is

a '*1*' if the feature is present in the ideal chair, and '0' if it not present. The only free parameter in the OR-of-ANDs classifier is the threshold of the output node (θ). If the value of the threshold is set below the total number of features present in the ideal object (for example $\theta = 2$), then the presence of any two of the four features will allow recognition of the object (i.e. flexible decoding). This can be written as a set of logical OR-of-ANDs operation. **(d)** The list of analogies between this object/chair recognition illustration and flexible odor decoding proposed in this manuscript are listed in a table.

The flexible decoding approach can be easily understood if the problem is recast as one of object recognition (**Fig. 4.15**). A simple approach to recognize an object, say a 'chair', is to first segment it into simple features (such as 4 legs, seat, back rest, and hand rest). While the presence of all relevant features (all four features in this example) allows robust recognition of the prototype chair, it may not allow generalization when other instantiations of this object are presented. Therefore, to allow generalization, it would be necessary to relax the constraint that all the relevant features need to be present. Instead, determining the presence or absence of a meaningful subset of these features, any m features out of the possible n features ($m < n$), can be used for achieving robustness. Higher values of m allow more specificity, whereas lower values allow generalization. Our results indicate that such a decoding approach can indeed allow robust recognition of odorants presented with different stimulus histories (note that odor identity is analogous to the object to be recognized, and activation of a projection neuron is analogous to the presence of a feature). While results presented used weight vectors with components that were either a *0* or *1*, we found further improvements in classification results could be achieved by using negative weights for non-responsive neurons (not shown).

Could such a flexible decoding scheme be implemented by the insect olfactory system? To understand this issue, it would be necessary to identify the basic components of the decoder: (i) convergence of input from multiple PNs onto downstream neurons, (ii) linear combination of the inputs, and (iii) a detection threshold that does not require all input neurons to be

simultaneously co-active. Existing anatomical and functional studies have shown that downstream Kenyon cells in the mushroom body linearly combine inputs from multiple projection neurons[29, 140]. Further, photostimulation of Kenyon cell dendritic claws in fruit flies have revealed that activating more than half of these input regions is sufficient for driving these cells to spike[70] (i.e. $n/2 < m < n$ is sufficient). Therefore, anatomical and functional evidences suggest that the downstream centers in the mushroom body can indeed implement such a decoding approach.

Our results also indicate that variations in the neural responses with stimulus history were not random. Rather, the response evoked by the current stimulus was reshaped to suppress overlap with the preceding cue and increase the responses of those PNs that responded uniquely to the current cue. This simple manipulation at the level of individual PNs resulted in contrast enhancement of population neural responses. Note that contrast enhancement in olfaction happens between stimuli over time, rather than in the spatial domain as in vision.

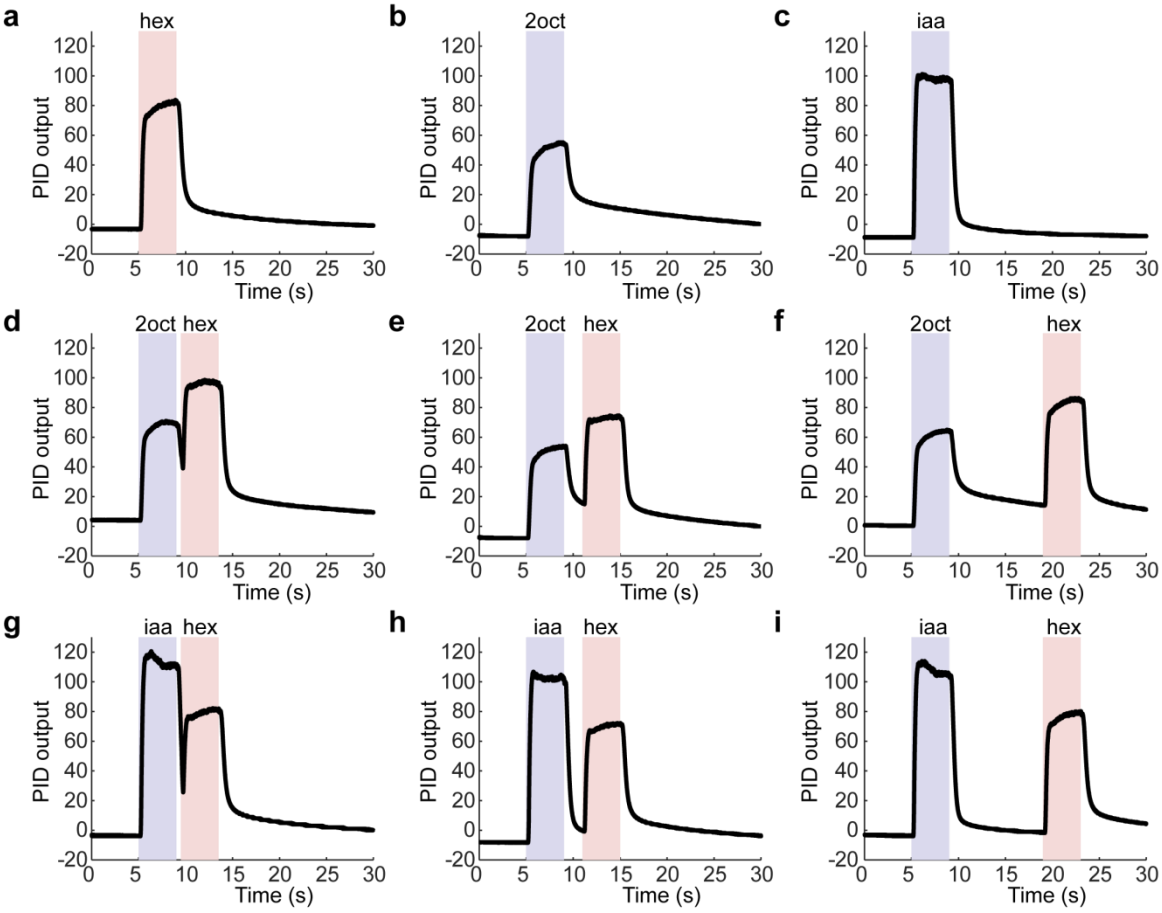

Figure 4.16: Characterization of stimulus overlap using photoionization detector. (a, b, c) Photoionization detector (PID) measurements are shown. The color bars indicate when a 4 s odor puff was presented. The three traces shown correspond to hex, 2oct and iaa presentations, respectively. Mean across five trials is plotted in each panel. **(d, e, f)** Similar PID traces are shown for 2oct-hex (distractor-target) odor sequences with three different lags between the two stimuli: 0.5 s, 2 s, and 10 s. **(g, h, i)** Similar plots as **panels d, e, f,** but for a different distractor-target (iaa-hex) odor sequence.

Could some or most of the results be simply explained due to mixing of vapors from the first delivered distractor stimulus with those from the target odorant (i.e. mixture coding)? A photoionization detector-based characterization of the stimulus overlap indicated that at least for some odorants (for example, 2oct followed by hex case), vapors from the first odor pulse lingered longer and overlapped with the target odor presentations (**Fig. 4.16**). As can be expected, the overlap reduced as the gap between the two pulses was increased. Notably, our

results indicate that hexanol presentation with a longer delay (2 s and 10 s after termination of distractor 2oct pulses) resulted in qualitatively similar contrast enhancement as that observed for shorter delays **(Fig. 4.17)**. These results indicate that the overlap between the first and second stimulus delivered in sequence is not necessary for the contrast enhancement results reported in this study.

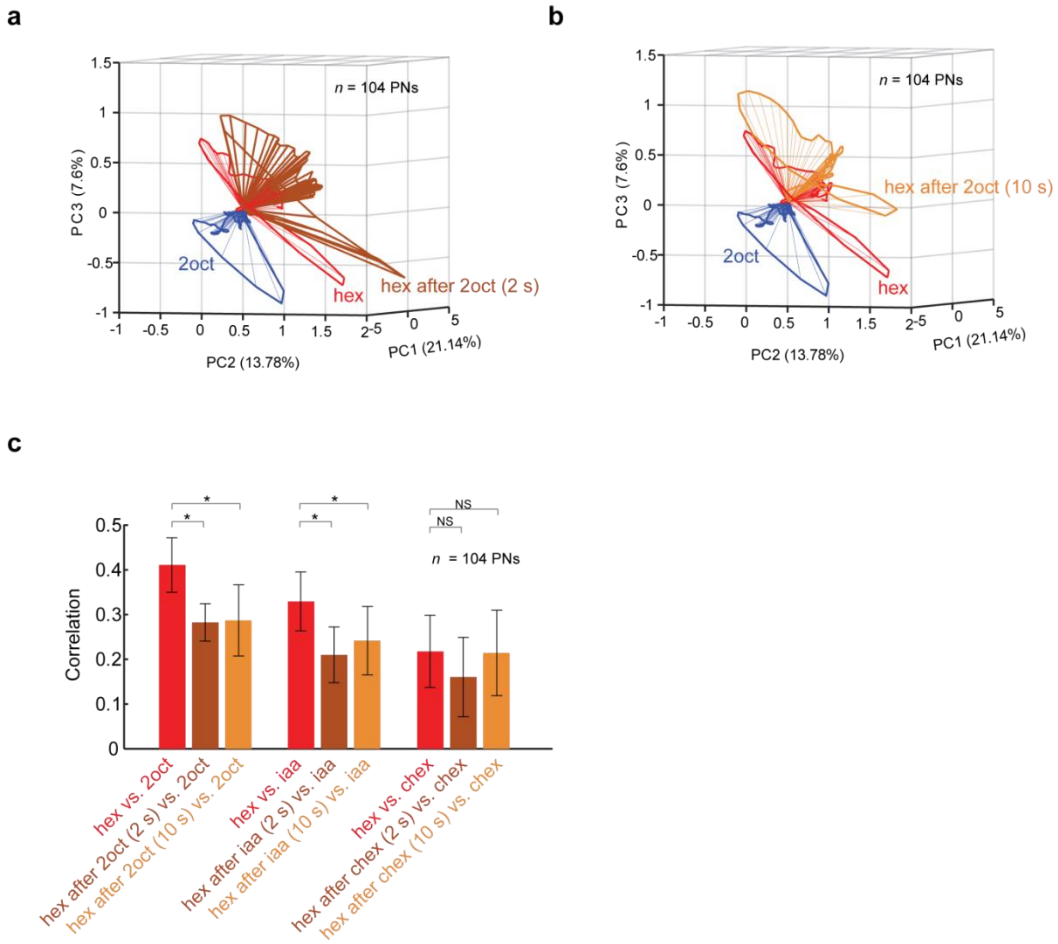

Figure 4.17: Contrast enhancement can be generalized for longer delays. (a, b) Response trajectories generated by two additional sequential presentations of hex are plotted: 2oct – 2 s – hex and 2oct – 10 s – hex. Similar method as in **Fig. 4.3a** was followed to analyze this dataset. **(c)** The mean of correlation values between the ensemble PN responses (n = 104 PNs) evoked by hexanol and the three distractor cues (2oct, iaa, and chex) are shown as bar plots. Error bars indicate ± s.d across ten trials. The mean odor-evoked responses during the initial 1 s after stimulus onset were used for computing these correlations. The odor-pairs that were compared are identified along the x-axis. Asterisks indicate a significant decrease in the correlation (*P < 0.025 (Bonferroni corrected for two comparisons), t-tests, n = 10 trials).

Nevertheless, since there is some overlap between vapors for shorter latencies, we also examined how similar or different were the processing of the binary mixtures with the odor sequences. To do this, we reanalyzed a published dataset of hex and 2oct binary mixture and 2oct-short lag-hex odor sequences (lag: 0.25 or 0.5 s). We found that a binary mixture of these two odorants evoked responses that were an additive combination of two component neural activities. Therefore, the binary mixture odor responses traced an odor trajectory in-between the two component response trajectories (i.e. green trajectory (hex-2oct mixture) was in-between the red (hex) and the blue (2oct) trajectories; **Fig. 4.18)**. However, note that for both hexanol presentations, even with 0.25 and 0.5 s lag following 2oct, the responses elicited during hex presentations were more similar to hexanol than the binary mixture or the distractor. Further, the responses shifted away from the 2oct response trajectory (i.e. magenta trajectory) indicating contrast enhancement of hex-evoked responses with respect to the preceding 2oct stimulus. Together, these results indicate that the odorants encountered in sequential fashion are processed differently than simultaneously encountered odor mixtures.

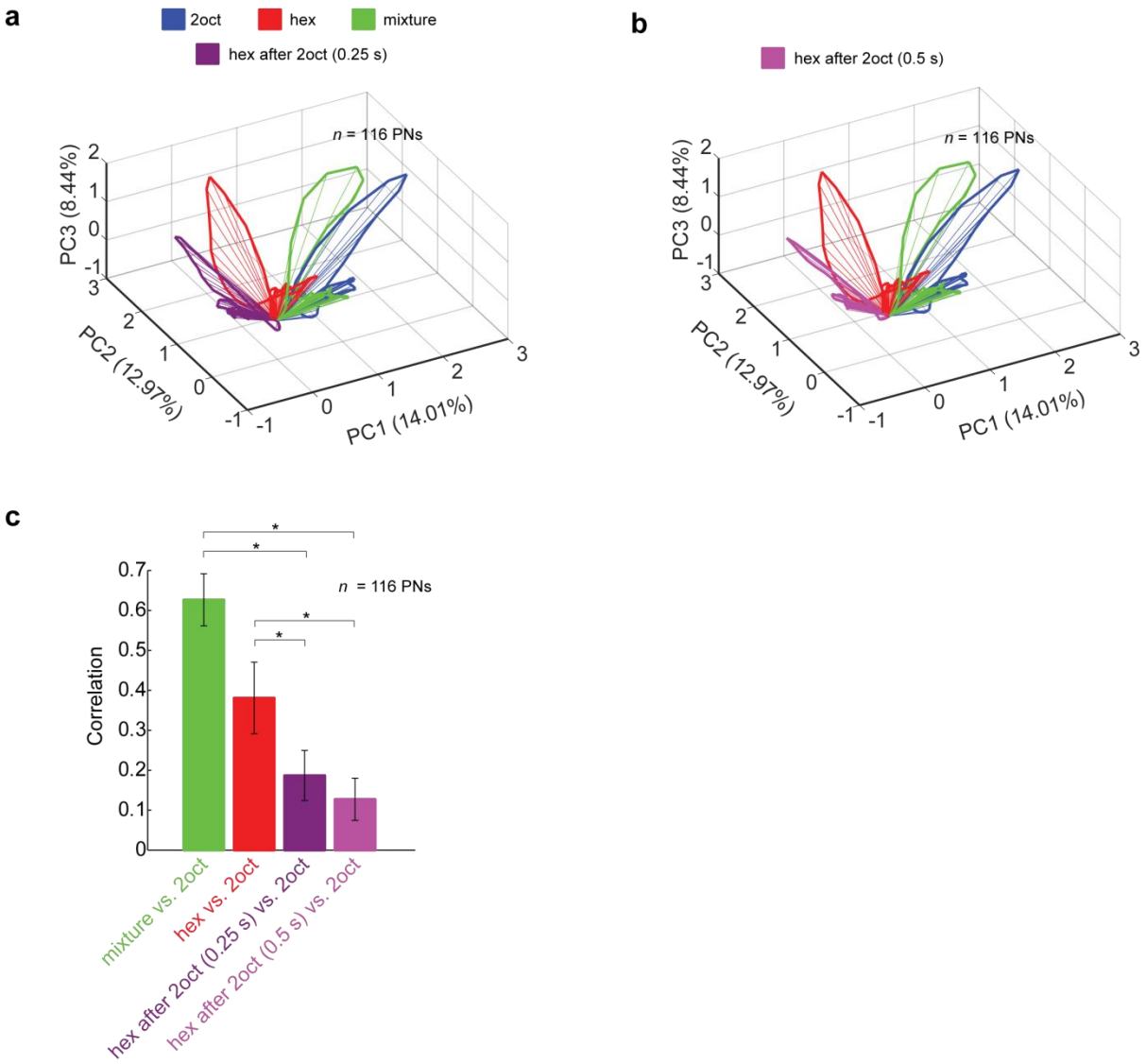

Figure 4.18: Sequential presentation responses are more dissimilar to distracting stimulus than binary mixture. (a, b) Similar plots as in **Fig. 4.3a** but showing ensemble response trajectories for the following stimuli: hex (red), 2oct (blue), a binary mixture of hex and 2oct (hex-2oct; green), 2oct – 0.25 s – hex (purple; top panel) and 2oct – 0.5 s – hex (purple; bottom panel). These data were re-analyzed from our previous studies [45]. **(c)** Correlation between binary mixture response, hex response, hex after 2oct (0.25 s) response, and hex after 2oct (0.5 s) response with 2oct-evoked neural activity were calculated and plotted as a bar graph (mean ± s.d; n = 10 trials). Mean ensemble activity during the initial 1 s after stimulus onset was used to compute these correlations. Asterisks indicate a significant decrease in the correlation (*P < 0.0125 (Bonferroni corrected for four comparisons), t-tests, n = 10 trials).

How do trial-to-trial variations compare against the changes in neural responses observed across stimulus histories? We found that individual PN responses did vary considerably across

trials (**Fig. 4.19a, b**). However, at the ensemble level, responses were highly consistent across trials. Odor-evoked response during the early, mid and late set of trials were still aligned and traced trajectories that evolved in the same direction (**Fig. 4.4 a,b).** These results were further quantified using a correlation analysis which also confirmed that variability across trials was indeed less than those observed across stimulus histories (**Fig. 4.19 c,d**).

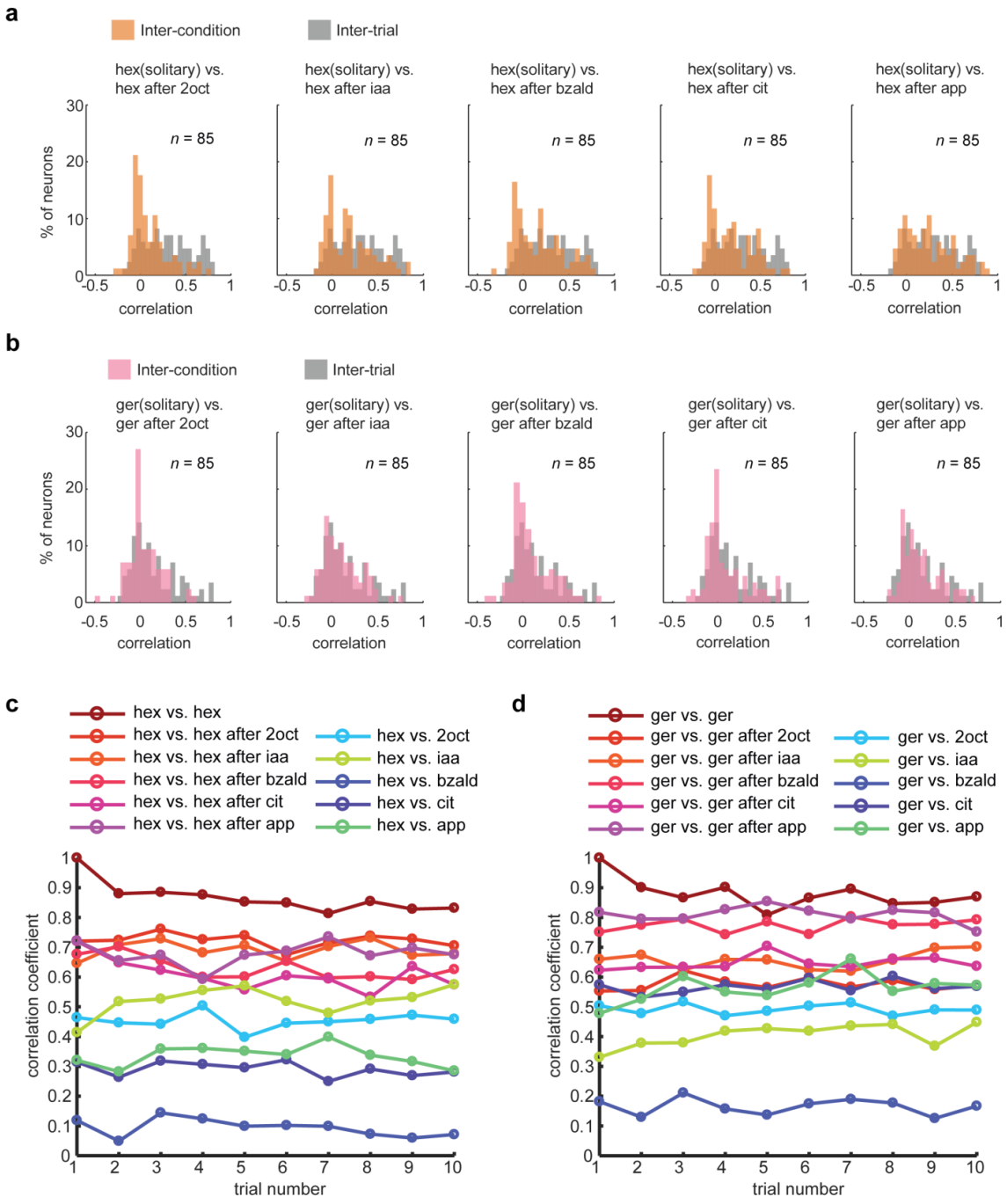

Figure 4.19: Trial-to-trial response variations are less compared to history-dependent changes. (a) Distributions of correlation values between inter-condition (colored) and inter-trial (gray) PN spike trains are shown. This analysis is similar to the one done for generating **Fig. 4.9e, f**. For computing correlation between trials, for each PN, we compared the similarity between the mean PN responses in the first five trials with the mean response in the remaining five trials of hex(solitary) stimulus. To allow for a fair comparison, the correlations for inter-condition correlations (plotted in orange) were calculated by estimating the similarity between the mean PN response in the first five trials of hex(solitary) exposures

with the mean response in the first five trials of sequential hex presentations. This was again done for each PN and for each sequential hex presentation to generate the five orange distributions shown in the plot. **(b)** Similar plots as in **panel a** but analyzing PN responses to geraniol. **(c)** Comparison of combinatorial PN response profiles activated by the same odorant across trials, same odorant across stimulus histories, and between different odorants is shown as a function of trial number. Note that all comparisons are made with respect to the ensemble PN responses elicited by solitary presentation of hexanol in the very first trial. **(d)** Similar plots as **panel c** but plotted when the target odor is ger.

Can such dynamic contrast enhancement lead to other potential confounds? For example, how are PN responses altered when back-to-back pulses of the same odorant are presented? To determine this, we reanalyzed a recently published PN response dataset to two back-to-back pulses of hexanol (**Fig. 4.20**). Our analysis revealed that in addition to a reduction in responses to the subsequent pulses[54], a few PNs that did not respond to the first pulse were activated in the second pulse, and some responding to the first pulse were inactivated. Note that the same OR-of-ANDs classifier can robustly recognize the stimulus after this subtle response perturbation.

While our results do not provide mechanistic insights on how this adaptive computing may arise, a few candidate mechanisms can easily be identified. Activity-dependent synaptic depression between the sensory neurons and projections neurons[141, 142], interference due to stimulus-evoked OFF responses[82], or adaptation at the level of sensory neurons[143, 144] can all contribute to the results observed in this study. Lastly, while we perturbed odor-evoked neural responses using variations in stimulus histories, other factors such as ambient conditions (humidity, temperature, air flow), presence of competing odorants, plasticity in central circuits have all been shown to introduce variations different from those that were examined here. Whether the same flexible decoding scheme proposed here can provide a generic framework for achieving trade-off between stability and flexibility remains to be determined.

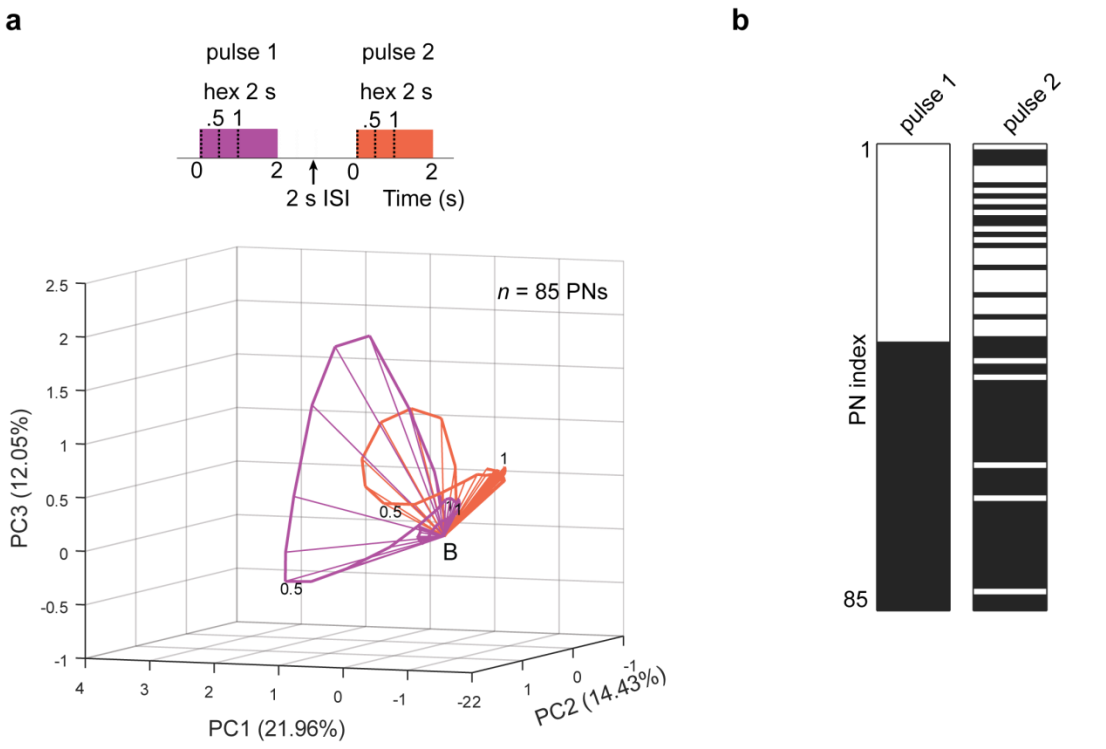

Figure 4.20: PN responses vary between sequential encounters of the same stimulus. (a) Similar trajectory plot as shown in **Fig. 4.3a** but comparing the population PN responses generated during the presentation of two hexanol pulses. The second pulse of hexanol was presented 2 s after the termination of the first pulse. These data were re-analyzed from our previous study[82]. **(b)** Similar barcodes as in **Fig. 4.7a** but identifying the responsive PNs in the first and the second pulse.

4.4 Author Contributions

The work described in this chapter has been published as : S. Nizampatnam, D. Saha, R. Chandak, and B. Raman. "Dynamic contrast enhancement and flexible odor codes." *Nature communications* 9 (2018).

B.R. conceived the study and designed the experiments/analyses. S.N. did all the analyses, generated all the figures and wrote the first draft of the manuscript. D.S. and S. N. performed the electrophysiological recordings. R.C. did the behavioral experiments. B.R. revised the paper taking inputs from all the authors. S.N., D.S., and R.C. are equally contributing first authors.

Chapter 5: Invariant Odor Recognition with ON-OFF Neural Ensembles

5.1 Introduction

Robustly recognizing a sensory stimulus is a necessity for the survival and propagation of all animals. Since this capability is demonstrated in all sensory systems, this raises the following question: what is the neural basis that underlies this feat of pattern recognition? Most stimuli are encountered in a multitude of ways in natural environments. Often, stimulus features such as intensity, duration, and recurrence could vary. In addition, external perturbances due to changes in environmental conditions (such as changes in humidity or temperature), the presence of other competing cues, or the temporal context (i.e. when it is received in a stimulus sequence) could also change independent of the variation in stimulus-specific features. An additional degree of interference can arise from changes in the sensory circuit due to plastic changes arising either from prior exposures or co-occurrence with other sensory cues. Given the complexity in carrying out the basic task of recognizing a stimulus, we wondered if there exists a computational framework that can compensate for all these disparate sources of variation and allow robust recognition of a stimulus. In particular, we sought to examine this issue in the well-studied locust olfactory system [11-14, 41, 45, 46, 48, 52, 54, 82, 97, 101].

In the locust olfactory system, odorants activate olfactory receptor neurons in the antenna. This signal is transmitted downstream to the antennal lobe (analogous to the vertebrate olfactory bulb) where it drives responses in cholinergic projection neurons (PNs) and GABAergic local neurons (LNs). The interaction between PNs and LNs transforms the sensory input received into complex patterns of activity distributed across ensemble of PNs that become the output of the antennal lobe circuit. Prior work has shown that information about the identity

and intensity of an odorant is encoded by spatiotemporal PN activity patterns. While individual PN responses were perturbed by manipulating stimulus dynamics [54, 102], stimulus history [55, 145], and presence of background chemicals [45], the ensemble neural patterns can still allow recognition of odorants. Behavioral evidences also support this interpretation and reveal that odorants can be recognized independent of background cues [45] and stimulus history [145].

It is worth noting that prior studies examined neural response variability that arises due to each of these perturbations in isolation. In natural contexts, such interferences could occur independently or in conjunction with one another. Could robust odor recognition still be achieved? Particularly, can the variable neural responses be decoded in a manner that can simultaneously allow invariant odor recognition independent of all these perturbations? If so, what neural response features would be important for achieving this result? We sought to examine these issues in this study.

5.2 Results

5.2.1 Stimulus dynamics, history and competing cues induce variations in PN responses

We began by examining how odor-evoked responses of individual projection neurons (PNs), in the locust antennal lobe, were perturbed due to variations in how the odorant was encountered. Changes in pulse durations and inter-pulse intervals (stimulus dynamics), presence of other competing odorants (i.e. background vs. no background), and alterations in stimulus history (following termination of another cue) were all explored. A photoionization detector was used to characterize this stimulus delivery protocol (**Figure 5.1**). For all odorants used, we found that the number of odorant molecules delivered reached a steady-state level within 500 ms of pulse onset.

Return to baseline was relatively slower and took ~1 s or more in some cases. Pulses with less than a second of inter-pulse interval, or that were overlapping, had an additive effect on the photoionization detector. Overall, the stimulus delivery was robust and a consistent steady-state level stimulus concentration was reached independent of how the odorant was delivered.

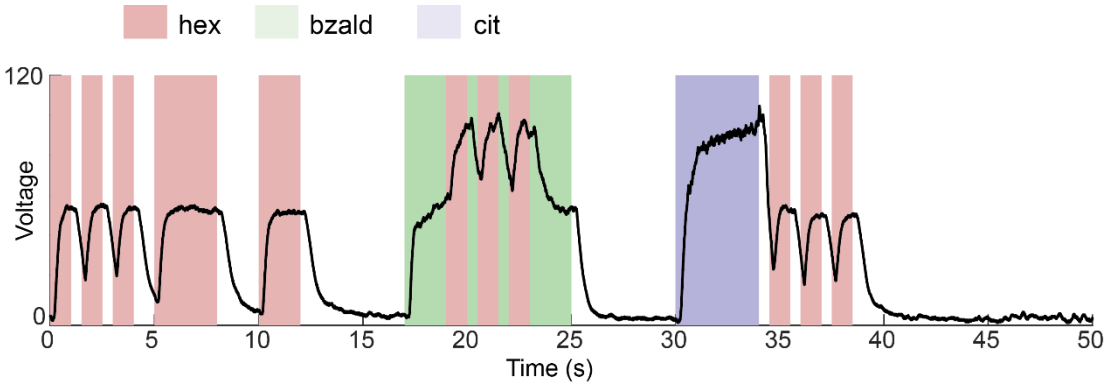

Figure 5.1: Characterization of the stimulus delivery. Voltage output of a miniPID (Aurora Scientific) is plotted as a function time to characterize the stimulus delivery protocol.

In total, we recorded responses of eighty-nine PNs in the locust antennal lobe (n = 25 locusts). First, we examined the ability of individual PNs to robustly encode the identity of two 'target' odorants, hexanol (hex) and isoamyl acetate (iaa), that were encountered during the complex stimulation procedure (**Figure 5.2a-d**). In the entire ensemble of PNs that were recorded, we found that four PNs responded robustly to all encounters of the target odorants (**Figure 5.2a, b**; PN1 and PN2). However, these 'reliable' PNs were activated by both the target odorants (hex and iaa) and therefore did not provide good discrimination between the two target odorants. For all other PNs that were reliably activated during the first pulse of the target odorants, the response during the subsequent encounters were either attenuated, or completely suppressed due to the presence of other competing odorants and/or changes in stimulus histories (**Figure 5.2c, d**; PNs 3-8).

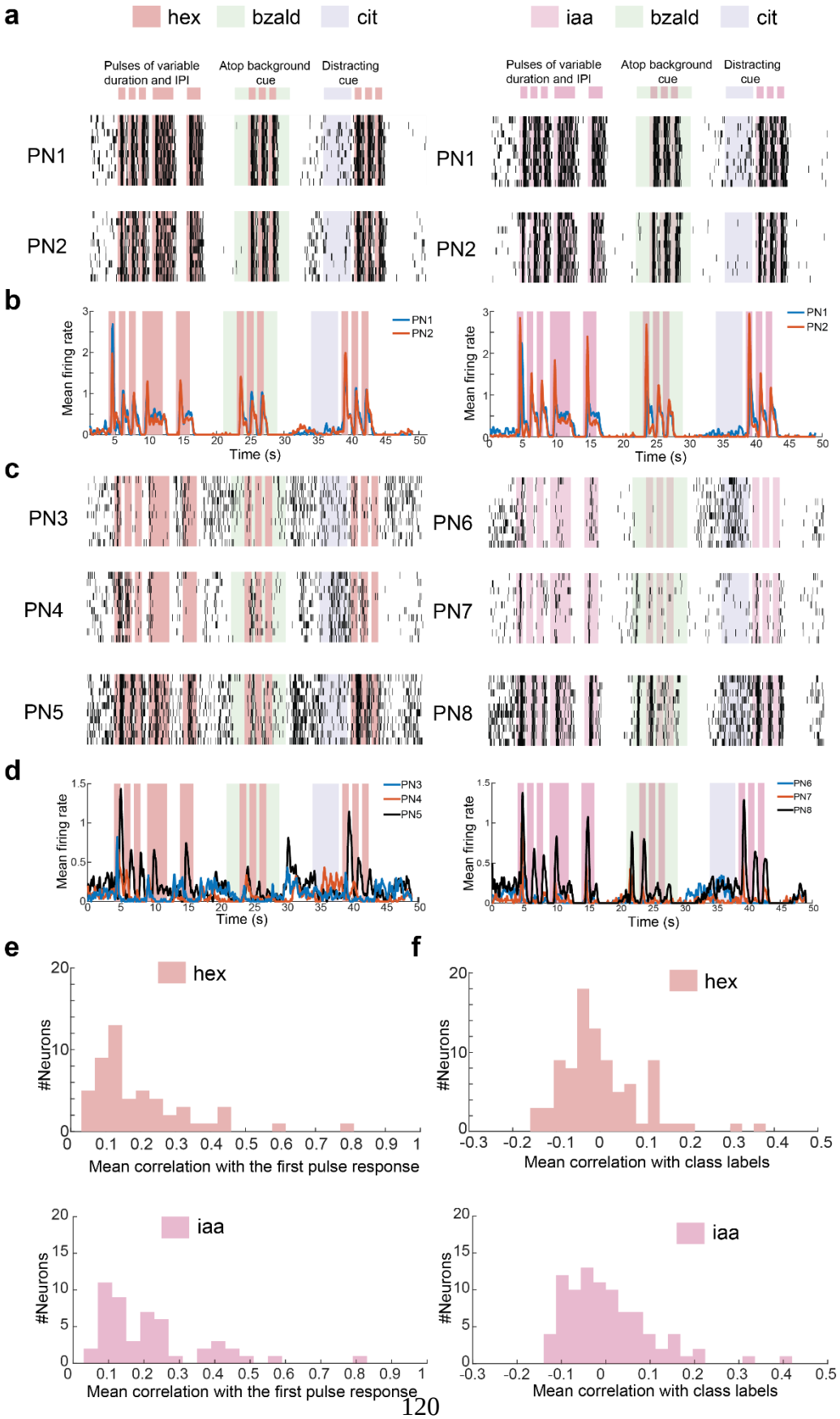
a
hex
bzald
cit
iaa
bzald
cit
Pulses of variable duration and IPI
Atop background cue
Distracting cue
PN1
PN2
b
Mean firing rate
Time (s)
c
PN3
PN4
PN5
PN6
PN7
PN8
d
e
f
#Neurons
Mean correlation with the first pulse response
Mean correlation with class labels

Figure 5.2: Individual projection neuron responses are highly variable. (a) Left plots, raster plots showing PN responses (PN1 and PN2) during a pulsatile presentation of a target stimulus (hexanol; *hex*) in back-to-back sequences of variable duration and inter-pulse intervals, atop a background cue (isoamyl acetate; *iaa*), following a distracting stimulus (citral; *cit*). Each black tick represents an action potential fired by the PN. PN responses are shown for 10 consecutive trials (10 rows). Right plots, similar plots as in the left, but the target stimulus was isoamyl acetate (*iaa*). Notice that these PNs responded reliably across all the presentations of both *hex* and *iaa*. **(b)** Firing rates of the two PNs (50 ms time bins; trial averaged) shown in **panel a** are now plotted as a function of time. While both the PNs responded strongly to the first pulse of the target odorant, the response diminished during later encounters of the same stimuli. **(c)** Similar plots as **panel a** but shown for three different PNs. Unlike the PNs shown in **panel a**, the responses evoked by the target odorant in these six PNs were highly variable. **(d)** Similar plots as in **panel b** but time histograms are plotted for the PNs shown in **panel c**. **(e)** Similarities between PN responses evoked during the first pulse of the target odorant with all other encounters were computed. For this quantification, PN response was first binned into 50 ms time bins and averaged across 10 trials. The first 1 s response following onset of each target odorant pulse was used to compare response similarity between different target odor encounters (i.e. 20-dimensional response vectors). For each PN, the mean similarity across odor pulses was determined, and the response similarity across PNs were then plotted as a distribution. Top and bottom plots reveal response similarity distribution for *hex* and *iaa*, respectively. **(f)** Similar plot showing correlation between the PN responses and the odor class label. The class label was set to '0' corresponding to timebins when the target stimulus was not presented and set to '1' for those timebins when the target stimulus was presented. Top and bottom plots reveal the correlation between individual PN responses and odor class labels for the two target odorants: *hex* and *iaa*.

To quantify the response variability observed at the level of individual PNs, we computed correlations between the PN response to the first pulse of target odorant and all the other introductions of the same chemical. The distribution of these response correlations revealed that spiking activities during subsequent encounters of the target odorant had only a weak pattern match with the responses elicited during the very first encounter of an odorant (**Figure 5.2e**). Furthermore, when individual PN responses were correlated with an 'odor label' (i.e. a binary vector of target odorant present or absent), the distribution was again centered around zero indicating that individual PN activities are not a reliable indicator of presence or absence of any target odorant (**Figure 5.2f**).

5.2.2 Variations due to changes in ambient conditions

Next, we also examined PN responses if variations in humidity conditions would further exacerbate the problem of robustly encoding the identity of an odorant. For this purpose, we used the same stimulus delivery protocol but using either 0% humid air or 100% humid air as the carrier stream. We again found that the four PNs that had robust responses to the target odorants also had reliable activity in varying humidity conditions (**Figure 5.3a, b**; PN1). But for all other PNs in our dataset the responses were again variable in both dry and humid conditions (**Figure 5.3a, b**; PN9, PN 11). The overall distribution of response similarity between the first pulse and the subsequent encounters of the same odorant was low but comparable in both dry and humid ambient conditions (**Figure 5.4a**).

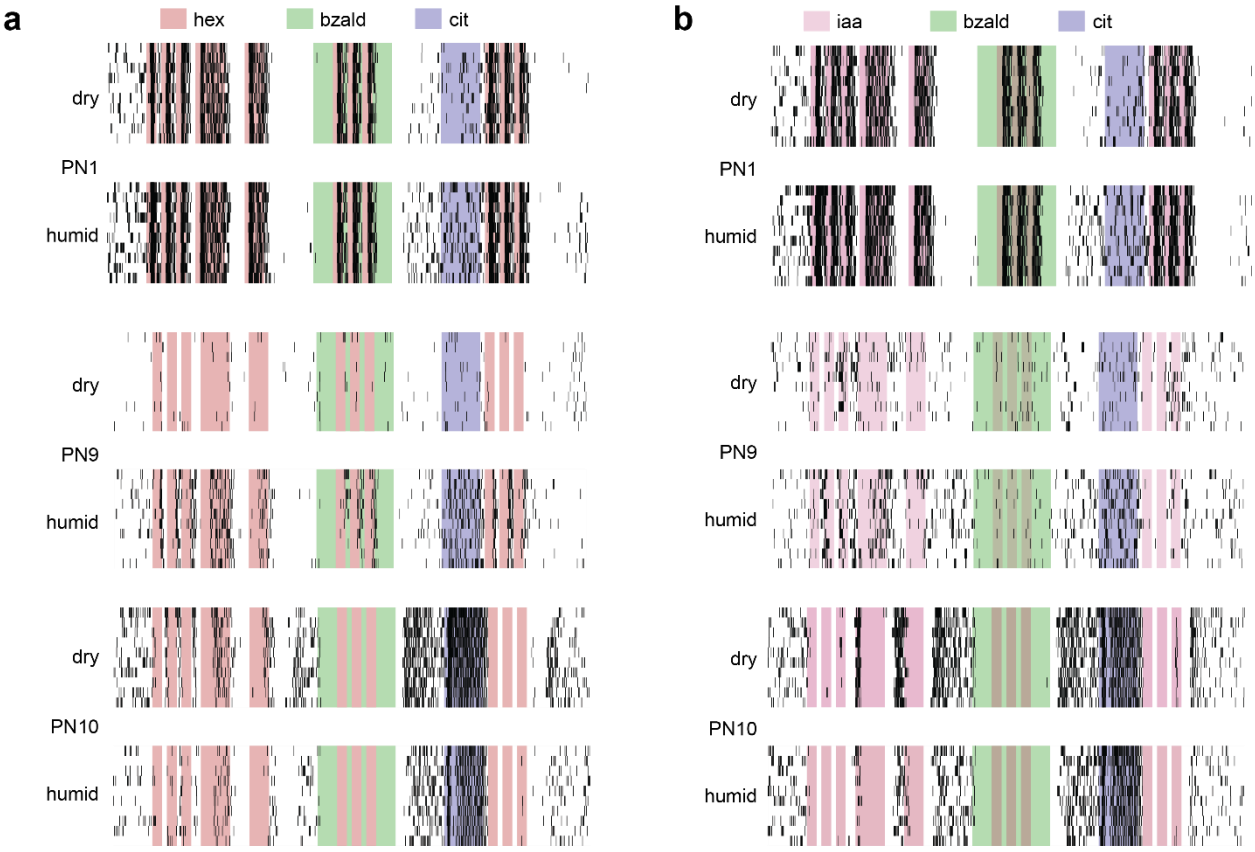

Figure 5.3: Variations in individual PN responses between dry and humidity conditions. (a) Similar raster plot showing PN responses to the stimulation protocol used in **Figure 5.2**. For each PN shown, the

top and bottom plots reveal the spiking activity of the same PN between dry (carrier stream – 0% RH) and humid (carrier stream – 100% RH) conditions are shown. Note that changes in humidity levels of the carrier stream resulted in increase or decrease in spiking activity in individual PNs. **(b)** Similar plots as in **panel a** but showing PN responses to a different target stimulus (*iaa)*. Note that the same set of PNs are shown.

Between dry and humid conditions, we found that both spontaneous activity and odor-evoked responses varied in ~ 50% of PNs recorded (**Figure 5.4b, c**). While most PNs had increased activity in the humid conditions, a smaller fraction had higher baseline activities and odor-evoked responses in dry conditions. These results suggest that changes in ambient conditions (i.e. dry or humid) can alter both spontaneous activities (i.e. initial state of a dynamical system), and odor evoked neural response dynamics at the individual and at the ensemble level in the antennal lobe.

These physiological results raise the following question: can locusts recognize an odorant independent of the changes in humidity conditions? To examine this, we trained locusts in an appetitive conditioning assay. In this paradigm, each locust was trained by presenting an odorant (conditioned stimulus; hexanol at 1 % v/v concentration) in dry conditions followed by a grass reward (unconditioned stimulus) in each training phase trial. Following six such trials, we tested the ability of the trained locusts to recognize the conditioned odor stimulus by presenting it in unrewarded test phase trials. Opening of palps (sensory appendages close to the mouth) in anticipation of grass reward, following the introduction of the conditioned odor stimulus was regarded as successful recognition. After the training phase in dry condition, we examined the ability of locusts to recognize the conditioned stimulus presented either in dry or humid conditions. Our results indicate that locusts opened their palps to all the introductions of the conditioned stimulus in both dry and humid conditions (**Figure 5.4d**). The performance was near identical indicating robust odor recognition that was invariant with respect to changes in ambient

conditions. Similar results were also obtained when locusts were trained in humid conditions and tested in both dry and humid conditions (**Figure 5.4d**). These results indicate that locusts can recognize trained odorants invariant to changes in ambient conditions.

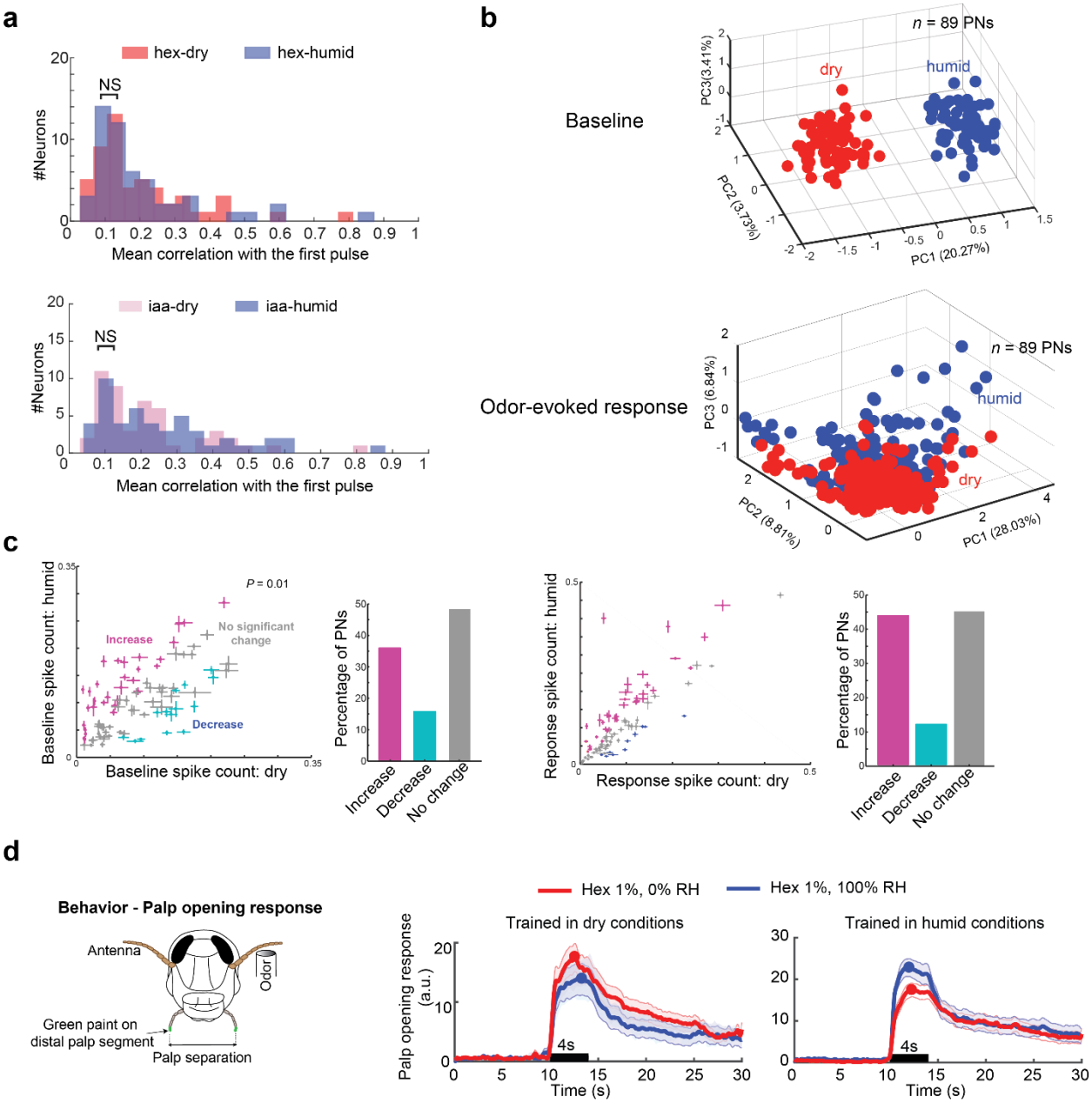

Figure 5.4: Spontaneous spiking activity and stimulus-evoked PN responses are both altered in different humidity conditions. (a) Similar plot as in **Figure 5.2d** but comparing response similarity between PN responses observed in dry and humid conditions. 'NS' indicates that the two distributions are not significantly different (Two-sample Kolmogorov-Smirnov test; P = 0.05). **(b)** Left, spiking activities of all 89 PNs during a 15 s pre-stimulus period (i.e. before odor stimulation begins) are shown after PCA

dimensionality reduction. Spikes in individual PNs were binned in 200 ms non-overlapping windows and treated as vector components. Each colored sphere represents a 89-dimensional PN spike count vector along the first three principal components. Red and Blue colored spheres are used indicate the differences observed in the spontaneous, ensemble PN spiking activity in dry and humid conditions, respectively. Right panel shows a similar plot but comparing odor-evoked responses in dry and humid conditions. **(c)** Top panel, Comparison of projection neuron spike counts during a 15-s pre-stimulus period (i.e. no odorant present). The *x* axis corresponds to spike counts in dry conditions. The *y* axis corresponds to spike counts in humid conditions. The mean ± s.e.m. over ten trials is shown for all PNs. Markers are colored to indicate significant increase (magenta), decrease (cyan), or no change in spike counts (paired t-test, $P = 0.01$, $n=10$ trials). On the right, bar plot is shown to summarize changes in baseline firings in individual PNs. Note that ~50% PNs had changes in baseline activity. Bottom panel, similar plots as in top panels but comparing odor-evoked PN responses to hexanol in dry and humid conditions are shown and summarized. **(d)** Behavioral palp-opening response assay is schematically shown. Locusts were trained to associate the conditioned stimulus (CS; hex 1% v/v) with a food reward (US; grass). Subsequently, in an unrewarded testing phase, trained locusts opened their sensory appendages close to their mouths called palps to indicate successful recognition of the conditioned stimulus. Note that the palps were painted with a non-odorous paint and tracked to quantify behavioral palp-opening response. Locusts were trained in either dry or humid conditions but subsequently tested in both conditions (see Methods for more details). Median palp opening response ± s.e.m. ($n=20$ locusts) is shown for the testing phase trials. Note that POR responses to the conditioned stimulus in shown for both dry and humid conditions.

5.2.3 Robust recognition with a 'ON minus OFF' classifier

Our results indicate that odor-evoked responses vary with stimulus dynamics, history, presence of competing cues and changes in ambient conditions. However, the behavioral recognition (i.e. the palp opening response or POR) remained invariant to such perturbations (Figure 2; also refer prior results on background [45] and history invariance [145]). Given this discrepancy between neural variability and behavioral robustness, we sought to determine (i) whether a neural decoder can be designed that can allow robust odor recognition, and (ii) what would be the simplest possible approach to achieve this mapping.

To investigate this issue, we regarded the ensemble activity across the 89 PNs recorded in a 50 ms time bin as a snapshot of high-dimensional neural activity to be decoded (i.e. 89-dimensional firing rate vector). To design the simplest decoder, we classified each PN as a ON

responsive or OFF responsive based on its response during the training phase trials that only included solitary exposures of the target odorants (**Fig. 5.5**). The classification approach had two components: an ON classifier that summed the contribution the all ON responders (achieved using a binary weight assignment of '1' to all ON neurons and '0' to all others) that was appropriately thresholded, and an OFF classifier that summed contribution the all OFF responders (achieved using a binary weight assignment of '1' to all OFF neurons and '0' to all others) followed by a thresholding step. The output of these two classifiers was combined by computing ON classifier output minus OFF classifier output. Only when the resulting output was positive then the prediction was target stimulus present (i.e. a rectifying linear unit or a 'ReLU').As can be noted, the only two free parameters in this approach are the classification thresholds that was set to minimize false positives during pre-stimulus, while maximizing true-positives in the training data.

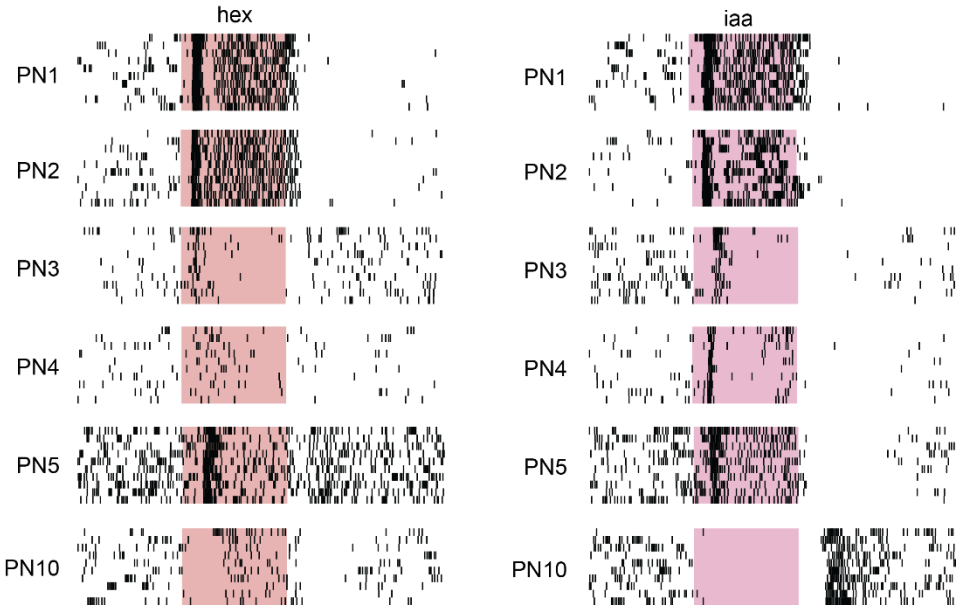

Figure 5.5: PN responses to solitary odor pulses. PN responses to 4 s solitary presentation of hexanol (hex; left) or isoamyl acetate (iaa; right) are shown. The colored boxes indicate the 4s duration of the odor pulse. Each tick corresponds to an action potential, and PN spiking activity is shown for 10 consecutive trials. Only PN responses to these solitary 4 s pulses was used to train all classification models (**Figure 5.6**).

Odor recognition results (trials-averaged) from this binary classification scheme for the complex, pulsatile stimulus delivery is shown in **Figure 5.6b**. As can be noted, both target odorants could be detected and recognized during most of the pulses. In general, recognition performance was better for *iaa* than *hex* as more PNs in our dataset were activated by *iaa*(**Figure 5.6d**). Best recognition was encountered in the very first odor pulse and the performance progressively dipped during subsequent encounters. Recognition of the target odorants were harder atop a background, and this particularly the case during the second and third pulse of *hex atop bzald* (**Figure 5.6b, c**). Overall, these results indicated that a very a simple but generic approach can achieve better than chance recognition of the target odorants.

Taken together, our results indicate that although individual PN responses vary unpredictably, a simple linear neural decoding scheme is sufficient to achieve invariant odor recognition.

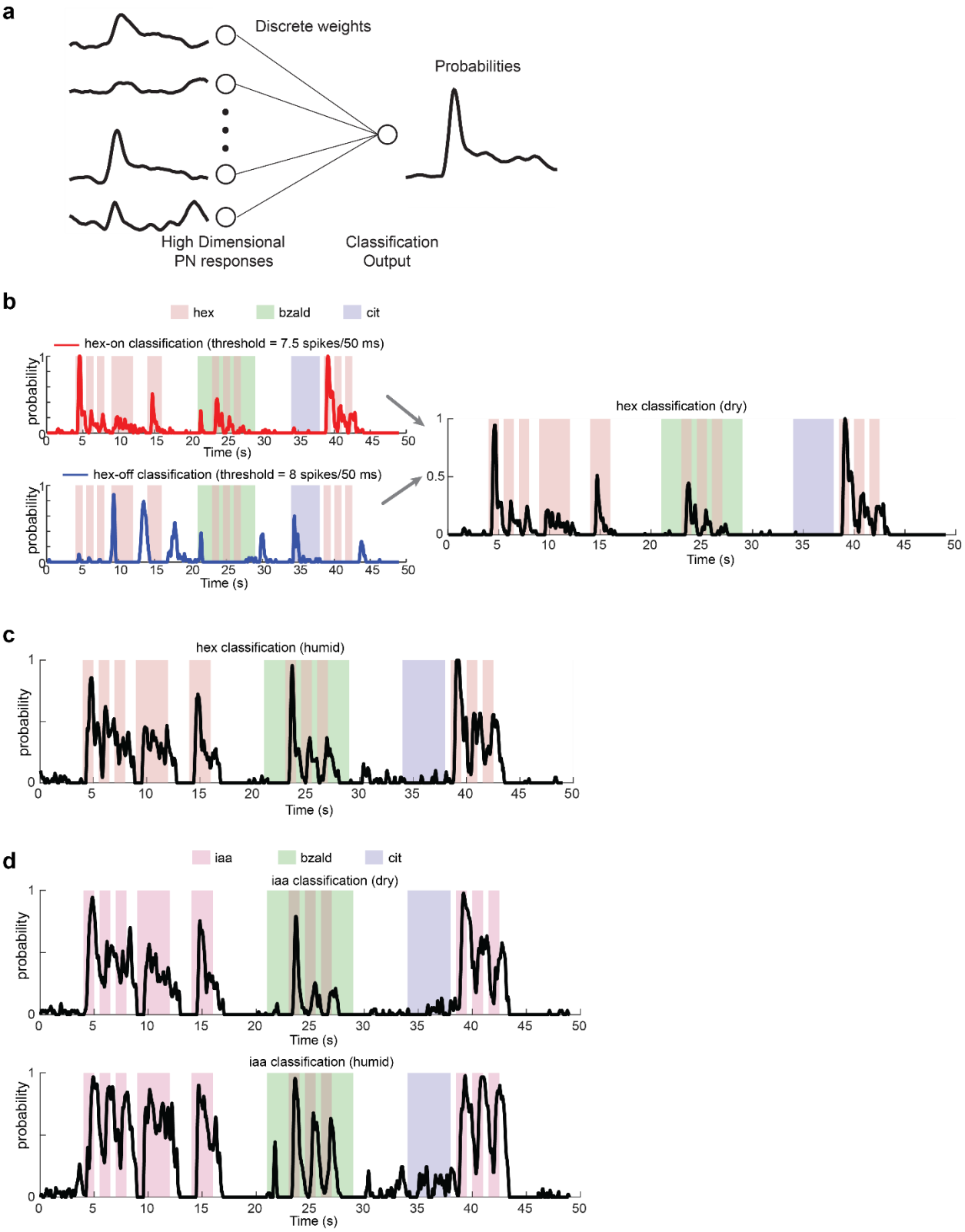

Figure 5.6: Decoding stimulus identity with a 'ON minus OFF' classifier. (a) Top, classification probability for *hex* as a function of time using a ON classifier is shown. ON responsive neurons were first

found using solitary presentation of *hex* (see Methods; **Figure 5.5**). In other words, a weight of '1' was assigned to the ON responsive PNs and 0 to the rest. At each time bin, PN firing rates from ON responsive neurons were summed and thresholded to classify each timebin. Trial-by-trial classification results were averaged to generate classification probabilities and plot them as a function of time. Bottom panel, similar plot but showing classification results using OFF classifier that predicts the absence of the target stimulus using OFF-responsive neurons. Thresholds used for both these classifiers are shown at the top of each panel. Right, ON and OFF classifications were merged with a rectified linear unit (ReLU) as an activation function that outputs non-zero only if the ON classifier output is greater than the output of the OFF classifier and zero elsewhere. **(b)** Classification probabilities predicted using a 'ON minus OFF' classifier is shown for hexanol stimulation in humid condition. **(c)** Similar plots as in **panels a and b** but showing classification probabilities for *iaa* predicted using ON minus OFF classifier. Top and bottom sub-panels show robust recognition results in dry and humid conditions, respectively.

5.3 Discussion

We examined how invariant recognition of odorants can be achieved in a relatively simple locust olfactory system. Our results indicate that individual PN responses can vary with one or several of perturbations we studied, including, stimulus dynamics, repetition, stimulus history, presence of background odorants and changes in humidity conditions. Nevertheless, at the population level information regarding the odorant's identity was still robustly encoded, and a simple classification scheme were sufficient to extract the relevant information out. The classifier essentially boiled down to adding the contribution of PNs that were strongly activated when the odorant was presented (ON neurons) and subtracting the contribution of PNs that were activated after the termination of the odorant (OFF neurons). In sum, these results indicate a neural basis for achieving sensory invariance.

We found that not all neurons were perturbed and only a small subset (4/89 PNs) of them responded reliably to all introductions of the target odorants. While these neurons allowed robust detection of the target odorants, they were not specific and responded to both the target odorants examined in this study. Therefore, it is possible that an approach based on a single or small

subset of neurons encoding for a stimulus under all conditions, may not be a fault-tolerant approach.

Prior publications [45, 54, 55, 102, 145] had also found individual neurons unreliable, but robustness emerging at an ensemble level. However, our prior results indicated that odorants delivered atop different background generated ensemble responses that only partially overlap across conditions [45]. Furthermore, features of ensemble responses pattern matched across backgrounds could vary unreliably. In other words, even at the ensemble level, there was not a single feature that could remain consistent when the odor-evoked responses were minimally perturbed. How then could sensory invariance be achieved?

If ensemble responses features varied across conditions how did this 'ON minus OFF' classification approach achieve invariance. It is worth breaking this classification scheme into its two components: ON component and OFF component. Assigning '+1' to most strongly responding ON neurons and setting a recognition threshold that is less that this sum allows the classification scheme to be flexible. Interpreted differently, this indicates that an odor can be classified as long as a subset of strongly responding ON neurons are activated so that their sum reaches the threshold. The composition of this subset can change across conditions thereby allowing this approach to be more flexible.

What then is the contribution of the OFF component of the classifier? In an earlier study[82], we had found that OFF responses were better at predicting when the behavioral response to a conditioned odorant terminated. Here, in this study we found that the OFF component increased separability between activation patterns of different odorants. This enhanced discrimination between odorants and thereby reduced false positives.

Our results indicate that not only the odor-evoked responses but even the spontaneous activity can change across conditions. Earlier studies have argued that the antennal lobe neural network can be viewed as a non-linear dynamical system[97, 146, 147]. Under this perspective, our results indicate that both the initial conditions and odor-evoked response dynamics can vary across conditions. Yet at direct odds with our neural data, we find the behavioral recognition is robust even during these drastic changes. No detectable differences in response latency, intensity or duration were found. Hence, our results indicate that the rules for translating neural responses and their dynamics to generate behavioral output that is also patterned over time needs further investigation.

Taken together, these results indicate that the neural circuits in the insect olfactory system delicately balance discrimination between odorants with flexibility necessary for robustness and fault tolerance to achieve sensory invariance.

Chapter 6: Switch in neural ensembles with odor intensity

6.1 Introduction

Sensory stimuli that are encountered in natural environment can vary several orders of magnitude in their intensity. This is true for all modalities including olfaction. Male moths are known to perform single molecule detection and travel substantial distance to track their female counterparts [148]. On the other end of the spectrum, having the odor source right under the nose/antenna, like a fly sitting on a rotting fruit, should generate vapors that are near saturation. While prior work has shown that animals can ignore information regarding odor intensity and perform invariant recognition of the stimulus [149, 150], under what conditions is this computation not feasible? Given that some odorants are attractive at lower intensities for insects and switch to being repulsive at higher intensities [151, 152], it is reasonable to expect that neural responses to the same stimulus must diverge at the extremum intensity values. In this study, we examined how individual and ensemble neural responses vary with intensity in the locust olfactory system.

How the neural responses vary with odor intensity has been well-investigated at multiple circuits in the olfactory pathway, in both the vertebrate [153-155] and the invertebrate [48, 156, 157] models. In the insect antennal lobe (AL) [11-14, 41, 46, 48, 52, 54, 82, 97], the first downstream center from olfactory receptor neurons (ORNs), spatiotemporal responses evoked by projection neurons (PNs) have been found to vary with, and therefore, encode both odor identity and intensity [8, 46, 48, 52, 158]. Increasing stimulus intensity is known to increase responses in individual neurons, and recruit activity in additional less-sensitive neurons [159, 160]. Therefore,

the ensemble responses vary with intensity, but to a lesser degree than changes in odorant identity [48].

The ability to compress neural responses and the variations that arise due to stimulus intensity have been attributed to antennal lobe circuitry involving local neurons [56, 63, 161]. Local neurons (LNs) receive feed-forward inputs from ORNs [56], and recurrent inputs from PNs [22, 57, 58]. The LN responses have been shown to scale with the total ORN input and thereby prevent PN activity from saturating – a gain control function [56, 63]. Since LNs are not a homogenous group [20], and not all PNs monotonically vary with intensity changes, whether there are different sub-groups of LNs that help carrying out different computations is not clear.

In this study, we examined when does the neural invariance with respect to stimulus intensity breaks down. We identify two types of local neurons and how they compete to alter neural responses evoked with odor intensity. Particularly, we show that odor intensity acts as a bifurcation variable and can switch the neural ensembles activated at the extremums. Finally, using a simplistic computational model we provide mechanistic insights regarding how inhibition could both squash and amplify variations in sensory input.

6.2 Results

6.2.1 Switch in odor-evoked responses with concentrations

We began by examining how responses in individual PNs vary over a wide range of odor intensities (four log units of dilutions; **Fig. 6.1a-c**). We found that at the lowest intensities, only a small fraction of PNs were activated (ON responders; 14/80 PNs) or inhibited (23/80 PNs were suppressed below baseline levels). As was observed in our earlier studies [82], the inhibited

neurons increased their firing rates after the termination of the stimulus (i.e. OFF responders). Increasing stimulus intensity increased the number of both activated (38/80 PNs) and inhibited (20/80 PNs) neurons. However, most PNs that were sensitive and were activated at lower intensities were inhibited at higher odor concentrations and vice versa (**Fig. 6.1 a-e**). In other words, most ON neurons at lower intensity of a stimulus switched and became OFF responders at higher intensities (**Fig. 6.1 b, d**), and most OFF neurons became activated during the stimulus presentation at higher intensities (**Fig. 6.1 c, e**). These results indicate that neural ensembles that get activated can switch between widely different intensities of the same stimulus.

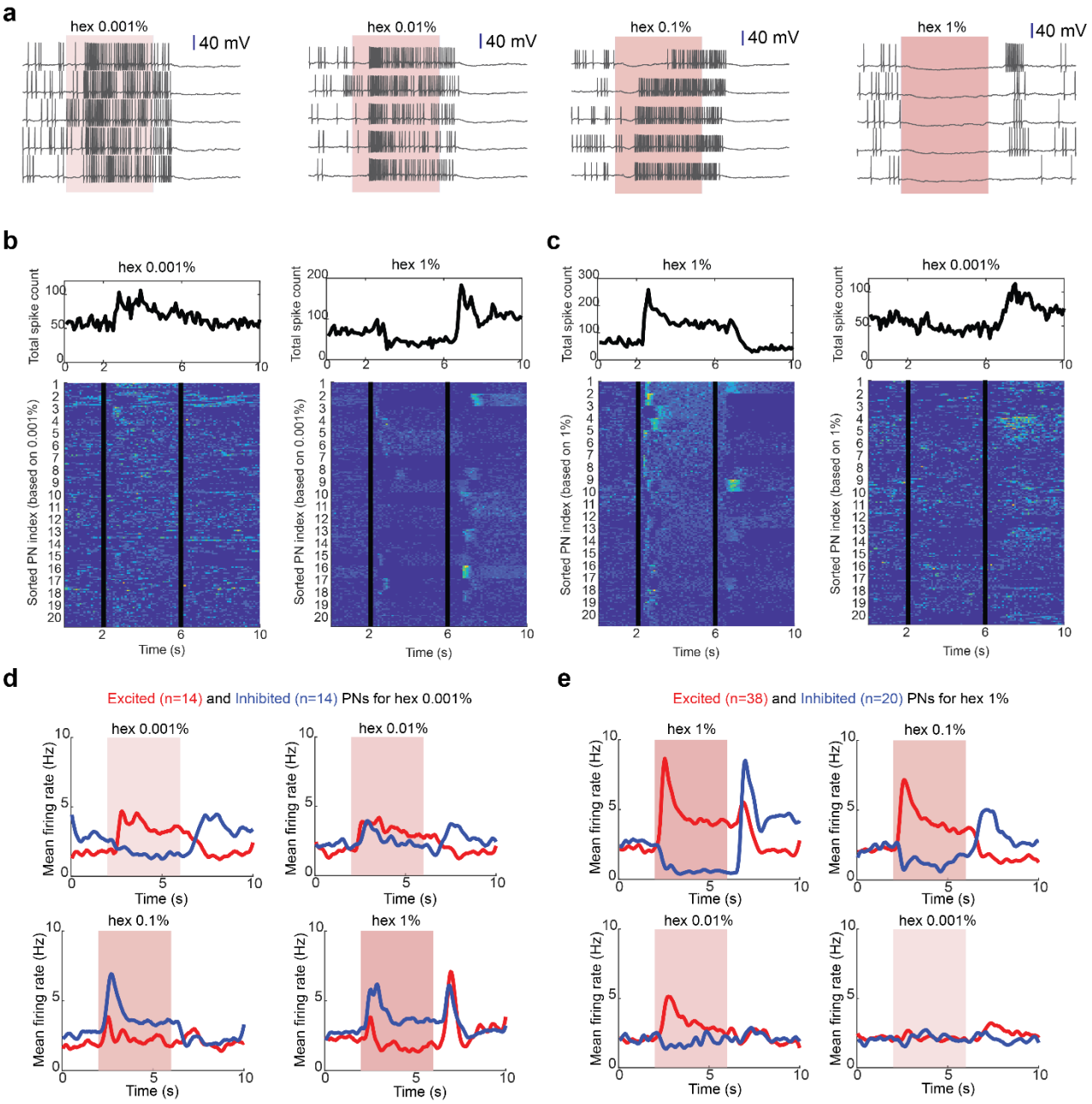

Figure 6.1: Individual PN responses switch from ON to OFF and vice versa with stimulus intensity. **(a)** Intracellular voltage traces showing responses of a projection neuron to four different intensities of hexanol (hex) are shown. Each panel shows PN responses in five trials to show reliability of activity patterns observed. A 40 mV scale bar is shown at the top of each panel. Note that the PN is activated at 0.001% but inhibited at 1%. **(b)** Firing rates of twenty PNs that had greatest increase in firing activity during hex 0.001% (v/v) are shown. Responses of each PN in ten trials are shown as ten consecutive rows in the heat map. The overall mean firing rate across these PNs as a function of time is shown at the top of the panel. The responses of the same twenty PNs but at a higher intensity of the same odorant (hex at 1% v/v) is shown on the right. **(c)** Similar plot as in **panel b** but showing the responses of top twenty PNs that were activated the most by hex 1%. **(d)** Mean firing rates of all excited (red) or inhibited (blue) PNs by

hex 0.001% are shown at four different intensities of hex. (e) Similar plots as in **panel d** but showing mean responses of all PNs that were excited (red) or inhibited during stimulation with hex at 1%.

6.2.2 Ensemble neural response variation with stimulus intensity

We next examined how PN ensemble activity varies with intensity. We visualized the odor-evoked responses distributed across the 80 recorded PNs using the principal component analysis (see Methods; **Fig. 6.2 a**). At a given stimulus intensity we observed the stimulus-evoked response comprised of two components: an ON-response trajectory during stimulus presentation and an OFF-response trajectory after the termination of the stimulus. Consistent with earlier observation, the ON and OFF response trajectories evoked by the same odorant evolved in different directions. Notably, our results indicated that the ON and OFF response trajectories evoked by the same odorant at two different intensities that were just a log-unit apart pattern matched (i.e. evolved in the same direction).

Comparison of odor-evoked responses evoked as the stimulus intensities varied by two log-units or greater revealed that the ensemble activity deviated and had less or no pattern match with those evoked at higher intensities (**Fig. 6.2 a**; right panel). The responses were less intense at the lower intensities and therefore evoked ensemble response trajectories that made smaller loops, but differed from the higher intensity responses nonetheless.

To quantitatively compare these results, we performed a complementary correlation analysis. We found that while PN ensemble activity during the stimulus presentation (hex 1%) was well correlated, the ON and OFF responses evoked were negatively correlated. As the odor intensity decreased, correlation between ON responses evoked gradually decreased thereby indicating a lack of similarity. Consistent with results in **Fig. 6.1**, we found that the ON responses evoked by hexanol at the highest intensity (hex 1%) was positively correlated with the

OFF responses evoked by the same stimulus at the lowest intensity (hex 0.001%; **Fig. 6.2**). The hex 0.001%-ON responses was correlated with hex 1%-OFF responses. Overall, these results show that odor-evoked neural responses varied drastically at widely different intensities of the same odorant.

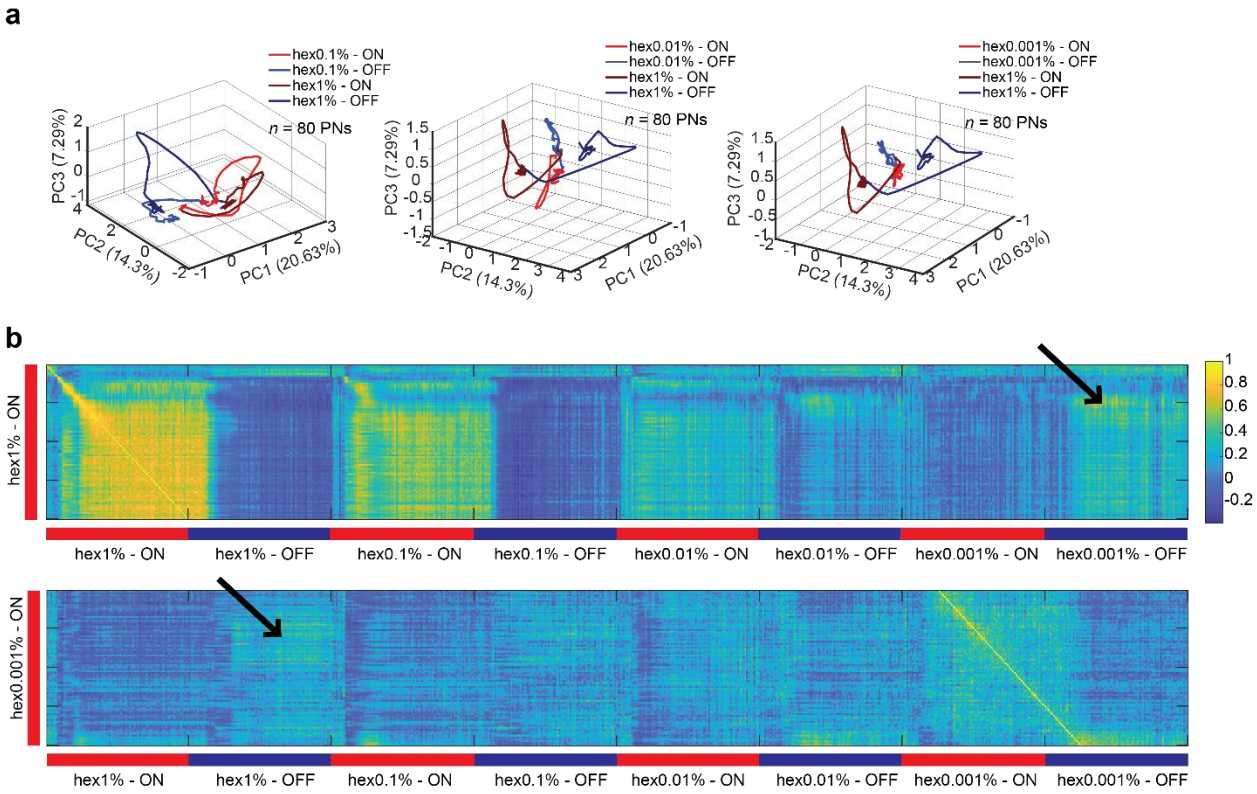

Figure 6.2 Ensemble PN responses vary markedly with stimulus intensity. (a) Population PN responses are shown after dimensionality reduction using principal component analysis. Each panel compares hex 1% response to responses at three other intensities (0.1%, 0.01%, and 0.001%). Both ON and OFF responses are shown. Note that ON and OFF responses for the same stimulus are quite distinct. **(b)** Results shown in **panel a** are quantified using correlation analysis. Top panel shows correlations between ON response evoked during hex 1% with both ON, OFF responses evoked at all the four intensities. Arrow heads indicate that correlation values are higher between hex 1% ON response and hex 0.001% OFF response. Bottom panel shows a similar plot, but correlations were computed with the ON response evoked during hex 0.001% presentation.

6.2.3 PN response variations due to odor identity vs. intensity

Are the response variations observed at widely different intensities comparable to those observed during exposures to different odorants? To understand this, we investigated PN responses evoked by three other odorants (isoamyl acetate or iaa, benzaldehyde or bzald, and citral or cit) at four concentrations (0.001%, 0.01%, 0.1% and 1% v/v). We found that for all these odorants, PN ensemble responses patterns diverged as the gap between the odor intensities widened (**Fig. 6.3a**)

To quantify our results, we performed classification analysis. First, we used training pattern templates at the highest intensity of these odorants and examined how robustly they help recognize odor responses evoked at lower intensities (**Fig. 6.3b; see Methods**). Our results indicate that this approach allowed recognition of responses evoked at slightly lower intensities, whereas response patterns evoked at the lowest intensities were either not detected or on many instances misclassified. Similarly, training templates using odor-evoked response patterns at the lowest intensity failed to robustly recognize at higher intensities (**Fig. 6.3c**). These results are further corroborated by a clustering analysis that showed that often response patterns at extremum values of stimulus intensity wrongly clustered (**Fig. 6.3d**). In sum, these results indicate that the variations in neural response patterns at widely different intensities can be comparable as those evoked by different odorants.

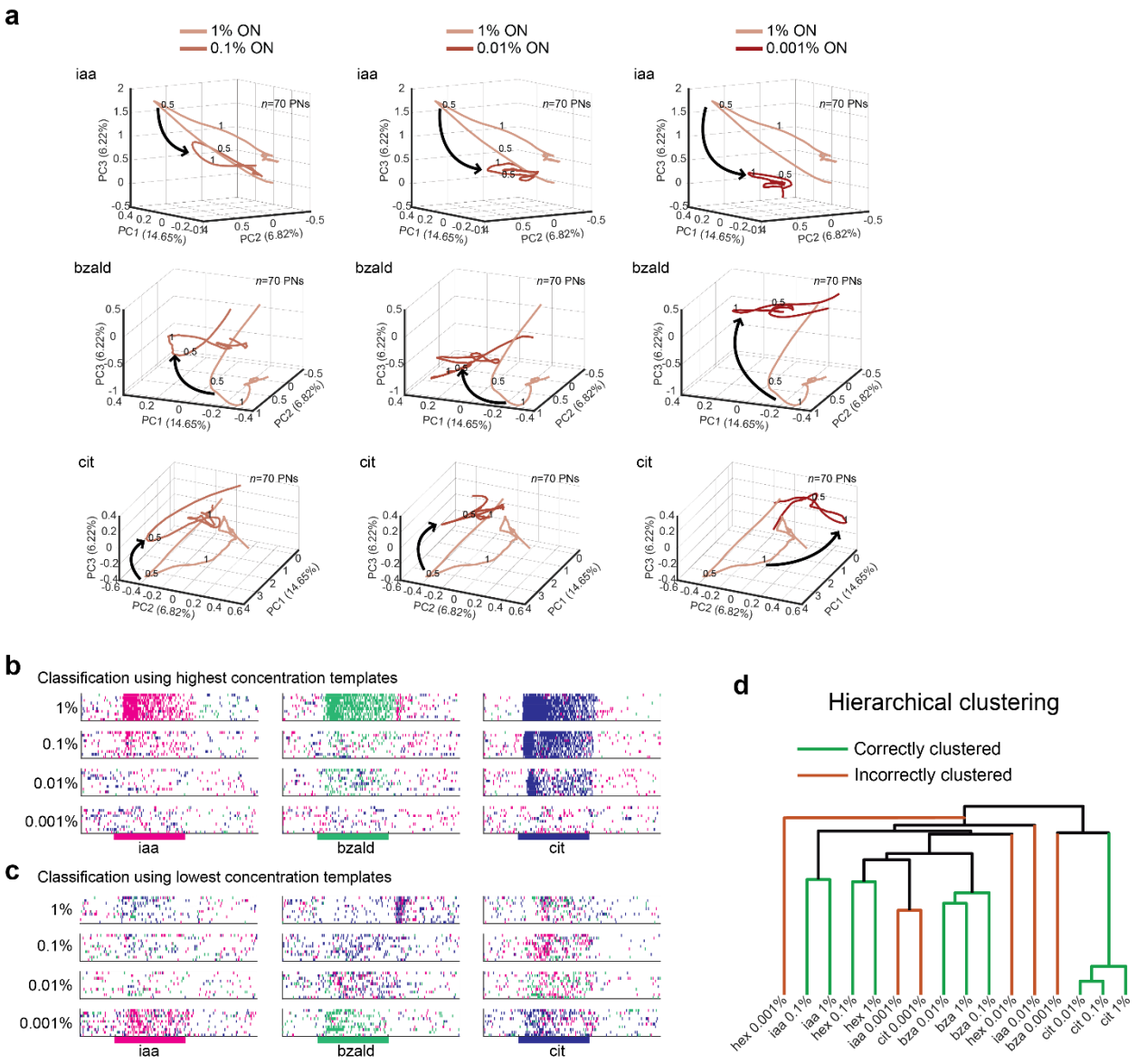

Figure 6.3: Comparison of PN response variations due to odor identity vs. intensity. (a) PCA trajectory plots comparing odor-evoked ON response patterns evoked at two different intensities are shown for three other odorants. **(b)** Results from a timebin-by-timebin, trial-by-trial classification analysis are shown. The mean ensemble response patterns during the first two seconds following stimulus onset were regarded as training templates for each odorant. Only the responses evoked at the highest intensity (i.e. 1% v/v) exposure of each odorant were used as training templates (one template per odorant; see **Methods**). Each timebin in each trial was classified into one of the following categories: response below detection threshold (white), pattern match with iaa 1% response template (magenta), pattern match with bzald 1% response template (green), or pattern match with cit 1% response template (blue). A leave-one-trial-out cross validation was performed to generate results for trials at the highest intensity (see **Methods**). **(c)** Similar plot as in **panel b** but showing classification results generated using templates created using activity patterns during exposures to the lowest intensity of the same set of

odorants. **(d)** Dendrogram generated using a hierarchical clustering analysis are shown. The trial-averaged activity during the 4 s odor exposure was used for each odorant. A cosine distance metric was used to determine the distance between the high dimensional activity patterns.

6.2.4 Two distinct local neuron types based on stimulus intensity variations

The projection neuron responses are modulated by GABAergic local neurons (LNs) in the antennal lobe. The local neurons have been shown to contribute to many different neural computations [56, 63, 161] including gain control [56, 63]. Therefore, we wondered how the LN activity varies with odor intensity.

We performed whole-cell recordings to understand LN responses to three odorants delivered at a wide range of concentrations (1%, 0.1%, 0.01%, 0.001%, and 10% v/v). As reported earlier [51, 58], LNs in the locust antennal lobe fire small spikelets and not full-blown sodium spikes (**Fig. 6.4a, b**). Based on the activity levels in the absence of any stimulus, we found that there are broadly two subtypes of LNs: one subtype that showed less spontaneous activity, and the other that showed higher levels of spontaneous activity (**Fig. 6.4a, b**). Interestingly, we found that these two types of LNs also differed in how they responded to odorants. While the LNs with less spontaneous activity depolarized during stimulus exposures, the LNs with higher spontaneous activity hyperpolarized during stimulus presentations (**Fig. 6.4a, b**).

To quantitatively understand how the LN responses varied as a function of odorant intensity, we used a differential area under curve (dAUC) metric. The dAUC metric took into account the overall deviation in membrane voltage during odor stimulation period and subtracted the value from the pre-stimulus period ($dAUC = mean(V_{odorON}) - mean(V_{preOdor})$). We found that the LN responses were less odor specific and tended to respond to all odorants in the panel used.

Further, as intensity increased, LNs with less spontaneous activity had monotonically increasing depolarization (**Fig. 6.4a**), whereas LNs with high spontaneous activity had monotonically increasing hyperpolarization (**Fig. 6.4b**). While the monotonic increase in LN depolarization response is consistent with their role in gain control functions, whether the hyperpolarizing LNs contributed to how information regarding stimulus intensity is processed was unclear.

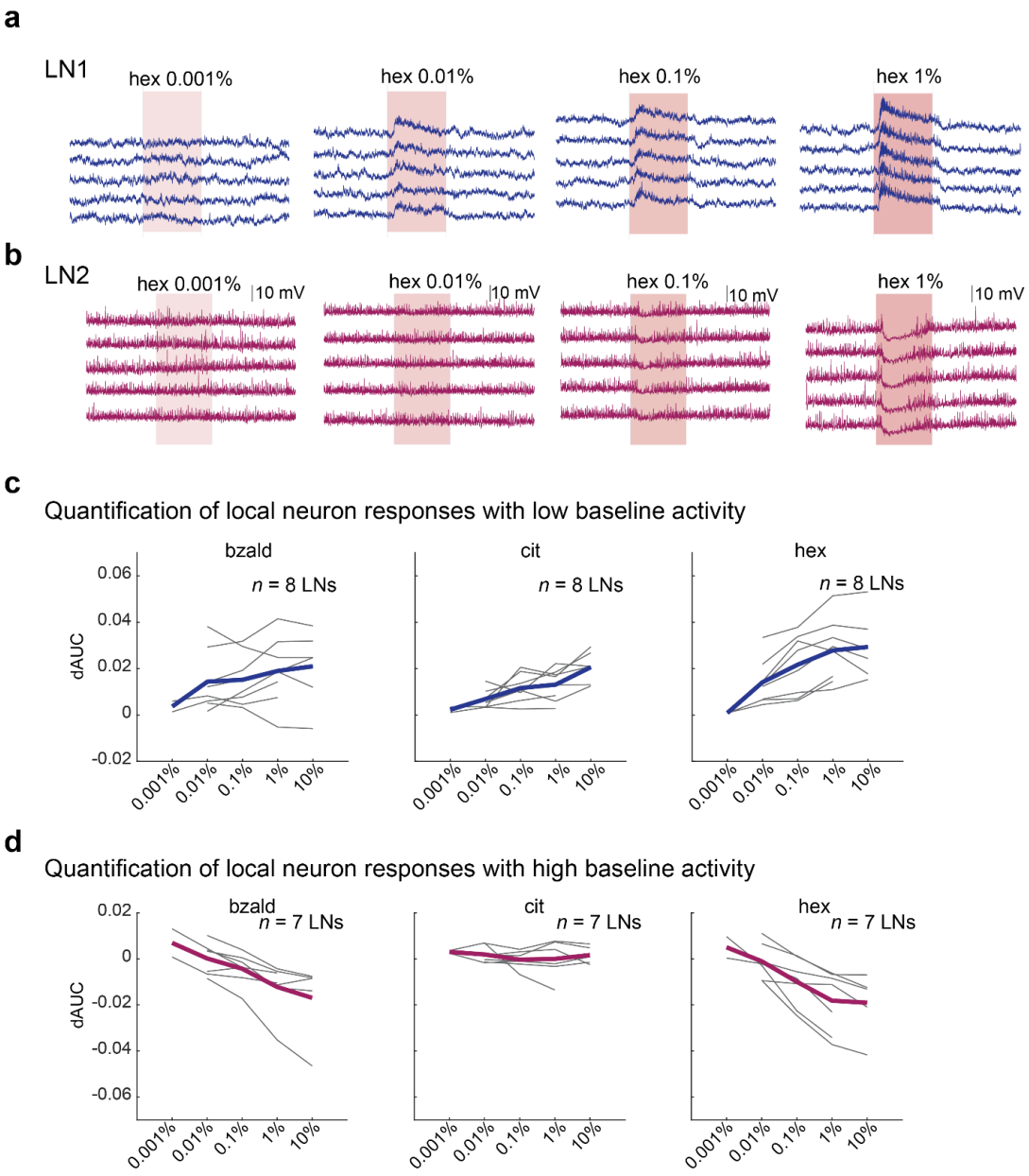

Figure 6.4: Two subtypes of local neurons that monotonically increase or decrease their activity with stimulus intensity (a) Intracellular voltage traces showing spontaneous and stimulus-evoked responses in a local neuron. The four panels correspond to sets of five trials when hexanol at four different intensities were presented. The color bar indicates the 4 s duration of the stimulus exposure. **(b)** Similar plot as in **panel a** but showing the responses of the second type of local neuron with high baseline activity that was hyperpolarized during odor exposure. **(c)** Dose-response curves quantifying LN responses as a function of odor intensity. Each panel shows the mean dose-response curves for individual local neurons to one of the following for three odorants: bzald, cit, and hex. LN responses were quantified using differential area under curve (dAUC) metric. dAUC was computed by finding the total change in membrane voltage during odor presentation and subtracting out the pre-stimulus activity level (see Methods). The mean across the local neurons are shown in solid blue. Note that local neurons that had low baseline and were depolarized during odorant exposure were segregated and are shown here (similar to LN1 in **panel a**). **(d)** Similar plots as in **panel c** but showing dose-response curves for the local neurons that had high baseline during pre-stimulus period and was hyperpoloarized during odor exposure (similar to LN2 in **panel b**)

6.2.5 A mechanistic model of antennal lobe circuitry with intensity-mediated response switching

Our results indicated that there are two type distinct types of local neurons that either monotonically increased or decreased their response as odor intensity was systematically changed. We wondered whether these two types of LN alone can explain the switch in the ON-OFF PN response ensembles observed at stimulus intensity extremums (refer **Fig. 1**). To examine this issue, we developed a well-constrained computational model of the antennal lobe with two distinct LN types we observed (**Fig. 6.5a**). The AL model had the following components: (i) feed-forward excitatory input from ORNs to all the PNs and to the first group of high-threshold LNs that depolarized only upon odorant exposure (LN_{sLow}) (ii) a second group of LNs with high baseline activity (LN_{sHigh}) that receives feed-forward inhibition from LN_{sLow} (iii) an additional source of input to the LN_{sHigh} to support its high spontaneous activity levels, and finally (iv) recurrent connections between PNs and both LN categories. Note that the PN

ensemble were split into two sub-groups, one that provided to input to the LN_{sLow}, and the other to the LN_{shigh}.

We simulated sensory neuron inputs at two different intensities to drive odor-evoked responses model (**Fig. 6.5b**). As different intensities were simulated by scaling the ORN responses, the input patters were highly similar at high and low intensities. At high intensity, the LN_{sLow} were activated strongly during the stimulus ON period interval as they received excitatory inputs from both ORNs and PNs (**Fig. 6.4c**). As a result, they suppressed activity in the LN_{sHigh}. This in turn had the effect of biasing the competition in favor of the PNs from ensemble 1 (PNs-set1) that received inhibition from LN_{sHigh}. Therefore, during the odor exposure, the identity of the stimulus was encoded by the combination of the PNs from the ensemble set 1 (PNs-set1; **Fig. 6.4d**).

At the lower intensity, this entire scenario was reversed. Matching our in vivo results, LN_{sLow} that had higher spiking threshold to ensure that they had lower spontaneous activity were not activated (**Fig. 6.4e**). As a result, LN_{sHigh} were not suppressed during the odor exposure period. This biased the competition in favor of the PN ensemble set 1 (PNs-set1; **Fig. 6.4f**). In sum, this resulted in the set of PNs that were activated at high and low intensity of the same pattern of input but with different scaling to be drastically different, matching the results that we observed *in vivo* (**Fig. 6.4g, h**).

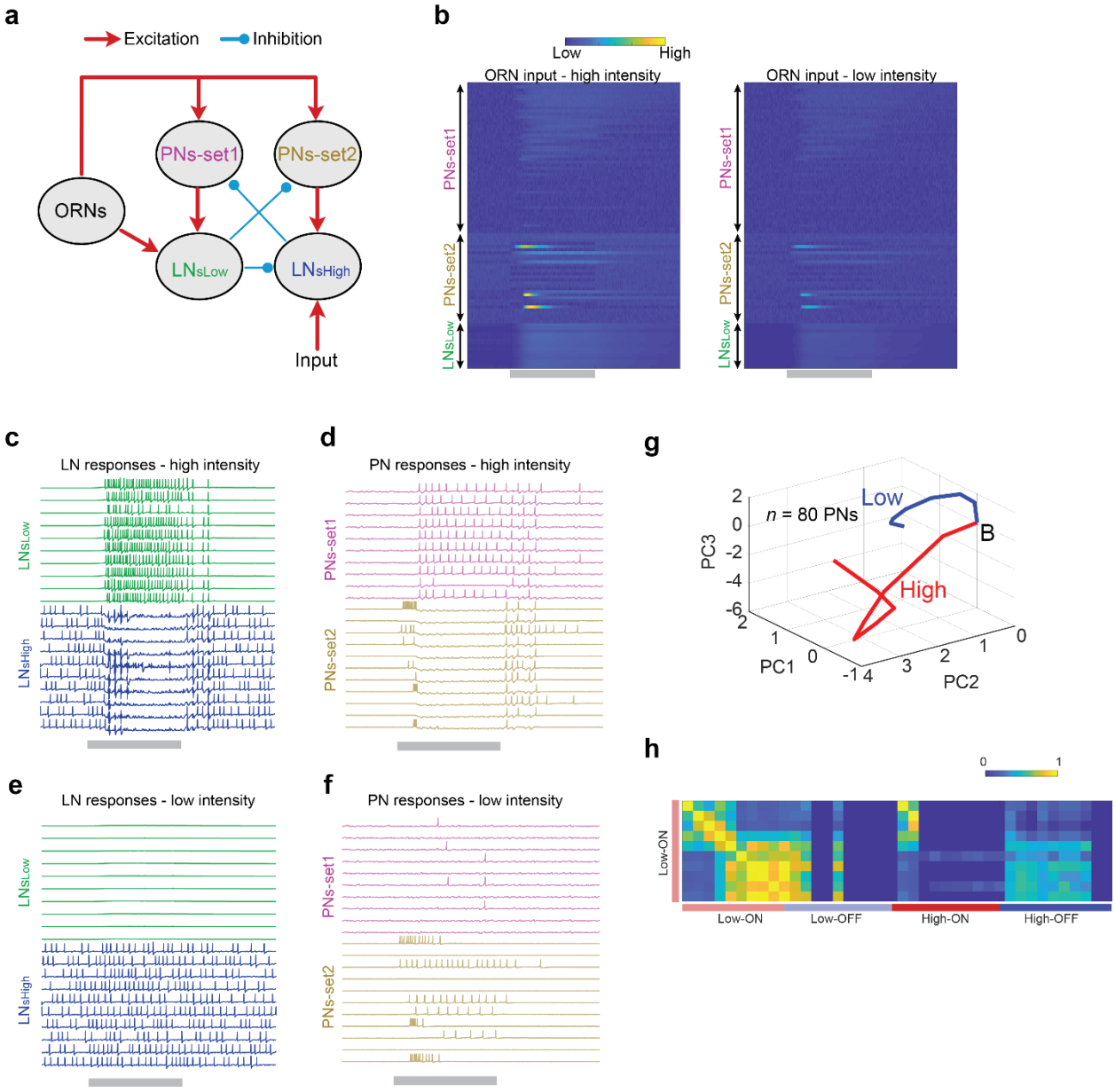

Figure 6.5: A computational model of antennal lobe for switching ensemble response patterns by varying input intensity. (a) A schematic of the model explaining the connectivity and the constraints set between ORNs, LNs, and PNs. LN_{sLow} and LN_{sHigh} correspond to two subtypes of local neurons with low and high baseline activity levels, respectively. While LN_{sLow} receive a direct ORN inputs, LN_{sHigh} receive input from a different source. When activated LN_{sLow} inhibits LN_{sHigh}. PNs-set1 and PNs-set2 correspond to two sub-populations of projection neurons that exclusively receive inhibition from LN_{sHigh} and LN_{sLow}, respectively. **(b)** Simulated sensory input to the model at two different intensities are shown. Inputs to PNs-set1, PNs-set2, and LN_{sLow} are stacked on top of each other and shown as a heat map. Hot colors indicate stronger input. Gray bar at the bottom of each panel identifies the duration of stimulus exposure. **(c, e)** Spontaneous and odor-evoked activities in a selected subset of ten local neurons from both categories are shown at high and low intensities. **(d, f)** A subset of ten PNs from two ensembles that vary

in which local neuron type inhibits them are shown at high and low intensities. Note that PNs-set2 were active during low intensity, whereas PNs-1 were activated during high intensity exposures of the same simulated odorant. **(e)** PCA trajectories of the ensemble PN responses (PNs-type1 and PNs-type2 both included) are shown for both high (shown in red) and low (shown in blue) intensities. 'B' indicates the starting point when the stimulus started. **(f)** Similar plot as in **Fig. 6.2b** but showing how correlation (or similarity) between ensemble PN activity elicited by the same odorant at high and low intensities.

6.2.3 Discussion

We examined whether PN responses remain invariant to stimulus identity when intensities are varied. Interestingly, we found that the same neuron can be excited i.e. ON responsive at a low intensity and inhibited at a high intensity, and therefore, OFF responsive. Moreover, at population-level, we found that a switch can happen between ON and OFF neural ensembles. Notably, PNs that were ON responsive at low intensities tended to be OFF responsive at high intensities, and the ones that were OFF responsive at low intensities tended to be ON responsive at high intensities. This result indicates that populations that were activated can vary drastically with minimal overlap when intensities are widely different.

We further examined spatiotemporal responses of PNs across intensities for the same odorant by comparing the response trajectories for different intensities with respect to trajectory for the highest intensity. We found that there was a systematic shift in the population PN response as intensity was reduced, and responses at the lowest intensity were aligning more to OFF response at highest intensity than with the ON response. A correlation analysis using all the n (number of PNs) dimensions also revealed the same. Prior studies have noted that OFF response of a stimulus tend to fall in an orthogonal subspace and is very distinct from its ON response [82]. Our result indicates that ON responses of the same stimulus can become very distinct even when intensities are changed. We further found that the response trajectories varied

similarly with intensity for three other odorants: iaa, bzald and cit – indicating that this result is more general. Next, we examined if these shifts in PN response patterns confounds the identity. From a multi-class classification analysis using pattern matching, we found that both the patterns at high and low intensities failed to reliably classify across all the intensities. Furthermore, when low intensity templates were used for classification, we found misclassifications (classified as a different odor) at higher intensities.

We examined the role of local neurons in reshaping PN activity at different intensities. We found that there are, broadly, two sub-types of local neurons based on their spontaneous activities. These two populations were also found to respond to odors in a contrasting manner. While the local neurons with no spontaneous activity depolarized in response to stimuli, the ones with high spontaneous activity got hyperpolarized.

Could the two sub-types of local neurons contribute differently in shaping PN activity at different intensities? To understand the role of LNs and a possible network-level mechanism, we developed a well-constrained model using the insights gained from local neuron recordings. Noting the inhibition of spontaneously active local neurons, we added inhibitory connections from one population of local neurons to the others, since there is no other known source of inhibition in the locust antennal lobe. Next, PNs responding at low intensities suggest a lack of inhibition to those PNs. Therefore, we constrained connectivity between PNs and LNs, where spontaneously active LNs connect to one sub-population of PNs and spontaneously inactive LNs connect to the other sub-population PNs. This modeling resulted in responses that are consistent with electrophysiological recordings of both PNs and LNs at high and low intensities. In sum, this study shows that PN responses can diverge to a large extent when intensity is varied, and a possible network-level mechanism that involves two types of LNs explains these variations.

Chapter 7: Conclusions and Future Work

7.1 Conclusions

The main objective of this work is to understand how neural representation of odorants is patterned across neurons and time, how it is altered when the same stimulus is encountered in multitude of ways and what are the adaptive features of this representation. The results presented clearly capture the complexity of neural response patterns in dynamic stimulus scenarios, where neural responses not only depend on the dynamics of stimuli but also on the internal adapted state. Additionally, we examined how could the olfactory system robustly encode the stimulus-specific information even though the stimulus-evoked neural responses are highly variable.

First, we examined odor-evoked neural responses both during stimulus presentation (ON response) and after its termination (OFF response). We found that, at the ensemble-level, ON and OFF responses are orthogonal to each other – a result that was consistent across all the stimuli, including mixtures. Using quantitative methods to analyze high-dimensional PN activity, we found that the OFF response of a stimulus was generally the most distinct response to ON response of the same stimulus. Further, OFF responses were found to carry similar amount of information (bits/s) as ON responses. However, these two epochs of responses were found to differ in one aspect: engaging the local inhibitory circuits, a necessary mechanism for oscillatory synchronization of PN responses.

Given that ORNs are prominently ON responsive, how are the OFF responses generated? We hypothesized whether an activity-dependent cell-intrinsic form of adaptation exits. Using a

computational model, where PNs were modeled with a bi-directional threshold adaptation, we found that the modeled PNs could generate OFF responses like results found *in vivo*.

Additionally, to understand why the PNs show a significant response following the termination of odors, and almost as informative as ON response, we investigated the behavioral significance of OFF responses. While ON responses correlated strongly with behavioral initiation, we found that OFF responses correlated better with the behavioral response termination. Establishing this link between PN responses and behavior helped us hypothesize that behavioral termination is also an active mechanism, similar to behavioral initiation.

We next examined the variability of neural responses when stimuli are encountered in sequence, when a target odor follows a distracting odor. We found that PN responses to a target odor varied drastically, depending on the stimulus history. In general, we found that the commonly activated PNs (common to both target and distractor odors) were suppressed, and uniquely activated PNs to target odor were enhanced. As such, PN responses to a target odorant were less correlated to responses elicited by the distracting odor i.e. 'Contrast Enhancement' when the two odorants were encountered in sequence. These history-dependent changes showed that both spatial and temporal response features were inconsistent to reliably encode identity. However, through behavioral studies, we found that locusts trained to recognize a target odorant can identify the presence of target odorant in all the sequential conditions.

To resolve this confound, we proposed a flexible coding approach – without having to rely on a fixed set of PNs or a specific temporal response motif. The core idea behind this coding approach is that activation of any subset, of a minimum size, of responsive PNs can reliably encode odor identity (m responsive neurons – out of – n total responders; $m < n$). Classification

results showed robust recognition of target odorant in all the conditions. Further, we predicted the behavior using ON and OFF responses of PNs. We found that the behavior predictions closely matched with the true behavior and showed fewer false positives after incorporating OFF responses for prediction – signifying a potential role of OFF responses in behavior.

Later, we examined the extent of PN response variability using a complex stimulation procedure, which varied pulse durations, inter-pulse intervals, introductions of other competing and distracting odorants, and changes in ambient conditions. While these aspects have been studied individually, we combined them into a single stimulation procedure to examine how the same set of PNs vary across a wide range of conditions. We found only a few PNs responded reliably across all the conditions of an odorant, but those PNs were not selective. This indicates that there was no unique combination of PNs that reliably responded across all the presentations of an odorant.

We found that changes in humidity not only altered the spontaneous firing of PNs but also odor-evoked responses—adding another layer of complexity to find a decoding solution. We tested whether the flexible decoding approach would classify the odor identity. Our results indicate that the m-of-n classification could provide robust recognition of the odorant across all the examined conditions. Moreover, classifiers using both ON and OFF responses resulted in fewer false positives, consistent with our earlier study. Taken together, these studies suggest that individual PN responses can be highly adaptive depending on the condition, however, a flexible subset of PNs remain activated across all instances when an odorant is encountered. These findings highlight the importance of incorporating flexibility in the neural encoding and decoding schemes to allow robust detection and recognition of a stimulus.

Finally, we examined when robustness could not be achieved. To study this, we examined neural responses to an odorant over a wide range of stimulus intensities. While it is true that some PNs that respond at high intensities do not respond at lower intensities, we found that the opposite is also true. Notably, PNs that responded at low intensities tended to be inhibited and OFF responsive at higher intensities. At the ensemble level, response trajectories of highest and lowest intensities were found to be almost orthogonal. Interestingly, the ON response at lowest intensity was more correlated to the OFF response at highest intensity than its ON response. After examining a diverse set of odorants, we found that this result is more general – leading to identity confound. Templates constructed using either the highest or the lowest intensities failed to reliably classify the odor identities across all the intensities. To resolve this confound, we investigated the contribution of feed-forward and feedback inhibition from LNs in intensity coding. From intracellular studies, we found that LNs can be broadly classified into two subtypes based on their spontaneous activity. Interestingly, these subtypes also differed in their odor-evoked responses. While the LNs with low spontaneous activity responded with monotonically increased response (more depolarization) as intensity increased, the LNs with high spontaneous activity responded with monotonically decreasing response (more hyperpolarization). We hypothesized that the subpopulation of LNs that get inhibited receives inhibition from the other group of LNs. Moreover, to investigate a possible mechanism, we developed a computational model of the antennal lobe network with the two LN subpopulations revealed in our experimental data. Our simple model of the antennal lobe not only replicated the local neuron response dynamics but also showed that activated PN ensembles can switch with intensity.

In sum, this study reveals insights on how a relatively simple invertebrate olfactory system performs complex adaptive computations and how it can achieve invariance.

7.2 Future work

What neural mechanisms could underlie contrast enhancement? While it was clear that common features were suppressed, and unique features were enhanced due to sequential presentations, the underlying neural mechanism is not understood. Are the underlying neural mechanisms that generate OFF responses also common to contrast enhancement computation? We investigated the role of two mechanisms: cell-intrinsic form of adaptation, and network-level adaptation due to LNs.

7.2.1 Activity-dependent plasticity in single projection neurons

Earlier in Chapter 3, we hypothesized that a cell-intrinsic form of adaptation would be necessary to generate the OFF responses observed *in vivo*. To examine whether this is indeed the case, we performed whole-cell recordings from individual PNs and monitored spiking activity before, during and after current injections (**Fig. 7.1**). We found that the PN firing rates following a positive current pulse decreased below the pre-pulse activity levels (**Fig. 7.1a**). However, for the same neuron, following a negative current pulse, the observed post-pulse activity levels were greater than the pre-pulse firing rates (**Fig. 7.1b**). Thus, it appears that the spontaneous PN activity is not a constant, but changes based on recent response history: a period of intense firing is followed by a prolonged period of low spontaneous activity (**Fig. 7.1a right panel**), whereas following an epoch of hyperpolarization, the spiking activity increases compared to the pre-pulse level (**Fig. 7.1b right panel**).

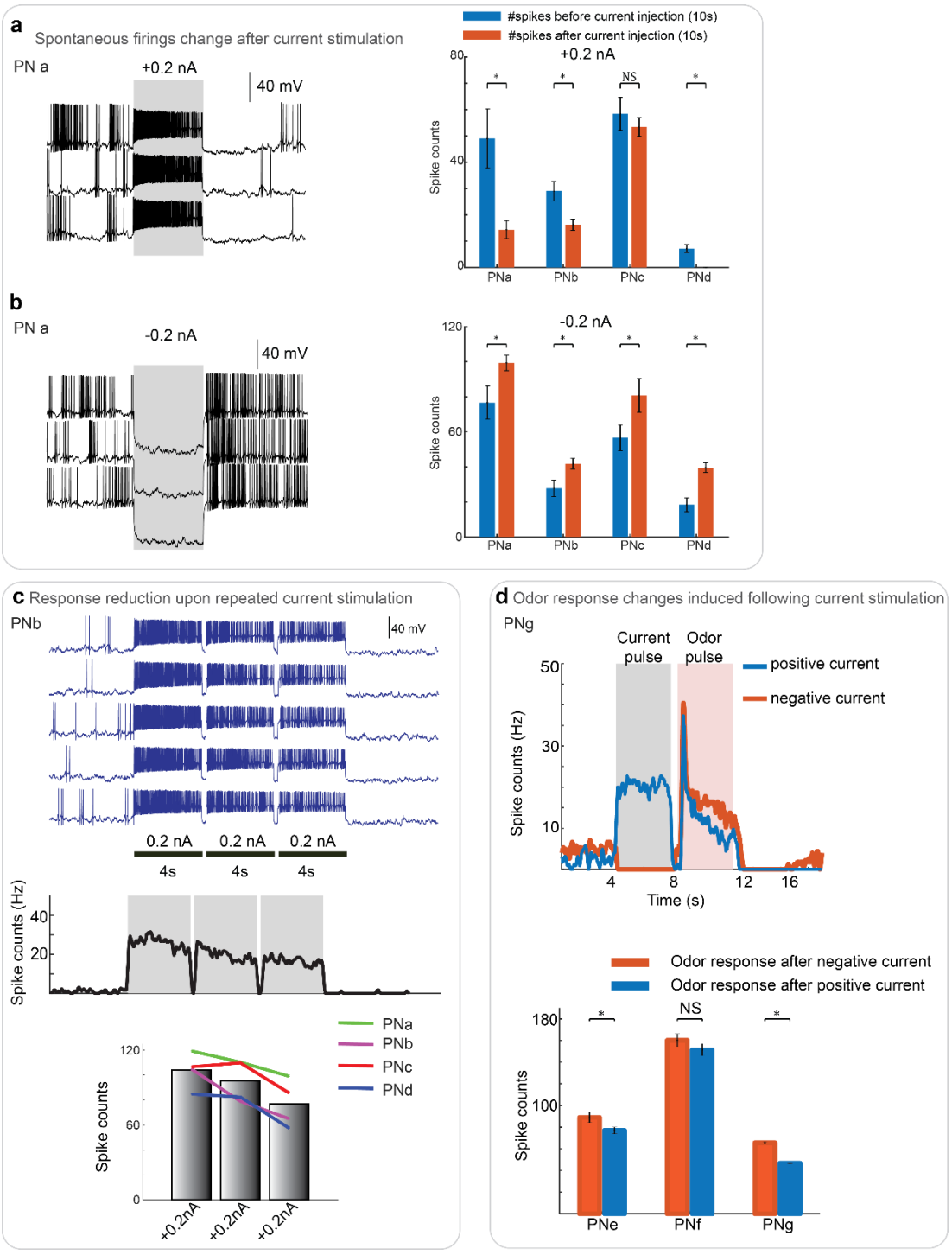

Figure 7.1 Activity-dependent plasticity in individual projection neurons. (a) Intracellular voltage traces revealing PN activity before, during and after a 4 s current pulse (+0.2 nA; gray box). Each row corresponds to one trial and current pulses in successive trials were 60 s apart. Right panel: Bar plots comparing PN spike counts during pre- (blue) and post- (orange) current injection periods. The height of the bar indicates the mean of spike counts and error bar indicates s.e. (standard error) across trials.

Asterisks indicate a significant decrease in spike count (*P < 0.05, NS: P > 0.05, paired t-tests, n = 3 trials for PNa and n = 5 trials for PNs b-d). (b) Bottom panel, similar plot as in the top panel but showing similar results but for a negative current injection (-0.2 nA). Note, asterisks in the right panel indicate a significant increase in spike count. (c) Top panel, intracellular voltage traces recorded from a PN are shown. Three consecutive positive current input of +0.2 nA (each 4s in duration) separated by a 250 ms IPI were used to evoke a firing response. Results from five consecutive trials are shown to illustrate repeatability. Middle panel, trial-averaged firing rates into 50 ms time bins are plotted as a function of time. Bottom panel, bar plot comparing trial-averaged spike counts in each of the three current injection pulses is shown. The height of the bar indicates the mean across four PNs, and individual PN responses are indicated using lines of different colors. (d) Top panel, Firing rates of a PN to a non-overlapping sequence of a 4 s current injection pulse followed by 4s odor presentation (500 ms gap) is shown. The blue line corresponds to the trial-averaged PN firing rates when a positive current (+0.1 nA) was injected before odor pulse (hex 1%) and the red line corresponds to the case when negative current (-0.1 nA) was injected before odor pulse (again hex 1%). Bottom panel, trial-average spike counts elicited by the odorant is shown as bar plots. Red bars correspond to odor responses (hex 1% for PNe, g and citral1% for PNf) following a negative current pulse (-0.2 nA for PNe, -0.1 nA for PNf, g) and blue bars correspond to mean response to the same odorant following a positive current pulse (+0.2 nA for PNe, +0.1 nA for PNf, g). Error bar indicates s.e. (standard error) across trials. Asterisks indicate a significant decrease in spike count (*P < 0.05, NS: P > 0.05, paired t-tests, n = 5 trials).

Next, we examined the response of individual PNs to back-to-back current pulses to determine whether the PNs response history can alter its response to subsequent inputs of equal magnitude (**Fig. 7.1c**). Our results indicate that the response to the first pulse in the sequence was the strongest and the spike count reduced systematically for the second and the third pulse in the sequence (**Fig. 7.1c middle and bottom panels**). This result shows that activity-dependent plasticity not only changes spontaneous firing rates but also firing rate responses to current pulses. Moreover, we examined how this form of plasticity impacts PN responses to odor stimulus. We changed the state of PNs by either depolarizing or hyperpolarizing right before an odor stimulus gets delivered and examined how PNs respond to odor stimulus. We found that the response to the odorant following a positive current pulse was weaker than the response to the same odorant when it was received after a negative pulse that hyperpolarized the cell (**Fig. 7.1d**).

This indicates that PN responses to odor stimuli can also be modulated in an activity-dependent manner.

7.2.2 Local neuron activity is also history-dependent

Could the local neurons in the antennal lobe also mediate a network level change that might mediate population-level neural contrast enhancement? To examine this, we presented a target odorant (hex) in solitary or sequential fashion while monitoring LN activity through whole-cell recordings. We found that not all the LNs responded to the target odorant reliably across all conditions (**Fig. 7.2a**). We found that LN responses were adapted when hexanol presentations followed prior exposures (**Fig. 7.2b**). This result is similar to observation in the PN activity that also showed a similar decrease (**Fig. 7.2c**), and not anti-correlated with the PN activity as would be necessary for mediating a contrast enhancement computation.

Further work will be necessary to determine the contribution of the second subtype of LNs i.e. with high spontaneous activity. To gain a deeper understanding, network-level mechanisms that contribute to adaptively reshaping PN activity, characterization of both the subtypes of LN responses would be necessary.

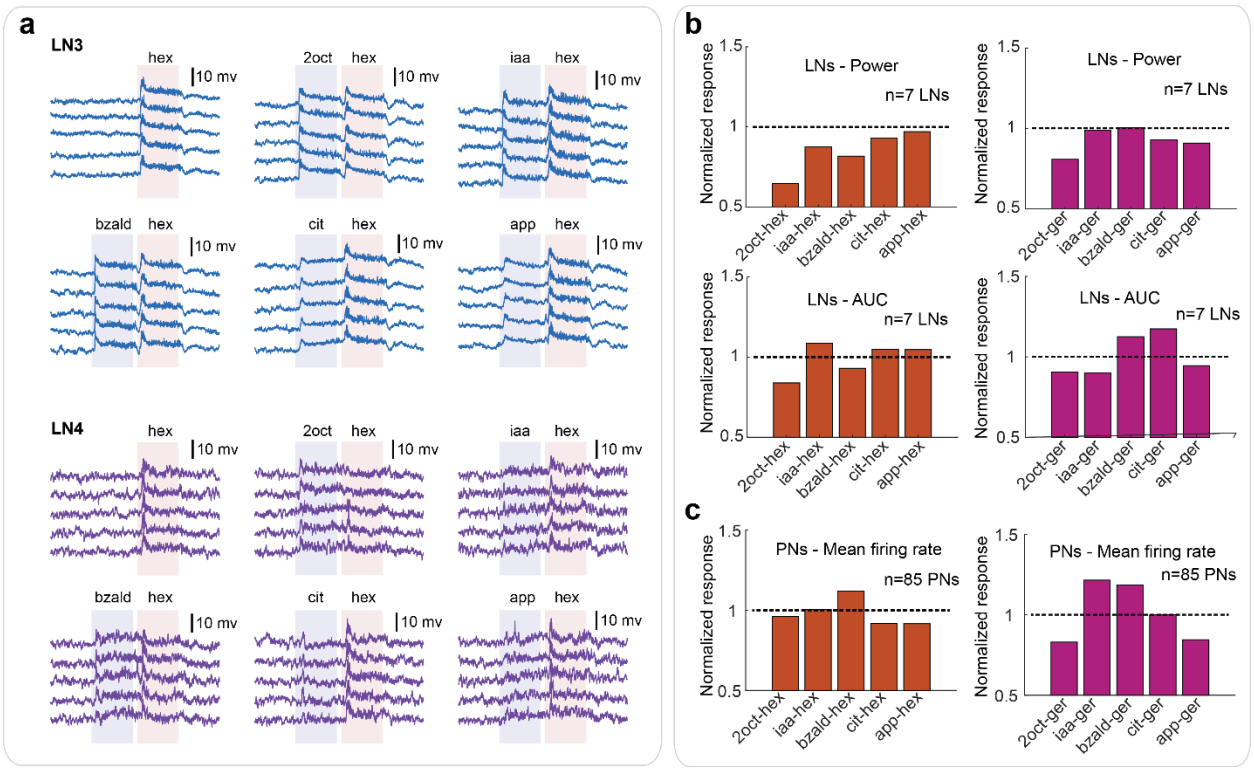

Figure 7.2: Stimulus-history dependent changes are also found in local neuron responses. (a) Intracellular voltage traces of two local neurons (LN3 and LN4) are shown. 6 panels shown for each LN correspond to 6 conditions of hexanol – 1 solitary and 5 sequential presentations following distracting stimuli. Note that LN3 response shows a consistent response to hexanol presentation in all the cases, but LN4 shows an adapted neural response when hexanol was presented after 2-octanol and benzaldehyde. **(b)** Local neuron responses are quantified using two metrics: power and AUC. Power was calculated from spectrogram (window-0.5 s, 90% overlap) by finding total power in 16-25 Hz frequency limits and first 2 s of odor presentation. AUC was calculated by first obtaining a moving RMS of membrane voltage and finding total deflection w.r.t 4 s of baseline period. Each bar in the bar plot shows mean response of LN responses (n = 7 LNs) to a sequential presentation of hexanol (or geraniol), when normalized w.r.t mean response to solitary presentation of hexanol (or geraniol). **(c)** Similar plot as in **panel b** but firing rates of 85 PNs were used to obtain bar plots for both hexanol and geraniol sequential cases.

7.2.3 Sequential odor encoding in Mushroom body

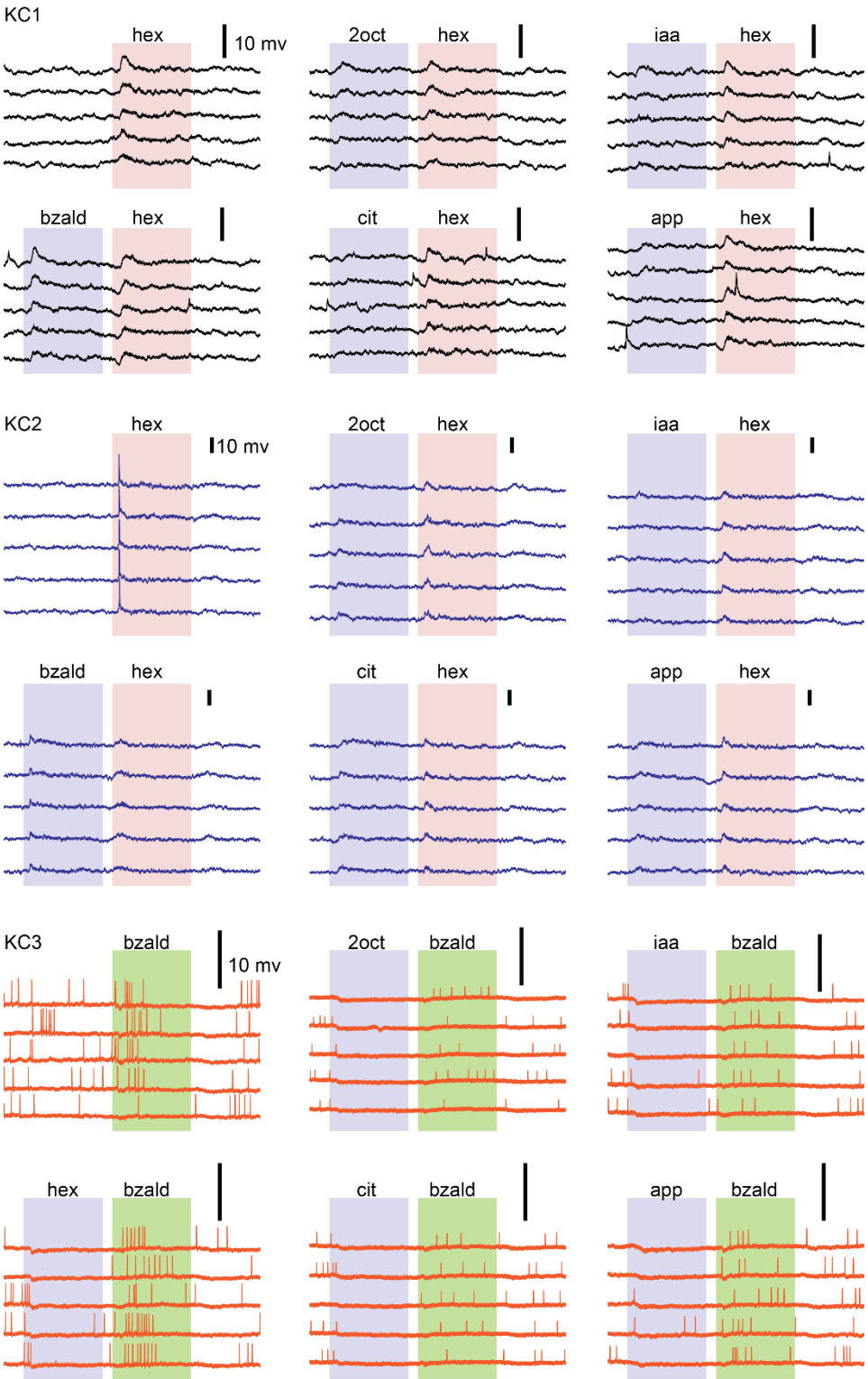

Figure 7.3: Individual Kenyon cells respond variably to sequential stimulus encounters. Intracellular voltage traces of three Kenyon cells (KCs) are shown. Responses to 6 encounters of the same stimulus (one solitary and 5 sequential) are shown for each KC. Responses of KCs 1&2 are shown for solitary and sequential encounters of hexanol (hex), and responses of KC3 are shown for solitary and sequential encounters of benzaldehyde (bzald). Scale bar shown on each panel corresponds to 10 mv.

PNs, in the antennal lobe, project downstream to Kenyon cells (KCs) in the Mushroom body. Given the range of response variations among PNs, we wondered how those adaptive computations – such as contrast enhancement – are exploited in this downstream center. Hence, we have also investigated how KCs respond to sequential stimulus encounters through whole-cell recordings on KCs (**Fig. 7.3**). Consistent with earlier studies, we found their response patterns to be highly sparse, and in some cases with almost no spiking activity (**Fig. 7.3 – KCs1&2**). These KCs, however, showed subthreshold depolarizations in the presence of odors. We found that some KCs could respond with a consistent depolarization across all the cases (**Fig. 7.3 – KC1**). We also found that some KCs that responded strongly to the solitary odorant encounters, but weaker activation in all the sequential presentations (**Fig. 7.3 – KC2**). While this is just the tip of the iceberg, further studies are needed to understand whether variable PN responses drive reliable activity in the mushroom body and lateral horns. This will remain an important direction for future investigation.

References

1. Chung, S., X.R. Li, and S.B. Nelson, *Short-term depression at thalamocortical synapses contributes to rapid adaptation of cortical sensory responses in vivo.* Neuron, 2002. **34**(3): p. 437-446.
2. Ulanovsky, N., et al., *Multiple time scales of adaptation in auditory cortex neurons.* J Neurosci, 2004. **24**(46): p. 10440-53.
3. Tetzlaff, C., Kolodziejski, C., Markelic, I., Wörgötter, F., *Time scales of memory, learning, and plasticity.* Biological Cybernetics, 2012. **106**: p. 715–726.
4. Gupta, N. and M. Stopfer, *Insect olfactory coding and memory at multiple timescales.* Current Opinion in Neurobiology, 2011. **21**: p. 768–773.
5. Hallem, E.A. and J.R. Carlson, *Coding of odors by a receptor repertoire.* Cell, 2006. **125**: p. 143-160.
6. Duchamp-Viret, P., M.A. Chaput, and A. Duchamp, *Odor response properties of rat olfactory receptor neurons.* Science, 1999. **284**: p. 2171-2174.
7. Friedrich, R.W. and S.I. Korsching, *Combinatorial and chemotopic odorant coding in the zebrafish olfactory bulb visualized by optical imaging.* Neuron, 1997. **18**(5): p. 737-52.
8. Raman, B., et al., *Temporally diverse firing patterns in olfactory receptor neurons underlie spatiotemporal neural codes for odors.* Journal of Neuroscience, 2010. **30**: p. 1994-2006.
9. Sicard, G. and A. Holley, *Receptor cell responses to odorants: similarities and differences among odorants.* Brain Research, 1984. **292**(2): p. 283-296.
10. Sanda, P., et al., *Classification of odorants across layers in locust olfactory pathway.* J Neurophysiol, 2016. **115**(5): p. 2303-16.
11. Stopfer, M., et al., *Impaired odour discrimination on desynchronization of odour-encoding neural assemblies.* Nature, 1997. **390**(6655): p. 70-74.
12. Vickers, N.J., et al., *Odour-plume dynamics influence the brain's olfactory code.* Nature, 2001. **410**(6827): p. 466-470.
13. Ito, I., et al., *Sparse odor representation and olfactory learning.* Nature Neuroscience, 2008. **11**(10): p. 1177-1184.
14. Kreher, S.A., et al., *Translation of sensory input into behavioral output via an olfactory system.* Neuron, 2008. **59**(1): p. 110-124.
15. Keil, T.A., *Fine structure of the pheromone-sensitive sensilla on the antenna of the hawkmoth, Manduca sexta.* Tissue Cell, 1989. **21**(1): p. 139-51.
16. Hallem, E.A., M.G. Ho, and J.R. Carlson, *The molecular basis of odor coding in the Drosophila antenna.* Cell, 2004. **117**(7): p. 965-79.
17. Malnic, B., et al., *Combinatorial receptor codes for odors.* Cell, 1999. **96**(5): p. 713-23.
18. Rospars, J.P., et al., *Relation between stimulus and response in frog olfactory receptor neurons in vivo.* Eur J Neurosci, 2003. **18**(5): p. 1135-54.
19. Nara, K., et al., *A large-scale analysis of odor coding in the olfactory epithelium.* J Neurosci, 2011. **31**(25): p. 9179-91.
20. Hansson, B.S. and S. Anton, *Function and morphology of the antennal lobe: new developments.* Annu Rev Entomol, 2000. **45**: p. 203-31.

21. Laurent, G., *A systems perspective on early olfactory coding.* Science, 1999. **286**(5440): p. 723-8.
22. Leitch, B. and G. Laurent, *GABAergic synapses in the antennal lobe and mushroom body of the locust olfactory system.* J Comp Neurol, 1996. **372**(4): p. 487-514.
23. Ernst, K.D. and J. Boeckh, *A neuroanatomical study on the organization of the central antennal pathways in insects. III. Neuroanatomical characterization of physiologically defined response types of deutocerebral neurons in Periplaneta americana.* Cell Tissue Res, 1983. **229**(1): p. 1-22.
24. Kay, L.M. and M. Stopfer, *Information processing in the olfactory systems of insects and vertebrates.* Semin Cell Dev Biol, 2006. **17**(4): p. 433-42.
25. Davis, R.L., *Traces of Drosophila memory.* Neuron, 2011. **70**(1): p. 8-19.
26. de Belle, J.S. and M. Heisenberg, *Associative odor learning in Drosophila abolished by chemical ablation of mushroom bodies.* Science, 1994. **263**(5147): p. 692-5.
27. Kido, A. and K. Ito, *Mushroom bodies are not required for courtship behavior by normal and sexually mosaic Drosophila.* Journal of Neurobiology, 2002. **52**(4): p. 302-311.
28. Laurent, G. and M. Naraghi, *Odorant-induced oscillations in the mushroom bodies of the locust.* J Neurosci, 1994. **14**(5 Pt 2): p. 2993-3004.
29. Jortner, R.A., S.S. Farivar, and G. Laurent, *A simple connectivity scheme for sparse coding in an olfactory system.* J Neurosci, 2007. **27**(7): p. 1659-69.
30. Eisthen, H.L., *Why are olfactory systems of different animals so similar?* Brain Behavior and Evolution, 2002. **59**(5-6): p. 273-293.
31. Liu, S.L., et al., *Olfactory Bulb Short Axon Cell Release of GABA and Dopamine Produces a Temporally Biphasic Inhibition-Excitation Response in External Tufted Cells.* Journal of Neuroscience, 2013. **33**(7): p. 2916-2926.
32. Panzeri, S., et al., *Cracking the Neural Code for Sensory Perception by Combining Statistics, Intervention, and Behavior.* Neuron, 2017. **93**(3): p. 491-507.
33. Jacobs, A.L., et al., *Ruling out and ruling in neural codes.* Proc Natl Acad Sci U S A, 2009. **106**(14): p. 5936-41.
34. Bialek, W., et al., *Reading a neural code.* Science, 1991. **252**(5014): p. 1854-7.
35. Laurent, G., *Olfactory network dynamics and the coding of multidimensional signals.* Nat Rev Neurosci, 2002. **3**(11): p. 884-95.
36. Stanley, G.B., *Reading and writing the neural code.* Nat Neurosci, 2013. **16**(3): p. 259-63.
37. Nicolelis, M.A. and S. Ribeiro, *Seeking the neural code.* Sci Am, 2006. **295**(6): p. 70-7.
38. Georgopoulos, A.P., A.B. Schwartz, and R.E. Kettner, *Neuronal population coding of movement direction.* Science, 1986. **233**(4771): p. 1416-9.
39. Rodrigues, V., *Spatial Coding of Olfactory Information in the Antennal Lobe of Drosophila-Melanogaster.* Brain Research, 1988. **453**(1-2): p. 299-307.
40. Knaden, M., et al., *Spatial Representation of Odorant Valence in an Insect Brain.* Cell Reports, 2012. **1**(4): p. 392-399.
41. Riffell, J.A., H. Lei, and J.G. Hildebrand, *Neural correlates of behavior in the moth Manduca sexta in response to complex odors.* Proc Natl Acad Sci U S A, 2009. **106**(46): p. 19219-26.
42. Haddad, R., et al., *Olfactory cortical neurons read out a relative time code in the olfactory bulb.* Nat Neurosci, 2013. **16**(7): p. 949-57.

43. Junek, S., et al., *Olfactory Coding with Patterns of Response Latencies.* Neuron, 2010. **67**(5): p. 872-884.
44. Bathellier, B., et al., *Dynamic ensemble odor coding in the mammalian olfactory bulb: Sensory information at different timescales.* Neuron, 2008. **57**(4): p. 586-598.
45. Saha, D., et al., *A spatiotemporal coding mechanism for background-invariant odor recognition.* Nature Neuroscience, 2013. **16**: p. 1830-1839.
46. Saha, D., et al., *Behavioural correlates of combinatorial versus temporal features of odour codes.* Nat Commun, 2015. **6**: p. 6953.
47. Stopfer, M. and G. Laurent, *Short-term memory in olfactory network dynamics.* Nature, 1999. **402**(6762): p. 664-8.
48. Stopfer, M., V. Jayaraman, and G. Laurent, *Intensity versus identity coding in an olfactory system.* Neuron, 2003. **39**(6): p. 991-1004.
49. Naraghi, M. and G. Laurent, *Odorant-induced oscillations in the mushroom bodies of the locust.* The Journal of Neuroscience, 1994. **14**(5): p. 2993-3004.
50. Meredith, M. and D.G. Moulton, *Patterned response to odor in single neurons of gold fish olfactory bulb: influence of odor quality and other stimulus parameters.* Journal of General Physiology, 1978. **71**: p. 572-597.
51. Laurent, G. and H. Davidowitz, *Encoding of Olfactory Information with Oscillating Neural Assemblies.* Science, 1994. **265**(5180): p. 1872-1875.
52. Galan, R.F., et al., *Odor-driven attractor dynamics in the antennal lobe allow for simple and rapid olfactory pattern classification.* Neural Computation, 2004. **16**(5): p. 999-1012.
53. Perez-Orive, J., et al., *Oscillations and sparsening of odor representations in the mushroom body.* Science, 2002. **297**(5580): p. 359-365.
54. Brown, S.L., J. Joseph, and M. Stopfer, *Encoding a temporally structured stimulus with a temporally structured neural representation.* Nat Neurosci, 2005. **8**(11): p. 1568-76.
55. Broome, B.M., V. Jayaraman, and G. Laurent, *Encoding and decoding of overlapping odor sequences.* Neuron, 2006. **51**(4): p. 467-82.
56. Olsen, S.R. and R.I. Wilson, *Lateral presynaptic inhibition mediates gain control in an olfactory circuit.* Nature, 2008. **452**(7190): p. 956-60.
57. Christensen, T.A., et al., *Local interneurons and information processing in the olfactory glomeruli of the moth Manduca sexta.* J Comp Physiol A, 1993. **173**(4): p. 385-99.
58. MacLeod, K. and G. Laurent, *Distinct mechanisms for synchronization and temporal patterning of odor-encoding neural assemblies.* Science, 1996. **274**(5289): p. 976-979.
59. Bazhenov, M., et al., *Fast odor learning improves reliability of odor responses in the locust antennal lobe.* Neuron, 2005. **46**(3): p. 483-492.
60. Sudhakaran, I.P., et al., *Plasticity of Recurrent Inhibition in the Drosophila Antennal Lobe.* Journal of Neuroscience, 2012. **32**(21): p. 7225-7231.
61. Twick, I., J.A. Lee, and M. Ramaswami, *Olfactory Habituation in Drosophila-Odor Encoding and its Plasticity in the Antennal Lobe.* Odor Memory and Perception, 2014. **208**: p. 3-38.
62. Das, S., et al., *Plasticity of local GABAergic interneurons drives olfactory habituation.* Proceedings of the National Academy of Sciences of the United States of America, 2011. **108**(36): p. E646-E654.
63. Olsen, S.R., V. Bhandawat, and R.I. Wilson, *Divisive normalization in olfactory population codes.* Neuron, 2010. **66**(2): p. 287-99.

64. Heisenberg, M., et al., *Drosophila mushroom body mutants are deficient in olfactory learning.* J Neurogenet, 1985. **2**(1): p. 1-30.
65. Dubnau, J., et al., *Disruption of neurotransmission in Drosophila mushroom body blocks retrieval but not acquisition of memory.* Nature, 2001. **411**(6836): p. 476-80.
66. Zars, T., et al., *Localization of a short-term memory in Drosophila.* Science, 2000. **288**(5466): p. 672-5.
67. McGuire, S.E., P.T. Le, and R.L. Davis, *The role of Drosophila mushroom body signaling in olfactory memory.* Science, 2001. **293**(5533): p. 1330-3.
68. Turner, G.C., M. Bazhenov, and G. Laurent, *Olfactory representations by Drosophila mushroom body neurons.* J Neurophysiol, 2008. **99**(2): p. 734-46.
69. Campbell, R.A., et al., *Imaging a population code for odor identity in the Drosophila mushroom body.* J Neurosci, 2013. **33**(25): p. 10568-81.
70. Gruntman, E. and G.C. Turner, *Integration of the olfactory code across dendritic claws of single mushroom body neurons.* Nat Neurosci, 2013. **16**(12): p. 1821-9.
71. Lin, A.C., et al., *Sparse, decorrelated odor coding in the mushroom body enhances learned odor discrimination.* Nat Neurosci, 2014. **17**(4): p. 559-68.
72. Stopfer, M., *Central processing in the mushroom bodies.* Curr Opin Insect Sci, 2014. **6**: p. 99-103.
73. Gupta, N. and M. Stopfer, *Functional Analysis of a Higher Olfactory Center, the Lateral Horn.* Journal of Neuroscience, 2012. **32**(24): p. 8138-8148.
74. Assisi, C., et al., *Adaptive regulation of sparseness by feedforward inhibition.* Nature Neuroscience, 2007. **10**(9): p. 1176-1184.
75. Lelito, J.P., A.J. Myrick, and T.C. Baker, *Interspecific pheromone plume interference among sympatric heliothine moths: a wind tunnel test using live, calling females.* J Chem Ecol, 2008. **34**(6): p. 725-33.
76. Simoes, P., S.R. Ott, and J.E. Niven, *Associative olfactory learning in the desert locust, Schistocerca gregaria.* J Exp Biol, 2011. **214**(Pt 15): p. 2495-503.
77. Bitterman, M.E., et al., *Classical conditioning of proboscis extension in honeybees (Apis mellifera).* J Comp Psychol, 1983. **97**(2): p. 107-19.
78. Wilson, R.I., *Neural and behavioral mechanisms of olfactory perception.* Curr Opin Neurobiol, 2008. **18**(4): p. 408-12.
79. Su, C.Y., et al., *Non-synaptic inhibition between grouped neurons in an olfactory circuit.* Nature, 2012. **492**(7427): p. 66-+.
80. Bhagavan, S. and B.H. Smith, *Olfactory conditioning in the honey bee, Apis mellifera: effects of odor intensity.* Physiol Behav, 1997. **61**(1): p. 107-17.
81. Mauelshagen, J., *Neural correlates of olfactory learning paradigms in an identified neuron in the honeybee brain.* J Neurophysiol, 1993. **69**(2): p. 609-25.
82. Saha, D., et al., *Engaging and disengaging recurrent inhibition coincides with sensing and unsensing of a sensory stimulus.* Nat Commun, 2017. **8**: p. 15413.
83. Saha, D., et al., *Multi-unit recording methods to characterize neural activity in the locust (Schistocerca americana) olfactory circuits.* J Vis Exp, 2013(71).
84. Pouzat, C., O. Mazor, and G. Laurent, *Using noise signature to optimize spike-sorting and to assess neuronal classification quality.* J Neurosci Methods, 2002. **122**(1): p. 43-57.

85. Laurent, G., K.J. Seymourlaurent, and K. Johnson, *Dendritic Excitability and a Voltage-Gated Calcium Current in Locust Nonspiking Local Interneurons.* Journal of Neurophysiology, 1993. **69**(5): p. 1484-1498.
86. Bishop, C.M., *Pattern recognition and machine learning*. 2006: springer.
87. Shannon, C.E., *A Mathematical Theory of Communication.* Bell System Technical Journal, 1948. **27**(3): p. 379-423.
88. Izhikevich, E., *Simple model of spiking neurons.* IEEE Transactions on Neural Networks, 2003. **14**: p. 1569-1572.
89. Farivar, S.S., *Cytoarchitecture of the locust olfactory system*, in *Biology*. 2005, California Technological Institute: Pasadena.
90. Hosoya, T., S.A. Baccus, and M. Meister, *Dynamic predictive coding by the retina.* Nature, 2005. **436**(7047): p. 71-7.
91. Peelen, M.V., L. Fei-Fei, and S. Kastner, *Neural mechanisms of rapid natural scene categorization in human visual cortex.* Nature, 2009. **460**: p. 94-97.
92. Machens, C.K., et al., *Single audtiroy neurons rapidly discriminate conspecific communication signals.* Nature Neuroscience, 2003. **6**(4): p. 341-342.
93. Murray, M.M., et al., *Rapid brain discrimination of sounds of objects.* Journal of Neuroscience, 2006. **26**(4): p. 1293-1302.
94. Jaramillo, S. and A.M. Zador, *The auditory cortex mediates the perceptual effects of acoustic temporal expectation.* Nature Neuroscience, 2011. **14**(2): p. 246-U340.
95. Uchida, N., A. Kepecs, and Z.F. Mainen, *Seeing at a glance, smelling in a whiff: rapid forms of perceptual decision making.* Nature Review Neuroscience, 2006. **7**: p. 485-491.
96. Abraham, N.M., et al., *Maintaining accuracy at the expense of speed: stimulus similarity defines odor discrimination time in mice.* Neuron, 2004. **44**(5): p. 865-876.
97. Mazor, O. and G. Laurent, *Transient dynamics versus fixed points in odor representations by locust antennal lobe projection neurons.* Neuron, 2005. **48**(4): p. 661-73.
98. Scholl, B., X. Gao, and M. Wehr, *Nonoverlapping Sets of Synapses Drive On Responses and Off Responses in Auditory Cortex.* Neuron, 2010. **65**(3): p. 412-421.
99. Fishman, Y.I. and M. Steinschneider, *Temporally dynamic frequency tuning of population responses in monkey primary auditory cortex.* Hearing Research, 2009. **254**(1-2): p. 64-76.
100. Deangelis, G.C., I. Ohzawa, and R.D. Freeman, *Receptive-Field Dynamics in the Central Visual Pathways.* Trends in Neurosciences, 1995. **18**(10): p. 451-458.
101. Geffen, M.N., et al., *Neural encoding of rapidly fluctuating odors.* Neuron, 2009. **61**(4): p. 570-86.
102. Aldworth, Z.N. and M.A. Stopfer, *Trade-off between information format and capacity in the olfactory system.* Journal of Neuroscience, 2015. **35**(4): p. 1521-1529.
103. Behnia, R., et al., *Processing properties of ON and OFF pathways for Drosophila motion detection.* Nature, 2014. **512**(7515): p. 427-30.
104. Wassle, H., *Parallel processing in the mammalian retina.* Nat Rev Neurosci, 2004. **5**(10): p. 747-57.
105. Hubel, D.H. and T.N. Wiesel, *Receptive Fields, Binocular Interaction and Functional Architecture in Cats Visual Cortex.* Journal of Physiology-London, 1962. **160**(1): p. 106-154.

106. Kuffler, S.W., *Discharge patterns and functional organization of mammalian retina.* J Neurophysiol, 1953. **16**(1): p. 37-68.
107. Friedrich, R.W. and G. Laurent, *Dynamic optimization of odor representations by slow temporal patterning of mitral cell activity.* Science, 2001. **291**(5505): p. 889-94.
108. Bhandawat, V., et al., *Sensory processing in the Drosophila antennal lobe increases reliability and separability of ensemble odor representations.* Nature Neuroscience, 2007. **10**(11): p. 1474-1482.
109. Nagel, K.I. and R.I. Wilson, *Mechanisms Underlying Population Response Dynamics in Inhibitory Interneurons of the Drosophila Antennal Lobe.* Journal of Neuroscience, 2016. **36**(15): p. 4325-4338.
110. Bazhenov, M., et al., *Model of transient oscillatory synchronization in the antennal lobe.* Neuron, 2001. **30**: p. 553-567.
111. Uchida, N. and Z.F. Mainen, *Speed and accuracy of olfactory discrimination in the rat.* Nature Neuroscience, 2003. **6**(11): p. 1224-1229.
112. Yao, H., et al., *Rapid learning in cortical coding of visual scenes.* Nature Neuroscience, 2007. **10**(6): p. 772-778.
113. R. F. Galán, et al., *Sensory memory for odors is encoded in spontaneous correlated activity between olfactory glomeruli.* Neural Computation, 2006. **18**(1): p. 10-25.
114. Gottlieb, Y., E. Vaadia, and M. Abeles, *Single unit activity in the auditory cortex of a monkey performing a short-term memory task.* Experimental Brain Research, 1989. **74**(1): p. 139-148.
115. Joesch, M., et al., *ON and OFF pathways in Drosophila motion vision.* Nature, 2010. **468**(7321): p. 300-U186.
116. Gollisch, T. and M. Meister, *Rapid neural coding in the retina with relative spike latencies.* Science, 2008. **319**: p. 1108-1111.
117. Mori, I. and Y. Ohshima, *Neural regulation of thermotaxis in caenorhabditis elegans.* Nature, 1995. **376**(6538): p. 344-348.
118. Kuhara, A., et al., *Neural coding in a single sensory neuron controlling opposite seeking behaviours in Caenorhabditis elegans.* Nat Commun, 2011. **2**: p. 355.
119. Chalasani, S.H., et al., *Dissecting a circuit for olfactory behaviour in Caenorhabditis elegans.* Nature, 2007. **450**: p. 63-70.
120. Merten, K. and A. Nieder, *Active encoding of decisions about stimulus absence in primate prefrontal cortex neurons.* Proceedings of the National Academy of Sciences of the United States of America, 2012. **109**(16): p. 6289-6294.
121. Choi, G.B., et al., *Driving opposing behaviors with ensembles of piriform neurons.* Cell, 2011. **146**: p. 1004-1015.
122. Grunewald, A. and M.J.M. Lankheet, *Orthogonal motion after-effect illusion predicted by a model of cortical motion processing.* Nature, 1996. **384**: p. 358-360.
123. Herry, C., et al., *Switching on and off fear by distinct neuronal circuits.* Nature, 2008. **454**(7204): p. 600-U28.
124. Oka, Y., M. Ye, and C.S. Zuker, *Thirst driving and suppressing signals encoded by distinct neural populations in the brain.* Nature, 2015: p. 349-352.
125. Koulakov, A., A. Gelperin, and D. Rinberg, *Olfactory coding with all-or-nothing glomeruli.* Journal of Neurophysiology, 2007. **98**(6): p. 3134-3142.
126. Mathis, A., et al., *Reading Out Olfactory Receptors: Feedforward Circuits Detect Odors in Mixtures without Demixing.* Neuron, 2016. **91**(5): p. 1110-1123.

127. Barnstedt, O., et al., *Memory-Relevant Mushroom Body Output Synapses Are Cholinergic.* Neuron, 2016. **89**(6): p. 1237-1247.
128. Semmelhack, J.L. and J.W. Wang, *Select Drosophila glomeruli mediate innate olfactory attraction and aversion.* Nature, 2009. **459**(7244): p. 218-U100.
129. Cury, K.M. and N. Uchida, *Robust Odor Coding via Inhalation-Coupled Transient Activity in the Mammalian Olfactory Bulb.* Neuron, 2010. **68**(3): p. 570-585.
130. Laurent, G., M. Wehr, and H. Davidowitz, *Temporal representations of odors in an olfactory network.* J Neurosci, 1996. **16**(12): p. 3837-47.
131. Bartlett, E.L. and X. Wang, *Long-lasting modulation by stimulus context in primate auditory cortex.* J Neurophysiol, 2005. **94**(1): p. 83-104.
132. Benucci, A., D.L. Ringach, and M. Carandini, *Coding of stimulus sequences by population responses in visual cortex.* Nat Neurosci, 2009. **12**(10): p. 1317-24.
133. Morcos, A.S. and C.D. Harvey, *History-dependent variability in population dynamics during evidence accumulation in cortex.* Nat Neurosci, 2016. **19**(12): p. 1672-1681.
134. Sun, Y., et al., *Neural signatures of dynamic stimulus selection in Drosophila.* Nat Neurosci, 2017. **20**(8): p. 1104-1113.
135. Wegel, R.L., and Lane, C. E., *The auditory masking of one pure tone by another and its probable relation to the dynamics of the inner ear.* Phys. Rev., 1924. **23**: p. 266-285.
136. Daly, K.C., et al., *The generalization of an olfactory-based conditioned response reveals unique but overlapping odour representations in the moth Manduca sexta.* J Exp Biol, 2001. **204**(Pt 17): p. 3085-95.
137. Guerrieri, F., et al., *Perceptual and neural olfactory similarity in honeybees.* PLoS Biol, 2005. **3**(4): p. e60.
138. Joseph, J., F.A. Dunn, and M. Stopfer, *Spontaneous olfactory receptor neuron activity determines follower cell response properties.* J Neurosci, 2012. **32**(8): p. 2900-10.
139. Min, S., et al., *Dedicated olfactory neurons mediating attraction behavior to ammonia and amines in Drosophila.* Proc Natl Acad Sci U S A, 2013. **110**(14): p. E1321-9.
140. Inada, K., Y. Tsuchimoto, and H. Kazama, *Origins of Cell-Type-Specific Olfactory Processing in the Drosophila Mushroom Body Circuit.* Neuron, 2017. **95**(2): p. 357-367 e4.
141. Nagel, K.I., E.J. Hong, and R.I. Wilson, *Synaptic and circuit mechanisms promoting broadband transmission of olfactory stimulus dynamics.* Nat Neurosci, 2015. **18**(1): p. 56-65.
142. Kazama, H. and R.I. Wilson, *Homeostatic matching and nonlinear amplification at identified central synapses.* Neuron, 2008. **58**(3): p. 401-13.
143. Kurahashi, T. and A. Menini, *Mechanism of odorant adaptation in the olfactory receptor cell.* Nature, 1997. **385**(6618): p. 725-9.
144. Nagel, K.I. and R.I. Wilson, *Biophysical mechanisms underlying olfactory receptor neuron dynamics.* Nat Neurosci, 2011. **14**(2): p. 208-16.
145. Nizampatnam, S., et al., *Dynamic contrast enhancement and flexible odor codes.* Nature Communications, 2018. **9**.
146. Rabinovich, M., et al., *Dynamical encoding by networks of competing neuron groups: winnerless competition.* Phys Rev Lett, 2001. **87**(6): p. 068102.
147. Laurent, G., et al., *Odor encoding as an active, dynamical process: experiments, computation, and theory.* Annu Rev Neurosci, 2001. **24**: p. 263-97.

148. Badeke, E., et al., *A Challenge for a Male Noctuid Moth? Discerning the Female Sex Pheromone against the Background of Plant Volatiles.* Front Physiol, 2016. **7**: p. 143.
149. Bolding, K.A. and K.M. Franks, *Recurrent cortical circuits implement concentration-invariant odor coding.* Science, 2018. **361**(6407).
150. Shusterman, R., et al., *Sniff Invariant Odor Coding.* eNeuro, 2018. **5**(6).
151. Semmelhack, J.L. and J.W. Wang, *Select Drosophila glomeruli mediate innate olfactory attraction and aversion.* Nature, 2009. **459**(7244): p. 218-23.
152. Faucher, C., et al., *Behavioral responses of Drosophila to biogenic levels of carbon dioxide depend on life-stage, sex and olfactory context.* J Exp Biol, 2006. **209**(Pt 14): p. 2739-48.
153. Kauer, J.S. and D.G. Moulton, *Responses of olfactory bulb neurones to odour stimulation of small nasal areas in the salamander.* J Physiol, 1974. **243**(3): p. 717-37.
154. Meredith, M., *Patterned response to odor in mammalian olfactory bulb: the influence of intensity.* J Neurophysiol, 1986. **56**(3): p. 572-97.
155. Wellis, D.P., J.W. Scott, and T.A. Harrison, *Discrimination among Odorants by Single Neurons of the Rat Olfactory-Bulb.* Journal of Neurophysiology, 1989. **61**(6): p. 1161-1177.
156. Silbering, A.F., et al., *Olfactory information processing in the Drosophila antennal lobe: anything goes?* J Neurosci, 2008. **28**(49): p. 13075-87.
157. Sachse, S. and C.G. Galizia, *The coding of odour-intensity in the honeybee antennal lobe: local computation optimizes odour representation.* Eur J Neurosci, 2003. **18**(8): p. 2119-32.
158. Laurent, G., *Dynamical representation of odors by oscillating and evolving neural assemblies.* Trends in Neuroscience, 1996. **19**(11): p. 489-296.
159. Friedrich, R.W. and S.I. Korsching, *Combinatorial and chemotopic odorant coding in the zebrafish olfactory bulb visualized by optical imaging.* Neuron, 1997. **18**(5): p. 737-752.
160. Rubin, B.D. and L.C. Katz, *Optical imaging of odorant representations in the mammalian olfactory bulb.* Neuron, 1999. **23**(3): p. 499-511.
161. Ng, M., et al., *Transmission of olfactory information between three populations of neurons in the antennal lobe of the fly.* Neuron, 2002. **36**(3): p. 463-474.